Influence of instruments performance and material properties on exposure assessment of airborne engineered nanomaterials

Levin, Marcus

Publication date:
2015

Document Version
Publisher's PDF, also known as Version of record

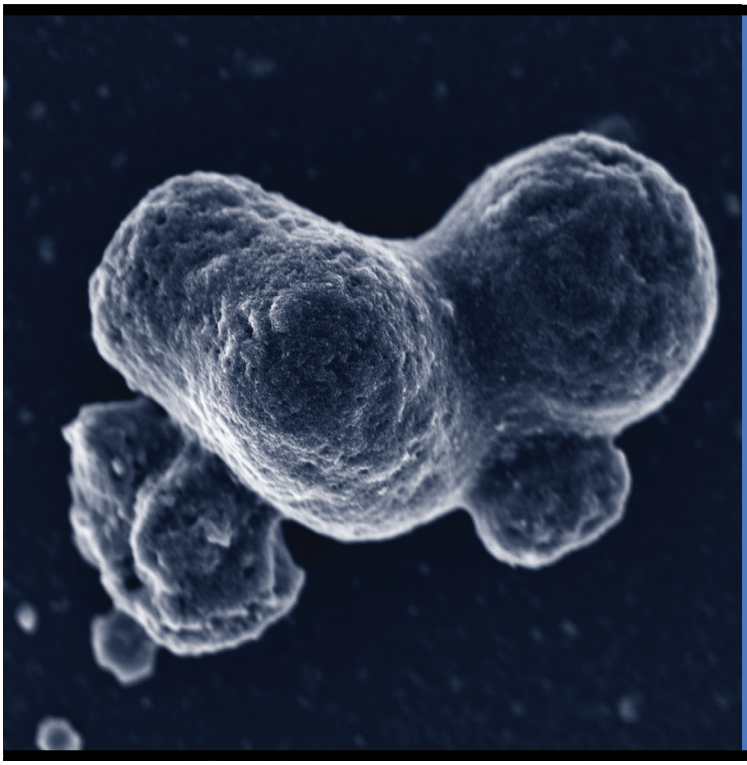

Influence of instrument performance and material properties on exposure assessment of airborne engineered nanomaterials

Marcus Levin
PhD Thesis July 2015

DTU Nanotech
Department of Micro- and Nanotechnology

Influence of instrument performance and material properties on exposure assessment of airborne engineered nanomaterials

Ph.D. Thesis by Marcus Levin

July 2015

Department of Micro- and Nanotechnology, Technical University of Denmark

National Research Centre for the Working Environment, Denmark

Abstract

Over the last decades, materials engineered of nanosized structures have increased tremendously, in terms of both produced tonnage and economic market share. This, together with the fact that some of these engineered nanomaterials have shown an increased toxicological effect in humans as compared to their bulk counterpart, has expanded the scientific field of exposure measurements to airborne nanoparticles. As the greatest potential for human exposure to engineered nanomaterials resides within the production, packaging and downstream powder-material handling, as well as at reworking/waste treatment facilities, exposure risk for workers has received great focus.

The studies described in this thesis come to four main conclusions: **1)** Mass-balance modeling of airborne engineered nanomaterials using dustiness index as a primary source term can be useful for assessment of material-specific exposure scenarios and in decision-making regarding powder choices. **2)** That such mass-balance modeling can, however, be highly sensitive to environmental conditions, especially humidity, during storage and use, which may cause a severe misrepresentation of the true emission if the conditions during dustiness testing differ from the modeled scenario. **3)** That particles with a geometrical mean diameter above 200 nm cannot be measured reliably with the Fast Mobility Particle Sizer (FMPS 3091, TSI Inc., MN, USA) but will instead be underestimated in terms of particle size and overestimated in terms of particle number concentration. Measured size distributions with particle modes above 150 nm should not be deemed reliable as they might arise from misclassification of larger size particles. **4)** That current methods for real-time measurement of lung-deposited surface area concentration for airborne engineered nanomaterials are cannot be relied upon to represent comparable levels for use in exposure assessments and for other regulatory purposes.

The work presented in this thesis provides understanding to improve assessment of airborne exposure to engineered nanomaterials in occupational settings. Based on conclusions drawn in this thesis, exposure assessment and control-banding models should review their use of dustiness index as a term of emission or ensure that the specific material of interest has been tested in relevant conditions. The work shows the limits of the capabilities of current techniques for measurement of airborne particle characteristics, and highlights necessary improvements for future adaptions of new metrics into regulatory testing and occupational exposure limits.

Table of Contents

1 Original papers

This thesis is based on the following four key research papers, which are referred to in the text by their roman numerals (**I-IV**):

I. Levin M, Koponen IK, Jensen KA. (2014) Exposure Assessment of Four Pharmaceutical Powders Based on Dustiness and Evaluation of Damaged HEPA Filters. Journal of Occupational and Environmental Hygiene. 11(3):165-77.

II. Levin M, Rojas E, Vanhala E, Vippola M, Liguori B, Kling KI, Koponen IK, Mølhave K, Tuomi T, Gregurec D, Moya S, Jensen KA. Influence of relative humidity and physical loading during storage conditions on dustiness of inorganic nanomaterials - Implications for testing and risk assessment. Journal of Nanoparticle Research 17(8):337.

III. Levin M, Gudmundsson A, Pagels JH, Fierz M, Mølhave K, Jensen KA, Koponen IK. (2015) Limitations in the use of unipolar charging for electrical mobility sizing instruments: A study of the Fast Mobility Particle Sizer. Aerosol Science and Technology 49(8):556-565 DOI: 10.1080/02786826.2015.1052039

IV. Levin M, Witschger O, Bau S, Jankowska E, Koponen IK Koivisto AJ, Jensen AJ, Clausen PA, Mølhave K, Asbach C, Jensen KA. Can we trust real time measurements of lung-deposited surface area concentrations in dust from powder nanomaterials? Submitted. (Aerosol and Air Quality Research)

2 Additional publications

Peer-reviewed research articles:

- Sørli JB, Hansen JS, Nørgaard AW, Levin M, Larsen ST. An in vitro method for predicting inhalation toxicity of impregnation spray products. ALTEX 02/2015; DOI: 10.14573/altex.1408191

- Halappanavar S, Saber ST, Decan N, Jensen KA, Wu D, Jacobsen NR, Guo C, Rogowski J, Koponen IK, Levin M, Madsen AM, Atluri R, Snitka V, Birkedal RK, Rickerby D, Williams A, Wallin H, Yauk CL, Vogel U. Transcriptional profiling identifies physicochemical properties of nanomaterials that are determinants of the in vivo pulmonary response. Environmental and Molecular Mutagenesis 12/2014; DOI:10.1002/em.21936

- Koivisto AJ, Jensen AC, Levin M, Kling KI, Dal Maso M, Nielsen SH, Jensen KA, Koponen IK. Testing a Near Field/Far Field model performance for prediction of particulate matter emissions in a paint factory. Environ. Sci.: Processes Impacts 11/2014

- Gomez V, Levin M, Saber AT, Irusta S, Dal Maso M, Hanoi R, Santamaria J, Jensen KA, Wallin H, Koponen IK. Comparison of Dust Release from Epoxy and Paint Nanocomposites and Conventional Products during Sanding and Sawing. Annals of Occupational Hygiene 07/2014; 58(8). DOI:10.1093/annhyg/meu046.

- Duch P, Nørgaard AW, Hansen JS, Sørli JB, Jacobsen P, Lynggard F, Levin M, Nielsen GD, Wolkoff P, Ebbehøj NE, Larsen ST. Pulmonary toxicity following exposure to a tile coating product containing alkylsiloxanes. A clinical and toxicological evaluation. Clinical Toxicology 06/2014; 52:498-505. DOI:10.3109/15563650.2014.915412.

- Nørgaard AW, Hansen JA, Sørli JB, Levin M, Wolkoff P, Nielsen GD, Larsen ST. Pulmonary toxicity of perfluorinated silane-based nanofilm spray products: Solvent-dependency. Toxicological Sciences 01/2014; 137(1):179-188. DOI:10.1093/toxsci/kft225
- Jensen ACØ, Levin M, Koivisto AJ, Kling KI, Saber AT, Koponen IK. Exposure Assessment of Particulate Matter from Abrasive Treatment of Carbon and Glass Fibre-Reinforced Epoxy-Composites – Two Case Studies. Aerosol and Air Quality Research 05/2015.

- Size-resolved characterization of particles and fibers released during abrasion of fiber-reinforced composite in a workplace influenced by ambient background sources. Kling KI, Levin M, Jensen ACØ, Jensen KA, Koponen IK. Submitted (Aerosol and Air Quality Research).

Books and Chapters:

- Rasmussen K, Mech A, Mast J, de Temmerman PJ, Waegneers N, van Steen F, Pizzolon JC, de Temmerman L, van Doren E, Jensen KA, Birkedal R, Levin M, Nielsen S, Koponen IK, Clausen PA, Kembouche Y, Thieriet N, Spalla O, Giout C, Rousset D, Witschger O, Bau S, Bianchi B, Shivachev B, Gilliland D, Pianella F, Ceccone G, Cotogno G, Rauscher H, Gibson P, and Stamm H, "Synthetic Amorphous Silicon Dioxide (NM-200, NM-201, NM-202, NM-203, NM-204): Characterisation and Physico-Chemical Properties JRC Repository: NM-series of Representative Manufactured Nanomaterials," JRC83506, 2013. ISBN: 978-92-79-32323-2

- Rasmussen K, Mast J, de Temmerman PJ, Verleysen E, Waegneers E, van Steen F, Pizzolon JC, de Temmerman L, van Doren E, Jensen KA, Birkedal R, Levin M, Nielsen SH, Koponen IK, Clausen PA, Kofoed-Sørensen V, Kembouche Y, Thieriet N, Spalla O, Giout C, Rousset D, Witschger O, Bau S, Bianchi B, Motzkus C, Shivachev B, Dimowa L, Nikolova R, Nihtianova D, Tarassov M, Petrov O, Bakardjeva S, Gilliland D, Pianella F, Ceccone G, Spampinato V, Cotogno G, Gibson P, Gaillard C, and Mech A, "Titanium Dioxide, NM-100, NM-101, NM-102, NM-103, NM-104, NM-105: Characterisation and Physico-Chemical Properties," JRC86291, 2014. ISBN: 978-92-79-38188-1

- Jensen KA, Levin M, Witschger O (2015) Methods for testing dustiness. In Ratna Tantra (Ed.) Nanomaterial Characterization: An introduction. John Wiley & Sons Inc (In Press). ISBN: 978-1-118-75359-0

Conference contributions as leading author

- Levin M, Koponen IK, Witschger O, Bau S, Jankowska E, Giout C, Spalla O, Jensen KA. Comparison of methods for measurement of surface area for six different nanomaterials. European Aerosol Conference 2012, Granada, Spain. A-WG06S1P15.
- Levin M, Lieke KI, Koponen IK, Jensen KA. Dustiness of inorganic nanopowders - Influence of humidity and physical loading during storage. 6th International Symposium on Nanotechnology, Occupational and Environmental Health, 2013. Nagoya, Japan. O-29-B-13.
- Levin M, Koponen IK, Jensen KA. Comparison of direct reading instruments for particle measurements. 6th International Symposium on Nanotechnology, Occupational and Environmental Health (NanOEH), 2013 . Nagoya, Japan. P-06-108.
- Levin M, Kling KI, Koponen IK, Jensen KA. Influence of humidity and physical loading during storage on dustiness of inorganic nanopowders. Aerosol Technology 2014. Karlsruhe, Germany. T230A08.
- Levin M, Gudmundsson A, Pagels JH, Rissler J, Mølhave K, Jensen KA, Koponen IK. Comparison of direct reading instruments for Particle Measurements. Aerosol Technology 2014. Karlsruhe, Germany. T320A12.
- Levin M, Gudmundsson A, Pagels JH, Rissler J, Mølhave K, Jensen KA, Koponen IK. Comparison of direct reading instruments for Particle Measurements. Nanosafety Forum for Young Scientists 2014. Syracuse, Italy.

3 Introduction

All ambient air surrounding the earth contains not only various gaseous compounds but also suspended particulate matter (PM). This colloidal system, called an aerosol, consists of solid and/or liquid particles with diameters ranging from ca. one nanometer up to 100 µm. There is a continuous production of new particles through natural processes such as e.g., sea-spray, soil dust, atmospheric nucleation and biological activity as well as anthropogenic sources such as combustion processes. In return, there are also several removal processes such as gravitational sedimentation and precipitation.

As there is a constant presence of PM in the air we breathe, we are also exposed to these particles and they can potentially deposit in the lungs through various processes. It has been estimated that in 2010 ambient PM air pollution accounted for 3.1 million deaths and around 3.1% of global disability-adjusted life years (Lim et al. 2012). The correlation between exposures to airborne PM and mortality and morbidity has been well established through epidemiological studies (Dockery et al. 1993; Pope 2000; Pope et al. 2002; Anderson 2009; Dadvand et al. 2013). PM air pollution from anthropogenic sources, such as traffic and combustion in households, caused an annual loss of an estimated 5 million years of life in Europe due to exposure to particles smaller than 2.5 µm ($PM_{2.5}$) (Almeida et al. 2005; EEA 2010). Ultra-fine particles (<100nm, $PM_{0.1}$) have been intensively studied in recent years as this is considered the most harmful size range of particles for pulmonary uptake (Oberdorster 2001; Donaldson et al. 2001; Nel 2005; Politis et al. 2008).

In the last two decades a new field has emerged within technology; nanotechnology (Siegel et al. 1999; Roco et al. 2011). As the use of nanoparticles, defined as a particle with all its external dimensions less than 100 nm (ISO 2013), has increased due to their ability to influence material properties such as catalytic activity, surface structure, etc. (Roco 2005), concerns have been raised regarding their possible impact on human health. Due to these concerns, there is a need for regulations and exposure limits to control the use of Engineered Nanomaterials (ENMs) in occupational settings. At the present, official occupational exposure limits are lacking due to insufficient knowledge of relevant exposure scenarios, measurement techniques, biologically relevant metrics, and incomplete epidemiological studies (Schulte et al. 2010; van Broekhuizen et

al. 2012). Further knowledge is therefore needed on the appropriate metrics of exposure measurements in workplaces as well as the applicability of replacing actual measurements with exposure assessment through mass-balance modelling of airborne particle dynamics (Brouwer 2010; Schneider et al. 2011; Brouwer et al. 2012)

In order to provide more accurate assessments of airborne exposure to engineered nanomaterials in occupational settings, the goal of this thesis is to increase the knowledge of how current techniques for measuring airborne particles responds to engineered nanomaterials, and to what extent modeling can be used to supplement these. The objectives of the research presented in this thesis work are:

- To demonstrate and evaluate the use of mass-balance modeling of exposure to ENMs with a material-specific emission potential (dustiness) as a primary source term in exposure assessment.
- To determine the effect of environmental storage conditions on powder dustiness and what implications such effects could have on mass-balance modeling of ENMs for worker exposure assessment.
- To investigate to applicability of the Fast Mobility Particle Sizer (FMPS 3091, TSI Inc., MN, USA) in measurements of ENMs by fully characterizing its unipolar charger effect on particle electrical mobility and studying its response functions to various aerosols.
- To compare methods for real-time measurement of lung-deposited surface area (LDSA) concentration in order to investigate the feasibility of LDSA concentration as a metric of choice in exposure assessment and regulatory approaches.

The thesis consists of: **1)** An introductory background section where the main concepts of exposure measurements of ENMs are described. **2)** A theoretical part where a selection of the techniques used to measure aerosols in general and ENMs specifically are described thoroughly. **3)** Research highlights of the project are described and discussed in a general perspective. Thereafter follow the main peer-reviewed articles of the thesis work.

4 Background

4.1 Engineered nanomaterials

Nano-sized materials are used within industrial applications to enhance certain aspects of other materials. These materials are often referred to as Engineered Nanomaterials (ENMs), and have been defined by the EU (2011) as:

> *"Any intentionally manufactured material, containing particles, in an unbound state or as an aggregate or as an agglomerate and where, for 50% or more of the particles in the number size distribution, one or more external dimensions is in the size range 1 nm to 100 nm."*

The production fields which use ENMs are highly diverse and include energy, electronics, food, medicine, cosmetics and construction (Sadik et al. 2009; Kuhlbusch et al. 2011).

ENMs are typically found either bound within a matrix, solid or liquid, or as unbound nanoparticles. In this sense unbound refers to the fact that, under reasonably foreseeable conditions, the individual particles are not contained within a matrix that would be expected to prevent the nanoparticles from being separately mobile and potentially airborne. ENMs are often desired for their special properties such as having a high specific surface area or outstanding magnetic, optical, catalytic and electronic properties.

The production of ENMs is estimated at an annual 20 to 30 thousand metric tonnes and in 2010 had a conservative market value of USD2.64 billion. The total annual production has been forecasted to reach 40 thousand metric tonnes in 2016 (Future Markets 2011).

4.2 Toxicity of engineered nanomaterials

The toxicity of ENMs might differ, either increase or decrease, from that of the same chemical compound in molecular or bulk form. In an inhalation exposure scenario, the respiratory

deposition of nanoparticles differs from larger particles and an increased toxicological effect can be seen for the same mass concentration exposure (Oberdorster 2001; Kreyling et al. 2006). This is partly due to differences in chemical reactivity of the materials due to changed surface effects and quantum effects (Roduner 2006). Furthermore, nano-sized particles may be able to cross boundaries within the human body that larger sized particle cannot (Donaldson et al. 2004), and could potentially migrate into the cells of humans (Oberdörster et al. 2005, Krug and Wick 2011). The field of nanotechnology can therefore not rely on previous studies of chemical and material toxicity.

There is currently increasing experimental evidence from animal studies that the toxicological effect of ENMs in the lung may, at least partially, be driven by the specific surface area dose of the test material (Oberdorster 2000; Maynard and Kuempel 2005; Duffin et al. 2007; Jacobsen et al. 2009; Donaldson et al. 2013; Saber et al. 2014). Due to the well-known sensitivity of the alveolar region, there is high concern about airway exposure to ultrafine air-pollution, and lately there have been concerns about exposure to the many different types of manufactured nanomaterials, which cover a wide group of nano-objects. It is characteristic of these exposures that they all have large surface-to-volume ratios, independent of their many different possible shapes, chemical compositions, surface chemical modifications and levels of agglomeration and aggregation.

4.3 Exposure assessment

The exposure of humans to ENMs can occur through three main routes of entry; *Inhalation, Ingestion* and *Dermal exposure*. In most cases, the route of exposure with the highest risk of activation within workplace-related exposure situations is the *Inhalation* route. For the purposes of studying the health effects from inhalation and deposition of ENMs, the respiratory tract is often split into three separate regions (ICRP 1994; McClellan 2000). **Figure 4.1a** shows a schematic overview of the human respiratory system and highlights the three regions: the *Head airways (H.A)*, consisting of the nose, mouth, pharynx and larynx; the *Tracheobronchial (TB)* region which starts with the trachea and splits into airway generations with decreasing size until the terminal bronchioles; the final region is the *Alveolar (Alv.),* where the gas exchange of the lungs takes place.

For any respiratory exposure to take place, the particles need to enter the respiratory system. The fractions of inhalable particles as a function of size are shown in **Figure 4.1b**. Below micron-size, basically all particles are considered to enter the respiratory system. As the particle size increases, the inhalable fraction decreases down to ca. 50% at 100 µm. Out of the inhalable fraction, not all particles are deposited within the lungs (**Figure 4.1b**).

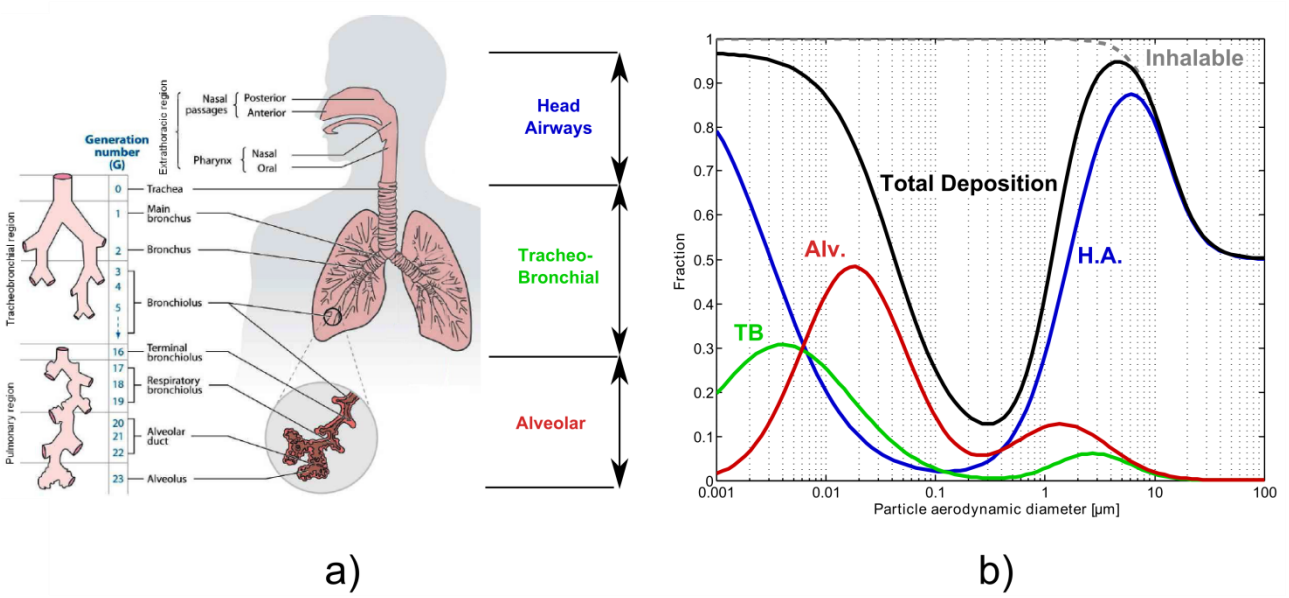

Figure 4.1 a) Schematic overview of the human respiratory system with the main three regions marked. Adapted from Hussein et al. (2011) **b)** Fractions of particles depositing in the different regions of the respiratory system based on their aerodynamic size according to Hinds' (1999) equations for the ICRP deposition model.

The three main physical mechanisms for deposition are Brownian diffusion, sedimentation and impaction, which can be related to particle size, d_p, particle residence time in the lung section, t_{rs}, and the volumetric flow rate, Q (Hinds 1999). Diffusion, which has a deposition probability proportional to $\left(\frac{t_{rs}}{d_p}\right)^{0.5}$, is the main cause of depositions of particles smaller than 500 nm. Gravitational sedimentation of particles within the respiratory system is proportional to $d_p^2 t_{rs}$, and therefore has a main effect for larger size particles. Finally, impaction has a deposition probability

proportional to $d_p^2 Q$, meaning it is predominately an effect for larger size particles in high velocity areas such as the H.A and TB regions (Hinds 1999).

Due to this clear size dependency of particle deposition in the respiratory system, a size-integrated measurement of exposure may not be properly linkable with the different toxicological effects that arise from the deposited particles, as the regional dose will differ depending on the particle size. As an example, a measurement of only number concentration could either lead to a 12% deposition, split between H.A and Alv., if the particle size corresponds to 300 nm. If the size was instead 20 nm, 75% of the particles would deposit in the respiratory system, with a majority of them in the Alv. region. It is therefore desirable to carry out all measurements of ENM exposure with size-resolved equipment, many types of which are described in **Section 5**.

The highest risk for respiratory exposures to ENMs can be found in workplaces such as research laboratories and within the nanomaterials production and handling. Since the number of people world-wide working within these settings is rapidly increasing, there is a rising need for assessment and control of exposures to ENMs (Brouwer 2010). In general, there are three possible approaches to studying the occupational exposure of ENMs; *Exposure measurements at the workplace, laboratory simulations of workplace exposure* and *numerical solutions to workplace exposures* (Dolez 2015).

4.3.1 Workplace measurements

The aim of a measurement of ENM exposure at workplaces is generally to assess the emission during a working process, quantify the workers' exposure, or assess compliance with occupational exposure limits.

The first attempts to study exposure to ENMs at workplaces were initiated in 1998 by the International Carbon Black Association (Kuhlbusch et al. 2004; Kuhlbusch and Fissan 2006). Since then, the number of workplace studies aimed at measuring exposure to ENMs has increased significantly, and guidelines on the methodology used have been established (ISO 2007). Despite this, there is still a lack of data and knowledge of cases with actual ENM exposure (Nasterlack et al.

2008; Brouwer et al. 2009; Kuhlbusch et al. 2011). New standards and guidelines for exposure assessments in workplaces (ISO, OECD) are, however, currently in progress.

One of the major challenges with measurements of ENMs in workplaces is the separation of particles emitted from processes within the workplace setting and environmental background particles (ECHA 2012). This challenge can be addressed to a certain extent by closing off the desired area with a tent-type protection and flushing filtered air into the area prior to the workplace activity (e.g. Maynard et al. 2004; Jensen 2015). It can, however, be argued that such an enclosure disturbs several important parameters in the exposure assessment of normal working routines, e.g. room ventilation.

4.3.2 Laboratory simulations

Many attempts have been made to replace actual workplace measurements with measurements of laboratory-simulated emissions of nanoparticles, e.g. for powder handling and dry aerosolization (Hsu and Chein 2007; Tsai et al. 2008; Nazarenko et al. 2012; Levin et al. 2014; Koivisto et al. 2015), abrasive treatments (Koponen et al. 2009; Goehler et al. 2010; Koponen et al. 2011; Golanski et al. 2011; Wohlleben et al. 2011; Gomez et al. 2014), spraying processes and wet release (Norgaard et al. 2009; Hagendorfer et al. 2010; Nazarenko et al. 2014). This can be highly useful as a work-around to an actual workplace measurement, which is often highly demanding in terms of time and money, and is prone to be disturbed by unforeseen events. Furthermore, laboratory simulations do not suffer from the need to distinguish emitted ENM from background particles, as the simulations can be conducted in a particle-free environment.

Laboratory simulation studies can be separated into activity-specific studies in which a process/activity is studied (e.g. sanding/grinding), and material-specific studies in which the same method is used to test the influence of different materials (e.g. dustiness testing of powder materials). Data from characterization of laboratory emission can be an important parameter in exposure modeling. However, unlike quantitative measurements of workplace exposure, it cannot

be used as a benchmark for good practices within the workplace and will not confidently replace the need for exposure measurements.

4.3.3 Numerical solutions

In recent years, a large number of exposure models and control-banding tools have been developed in an attempt to overcome the high demand for exposure assessment, something which is not feasible to do with full-scale measurements for all settings and variations. Control banding offers a simplified solution for controlling worker exposure, by ranking a specific scenario in a semi-quantitative manner to determine what control measures are necessary. Some of the current tools for such modeling include NanoSafer (Kristensen et al. 2010), Advanced REACH tool (ART, Tielemans et al. 2011), Stoffenmanager (Marquart et al. 2008; Van Duuren-Stuurman et al. 2012), ECETOC TRA (ECOTOC 2012) and EMKG-Expo-Tool (Arndt et al. 2005; Tischer et al. 2009). Several of the models are based on the Near Field/Far Field (NF/FF) mass-balance model, which is a common and well accepted approach to exposure modeling (Cherrie and Schneider 1999; Jayjock et al. 2011). The simplest version of the NF/FF-type of model uses a single-source term (e.g. mass or number concentration) of emission related to a specific process and/or material being handled to determine an emitted concentration in the close presence (NF) of the activity. It thereafter uses aerosol transport physics and mass-balance equations to calculate particle concentrations in the remainder of the room (FF). However, particles with different sizes generally behave differently based on their physical properties. Thus, each size fraction should be dealt with in a single mass-balance equation in order to estimate particle transport, interaction and deposition. In addition to this, a term should be added to each mass-balance equation to describe the change rate between the equations due to agglomeration, chemical reactions and vapor interactions (condensation/evaporation) (Hussein et al. 2015). The addition of these parameters to the modeling would require much more detailed knowledge about the source emission, and in many cases this is not available. It is therefore often not feasible to model the full scale of aerosol dynamics, and a simplified method is chosen instead.

Comparisons between estimated concentration levels through use of NF/FF modeling and actual measurements have given various levels of agreement, with a fair correlation ($R^2 \approx 70\%$) for small-scale powder handling (Brouwer et al. 2006), but less consistent results for larger-scale handling (Heitbrink et al. 1990; Liden 2006; Koivisto et al. 2015). All the above studies have in common the use of powder dustiness as a source parameter.

4.4 Powder dustiness

Dustiness is a non-intrinsic property of powders, describing their propensity to emit particles during physical agitation. It is a relative measurement wherein, given a certain agitation process, the amount of emitted material per mass of agitated material (mg/kg) can be ranked for different powder materials (Liden 2006). During testing it is known to vary with several material factors such as chemical composition, surface coating, primary particle size and aggregate size as well as testing factors such as applied energy and environmental conditions during powder storage (Plinke et al. 1995; Breum 1999; Jensen et al. 2009; Tsai et al. 2012; Burdett et al. 2013; Evans et al. 2013).

Due to this relative ranking of dustiness and the influence of environmental testing conditions, there is a strong case for standardization of its measurement. Despite this, only a single standard document exists thus far regarding testing of powder dustiness, namely the EN:15051 (BS EN:15051 2006). This standard concerns two separate methods for testing powder dustiness; the rotating drum method and the continuous drop. The difference between the methods is that, while in the rotating drum a powder sample is being repeatedly agitated, in the continuous drop method is all the time using 'un-tested' material. While the rotating drum may require less material than the continuous drop method, the standard still calls for triplicate tests, with 35 cm^3 of powder used in each. As the development and use of nano-structured materials has increased, the desire to test their dustiness has followed. However, due to high costs and low availability, the required amount of test material needed for tests is no longer been feasible. This, together with the wish for a system that could fit into standard fume-hoods to test for highly toxic materials, such as carbon nano-tubes, has led to the development of a down-sized system; the small rotating drum.

The small rotating drum was first developed by Schneider and Jensen (2008) and is a miniaturized version of the drum described in EN:15051. It consists of a 5.93 L cylindrical drum with conical ends, equipped with three lifter vanes used to lift and drop the tested powder, **Figure 4.2**. An 11 L/min humidity-controlled airflow passes through the drum and carries aerosolized materials to the sampling line. A variety of different sampling equipment can be connected to the small rotating drum (see e.g. **Paper I**, **II**, **IV**) but in the original setup it was equipped with filter sampling for determination of the inhalable dustiness index, as well as instruments for real-time reading of particle size distributions. The test procedure using the small rotating drum follows that of the EN:15051 rotating drum, but uses only 6 g of material for each triplicate test.

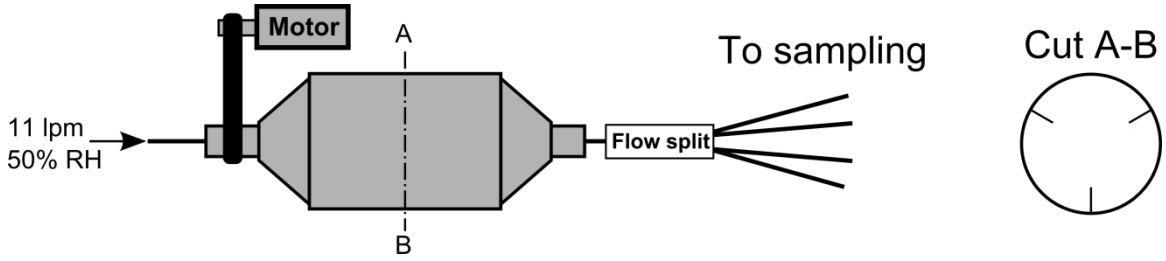

Figure 4.2 Schematic overview of the small rotating drum flow splitter for sampling devices. A-B-cut show internal drum design.

Other methods for testing the powder dustiness of ENMs have been developed simultaneously with the small rotating drum. These include the Vortex shaker (Baron et al. 2002), the Venturi device (Evans et al. 2013) and the Heubach Dustmeter (Type 2000, Heubach GmbH, Germany).

4.5 Measurement challenges

Due to the unclear metric dependency of nanoparticle toxicity, the biologically relevant metric to characterize during measurement of ENMs in workplaces is still not fully understood. Maynard and Aitken (2007) concluded that the LDSA concentration is a relevant metric in many cases, but not a

universal metric of exposure. They also noted that mass-concentration measurements, which many occupational exposure limits are based on, are useful to monitor under some, but not all, circumstances. It has been proposed that measurement of a wide range of characteristics could be needed for exposure measurement in order to cover the wide range of ENMs (Oberdorster et al. 2005; Grassian 2008; Quadros and Marr 2010; Abbott and Maynard 2010; Kuempel et al. 2012; Koivisto et al. 2014):

- Material properties of ENMs: size, shape, chemical composition, crystal structure, number and mass concentration.
- Surface properties: surface structure, chemistry, charge and area.
- Environmental influence: particle size, chemical composition, number/mass/surface area concentration of environmental background particles. Chemical composition and concentration of gases that may condense onto particles.

However, such variety in measurement adds further to the already work-intensive and costly process of exposure measurements at workplaces.

In addition to the challenge of the pure number of parameters in an exposure measurement, several particle characteristics, such as particle size and concentration, can be obtained through a wide variety of methods. As the different methods are based on observations of different specific properties of the particles, variations in the exposure measurements can be seen depending on which instrument is used, especially in cases with measurements of ENMs of complex morphology (Leskinen et al. 2012; Kaminski et al. 2013; Mills et al. 2013; Fissan et al. 2014; Zimmerman et al. 2014; Hornsby and Pryor 2014; Price et al. 2014). Further information on the reliability and material-specific comparability of the real-time methods for measuring particle properties is needed before these methods can be properly included in exposure assessments and regulatory decisions.

5 Measurement theory & techniques

For any assessment of exposure to ENMs, the use of proper and reliable techniques to characterize the airborne particles is of utmost importance. The techniques used vary in what fundamental property is being measured, and can further be separated into different classes based on their resolving power. An instrument can either be time-integrated, e.g. filter sampling with subsequent analysis, or it can be conducted semi-continuously with time resolution up to several Hz. Furthermore, a technique can either measure a size-integrated total concentration of some metric, e.g., mass, number, surface area, etc., or classify a metric according to particle size. This can either be done by selective measurement of a concentration in a specific size-range or by resolving it into a size-distributed concentration. This section aims to introduce some of the most common techniques used in measurement of aerosols and the underlying theory. These are split into categories of *particle counting* and particle size classification through *electrostatic* and *inertial* methods. In addition to this, other techniques such as optical sizing exist, but these will not be covered within this thesis.

There is currently no feasible way to measure the *absolute* size of a nanoparticle in air, especially not for highly time-resolved (down to one-second resolution in many cases) measurements. This, together with the fact that the particle size and shape are often complex, makes a complete description of the particle hard to obtain and impractical to use in aerosol measurements. The size measurements are rather based on observation of a particle property which can be linked to an *equivalent diameter* of particle. This means that when a particle is measured by a technique, it reports the size of a spherical particle that has the same value for a specific physical property on which the particle is measured. Some common observations and their links to equivalent diameters are shown in **Figure 5.1**. Only in the cases of the ideal spherical particle will the equivalent diameters be equal, and in cases of complex particle shape and chemical composition, they can vary strongly from each other.

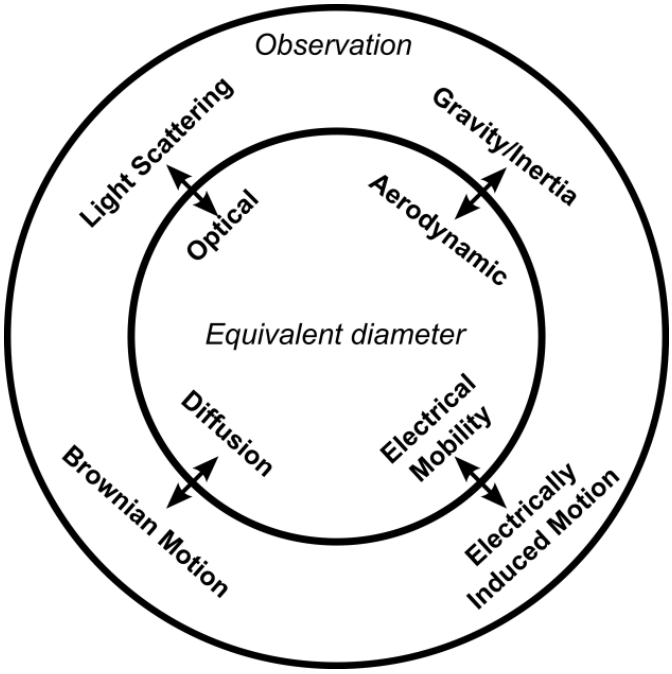

Figure 5.1 Particle observations that depend on particle properties or behavior.

5.1 Particle counting

The most common technique for counting particle number concentration is through light scattering of the particles. A continuous light source, such as a laser beam, is introduced into the pathway of the aerosol. As a particle crosses the beam, light will be scattered and can then be detected by a photo-detector. In the simplest case, a single pulse on the detector corresponds to one particle. The advantage of such detection is that it is non-intrusive and the aerosol flow can continue for further analysis. It can also be further evolved to give more information about the particle. The main disadvantage of the method is that particles with smaller size than the wavelength of the light source become increasingly hard to detect. As smaller particles scatter less light, the signal from the light scattered by the particles becomes increasingly hard to separate from the scattered light from gas molecules and therefore this technique of particle detection is generally limited to particles larger than 200 nm (Kulkarni et al. 2011).

There are, however, work-around techniques to use light scattering to detect particles smaller than 200 nm, normally through condensational growth of the particle up to a size range were its light scattering is sufficient for detection. This technique is the working principle of the commonly used Condensation Particle Counter (CPC), of which there are three main varieties. In the *Expansion-type* CPC (Aitken 1888; Rich 1955; Pollak and Metnieks 1958; Rich 1961; Skala 1963; Hogan and Gardner 1968), a volume containing the aerosol is saturated with a working fluid, commonly water, and then adiabatically expanded. As the expansion cools the air, it becomes supersaturated with water, which then condenses onto the particle and increases their size. An early disadvantage of this method was that as the particle growth and counting is completed, a new air-volume is sampled and initial conditions are regained, meaning that the instrument works in a non-continuous, cyclic fashion. Skala (1963), however, developed an Expansion-type CPC with rotary valves to control expansion cycles, allowing up to 5 cycles per second. The second type, the *Mixing-type* CPC (Fuchs and Sutugin 1965; Kousaka et al. 1982; Okuyama et al. 1984; Kousaka et al. 1992; Gamero-Castano and de la Mora 2000; Sgro and de la Mora 2004; Vanhanen et al. 2011) uses a cool (room temperature) aerosol flow saturated with the working fluid which is mixed rapidly and turbulently with a warm air saturated with the same fluid. The resulting vapor becomes supersaturated and condenses onto the particles at a steady-state continuous flow. A wide range of working fluids, ranging from water to organics such as dibutyl phthalate or dioctyl sebacate, can be used in the Mixing-type CPC. The third type of technique used is the *Laminar flow-type* CPC, sometimes also called Continuous flow CPC, (Sinclair and Hoopes 1975; Bricard et al. 1976; Agarwal and Sem 1980; Ahn and Liu 1990; Zhang and Liu 1990; Stolzenburg and Mcmurry 1991) in which a continuous laminar aerosol flow is saturated with a vapor, often n-butyl alcohol, in a heated saturator. The saturated aerosol flows into a condenser, which is kept at a lower temperature so that the aerosol is cooled due to convective heat transfer; the alcohol becomes supersaturated and condenses onto the particles (**Figure 5.2**). Hering et al. (2005) developed a modified version of the laminar-flow CPC by which the working fluid was replaced with water and the condenser tube was kept at a higher temperature than the saturator. This was made possible due to the high diffusivity of water vapor compared to the thermal diffusivity of air, which means that the water diffuses from the warm walls of the condenser tube into the center, where it becomes supersaturated and condenses onto the particles.

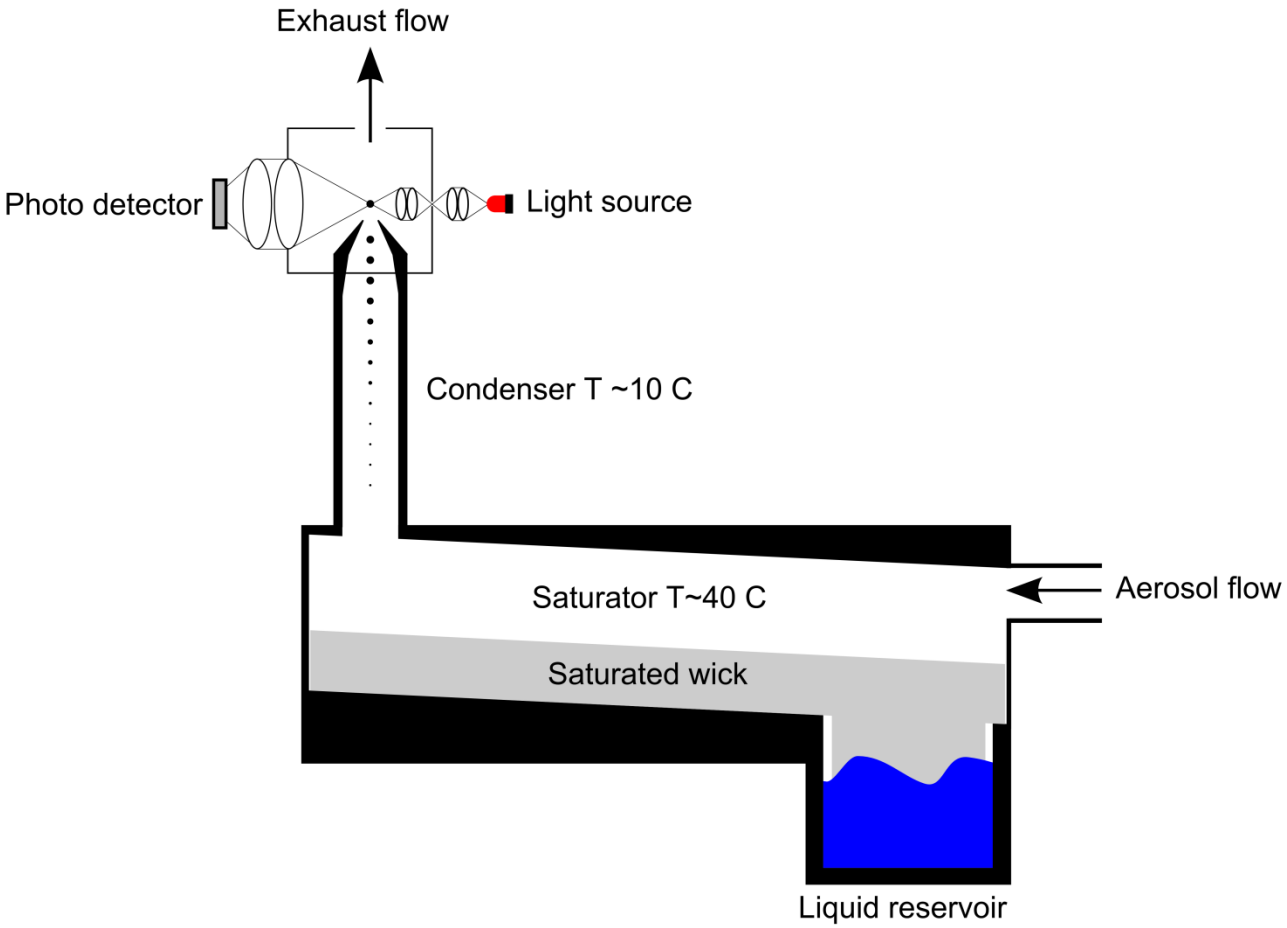

Figure 5.2 Laminar flow type CPC with alcohol working fluid.

5.2 Electrical classification

All aerosol particles are to some extent susceptible to acquiring a non-zero charge state during their generation by various charging mechanisms depending on the nature of the emission (Kulkarni et al. 2011). After this, a particle that carries n_e elementary charges, e, can only change its charge, positively or negatively, by attachment of gas ions of respective polarity (Flagan 2008). A particle's charge state can therefore be seen as a function of its initial state after emission combined with its exposure to gas ions during its lifetime. If a particle with a non-zero charge state is placed in an electrical field of known strength, it will migrate due to electromagnetic forces at a velocity determined by the field strength and particle size, shape and charge as well as

properties of the carrier gas (Davies 1945; Kulkarni et al. 2011). As a result of this, the particle size can be determined if the other factors are known or assumed, as the force, *F*, applied onto the particle in the electrical field with strength *E* will be:

$$\boldsymbol{F} = n_e e \boldsymbol{E} \qquad \textbf{(Equation 5.1)}$$

For time-frames that are sufficiently longer than the aerodynamic relaxation time, the particle will migrate at a steady-state velocity, v_e, of:

$$\boldsymbol{v}_e = Z_p \boldsymbol{E} \qquad \textbf{(Equation 5.2)}$$

where Z_p is the electrical mobility of the particle. For a spherical particle of size d_p , in the Stokes' regime where the Reynold's number is low ($Re < 1$), Z_p is given by:

$$Z_p = \frac{n_e e C_C}{3\pi\eta d_p} \qquad \textbf{(Equation 5.3)}$$

where η is the carrier gas viscosity and C_C is the Cunningham slip correction factor (Cunningham 1910) that corrects for the effect of non-continuous behavior of the carrier gas as the particle size becomes comparable or smaller than the mean free path of the gas, λ. The correction factor is given by:

$$C_C = 1 + \frac{2\lambda}{d_p}\left(\alpha + \beta e^{-\frac{\gamma d_p}{2\lambda}}\right) \qquad \textbf{(Equation 5.4)}$$

where α, β and γ are empirically determined coefficients; α=1.142, β=0.558 and γ=0.999 (Allen and Raabe 1985).

There are several methods for employing electrical mobility to determine particle size, using different techniques and geometries. However, they all share the need to measure on a well-known charging state of the particles to link their electrical mobility with particle size. The techniques of achieving this well-known charge state can be divided into two main categories; 1) *bipolar charging,* where the particles are given a well-known distribution of charges while the aerosol system maintains a net charge of zero and 2) *unipolar charging*, were the entire aerosol system is charged with the same polarity to a predictable level. Further details of these two techniques follows below.

5.2.1 Bipolar diffusion charging techniques

Bipolar charging, often referred to as *aerosol neutralizing*, is a process where the aerosol is introduced to a gaseous environment containing a high level of positive and negative ions. In this environment the charge state of a particle may increase by the attachment on an ion of the same polarity or decrease by attachment of an ion of the opposite polarity. The driving mechanism of attachment is random thermal motion of both ions and particles that leads to collisions between the two. The theory of particle diffusion charging is described in Fuchs' limited sphere theory (Fuchs 1963) together with corrections by Hoppel and Frick (1986). If the balance between ion polarities in the charging environment is initially balanced, the charge state of the aerosol will asymptotically reach a quasi-steady state given enough time. The balance in the steady state is, however, not truly neutral due to different diffusivities and mobilities of positive and negative ions, and a slight negative net charge can be observed after bipolar charging (Flagan 1998). Wiedensohler et al. (1988) described an expression for the fraction of particles, *f(n)*, in the size range of 1-1000 nm carrying *n* charges in this condition as:

$$f(n) = 10^{\sum_{i=0}^{i=5} a_i(n) \log(d_p)^i} \qquad \textbf{(Equation 5.5)}$$

where $a_i(n)$ is an empirically fitted function to Fuchs' theory. **Figure 5.3** shows fractions of particles in the five lowest charging states as a function of particle size. Noticeable here is that the charged fraction of particles at the ultrafine end is small, meaning that only a small portion of these particles can actually be analyzed with electrical methods and that high particle concentrations are needed for good statistics. Furthermore, as the particle size increases to 100 nm and above, the probability of multiple charges increases. This multiple charging means that several particle sizes will have the same mobility as described in **Equation 5.3**, which complicates data analysis of electrical-mobility-based instruments.

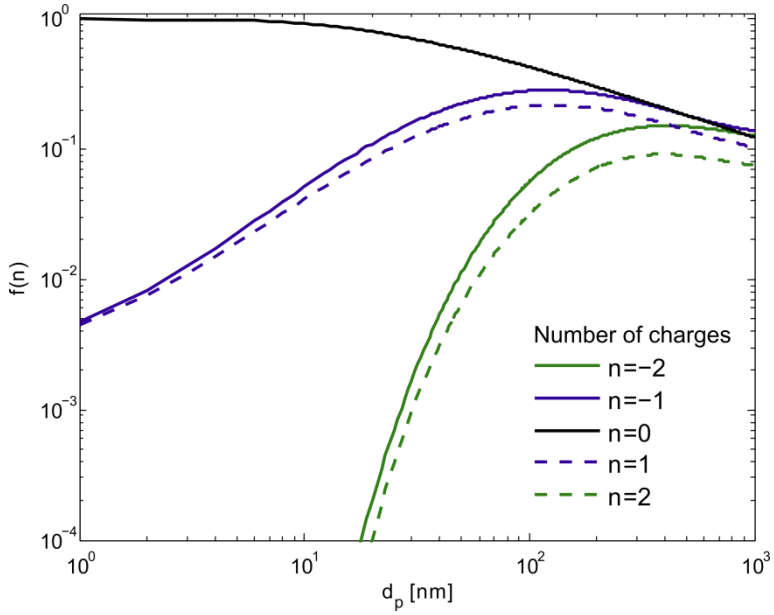

Figure 5.3 Fraction of particles carrying charge *n* as a function of particle size, calculated from Wiedensohler et al. (1988).

The traditionally most common mean of producing a high concentration of ions is by exposure of the carrier gas to ionization radiation from a radioactive source (Cooper and Reist 1973). While this may be considered sufficient for some cases, the radioactive source can create problems in terms of health and safety as well as transportation restrictions. It is therefore often not the desired option. Efforts to replace it using photo-electric charging processes have had limited results (Burtscher et al. 1982; Jung et al. 1988; Li and Chen 2011). The most common alternative to the radioactive bipolar charging is the use of soft X-ray with photon energies of up to 10 KeV. This technique has the capability of producing high ion concentrations while being easily shielded, leading to an increased use in nanoparticle charging (Shimada et al. 2002; Kulkarni et al. 2002; Han et al. 2003; Lee et al. 2005; Yun et al. 2009; Modesto-Lopez et al. 2011).

The most common instrument for particle sizing is one using the well-known characteristics of bipolar charged particles, namely the Differential Mobility Analyzer (DMA). It should be noted that the DMA is not a stand-alone instrument but rather a size classifier or separator, commonly used in series with a detector of some sort. The DMA uses a well-defined electric field to measure how fast a particle migrates, which in turn can be linked to its electrical mobility, **Equation 5.2**. The

DMA method was first described in detail by Hewitt (1957) and then further developed by Knutson and Whitby (1975). The basic design of a DMA consists of two electrodes with a flow channel in-between them. The aerosol flow is introduced near one of the electrodes and a larger sheath flow passes through the remainder of the gap between the electrodes. An applied voltage difference between the two electrodes creates an electrical force on the charged particles perpendicular to the combined aerosol and sheath flow. Particles of the correct polarity will move in trajectory towards the opposing electrode. Downstream, on the opposing electrode, a small exit flow is extracted from the main flow, **Figure 5.4**. This flow will only carry particles of a specific narrow range of mobilities, depending on the DMA geometry, flows and applied voltage.

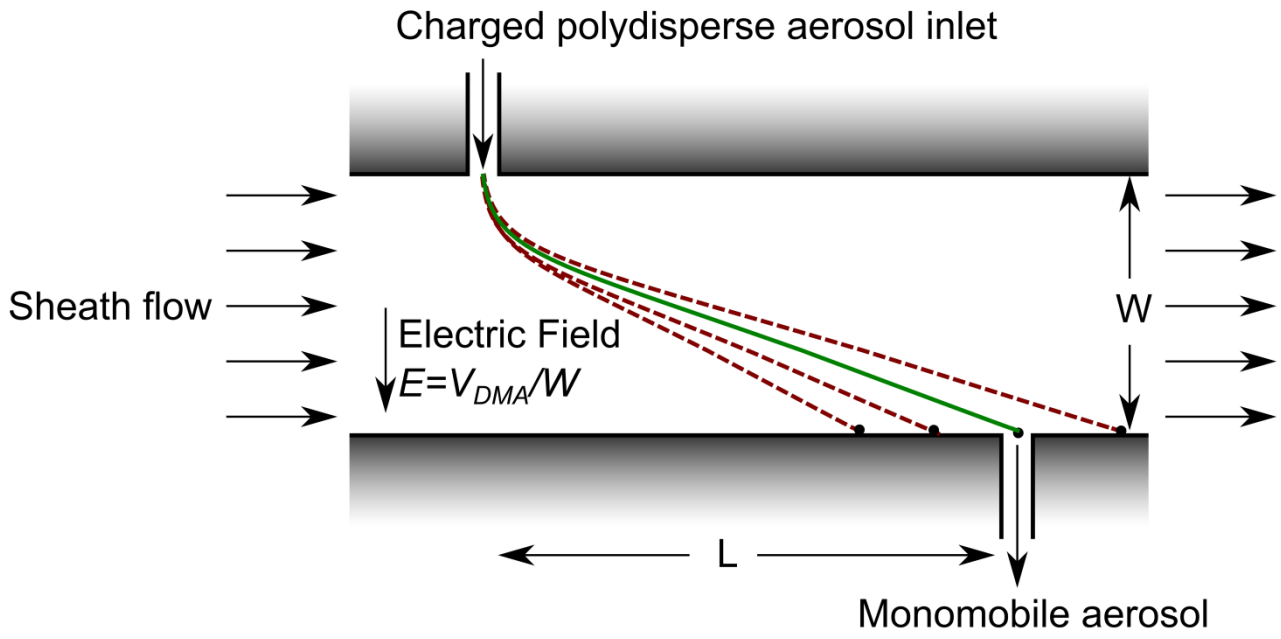

Figure 5.4. Schematic figure of a DMA with trajectories of four particles with different electrical mobility.

While several different geometries of DMAs exist, the most commonly used is the cylindrical DMA in which the two electrodes are concentric cylinders (Knutson and Whitby 1975; Winklmayr et al.

1991; RosellLlompart et al. 1996; Chen et al. 1998; Heim et al. 2004). In a cylindrical DMA, the particles passing through the exit slit will have a nominal mobility, *Z**, according to (Flagan 2008):

$$Z^* = \frac{Q_s \ln(R_2/R_1)}{2\pi V L} \qquad \textbf{Equation 5.6}$$

where Q_s is the sheath air flow, R_1 and R_2 is the inner and outer cylinder radius, V is the potential difference between the two cylinders and L is the cylinder length as shown in **Figure 5.4**.

Other geometrical designs include radial DMAs with radial flows in-between two disc electrodes (Zhang et al. 1995; Fissan et al. 1996) and rectangular channel DMAs (Kulkarni and Wang 2006; Zhang and Wexler 2006).

While an ideal mobility classifier would be able to classify and select only particles of a single nominal mobility, in practice the penetrating particles in the DMA will also have a certain probability of containing particles with mobilities of slightly higher and lower values, determined by the so-called *transfer-function*. The kinematic limit transfer function will have a triangular distribution around the nominal moblility with a width determined by relations between the aerosol flow, sheath flow and the classified flow. This transfer function can, however, only be approached in an ideal DMA at very high voltages, as there will always be an effect from Brownian diffusion of the particles between the electrodes.

Since the DMA is only a particle classifier and not a counter, it needs to be coupled with a detector. The most common option is a CPC, described in **Section 5.1**, due to its high counting efficiency. The second option is an electrometer, which can be useful for very high number concentrations of particles. Since the electrometer detection is based on a fundamental property of the aerosol, charge, it is often used with spherical test particles for calibration of other types of detectors, such as the CPC.

By using a DMA coupled with a CPC and making measurements at varying voltages that span the range of the DMA, a *differential* measurement of number concentrations in mobility bins is achieved. The simplest setup where this is done is known as the Differential Mobility Particle Sizer (DMPS). While this method is simple enough in its inversion of measured data to particle size distributions, the physical size of the instrument and flow rates used means that most of the time

spent during a measurement is spent waiting for a steady-state to be achieved at a selected voltage. To decrease the time-resolution with which a particle size distribution could be measured, Wang and Flagan (1990) constructed a system where the voltage is scanned and particles are counted continuously. This is known as the Scanning Mobility Particle Sizer (SMPS).

5.2.2 Unipolar diffusion charging techniques

For unipolar charging of particles, Fuchs' limited sphere theory (Fuchs 1963) is widely accepted for spherical particles larger than 50 nm in diameter, based on experimental data (Adachi et al. 1985; Pui et al. 1988; Romay and Pui 1992; Biskos et al. 2005; Qi et al. 2007). For particles smaller than 50 nm, Filippov (1993) compared Fuchs' theory with Monte Carlo simulations and found agreement down to 30 nm. Adachi et al. (1985) also supports the use of Fuchs' theory for particles smaller than 50 nm. For smaller particles, the image force between the particle and the ions is not negligible and has an increasingly larger impact. Keller et al (2001) calculated that the image force is no longer negligible as particle size goes below 30 nm, while Rogak and Flagan (1992) estimated this level to be 40 nm.

In unipolar diffusion charging, the aerosol is introduced into a volume with a high concentration of gaseous ions of a specific charge, which are captured by the particles through the high diffusion coefficient of the ions. After passing through the charger volume, an average charge per particle, $\bar{q}$, has been imposed onto the particles. The average charge depends on the particle diameter, d_p, the ion concentration within the charger volume, N_i, and the particle residence time within the charger volume, t. The latter two relate to charging conditions and are properties of the charger design; they are often described as the so-called $N_i t$-product. Pui et al. (1988) showed that the charged fraction of particles depends on the $N_i t$-product, the particle size and the ion-particle combination coefficient. For a specific $N_i t$-product and within a specific particle size range, the average charge per particle can be related to the particle diameter through a power law such as (Fierz et al. 2002; Jung and Kittelson 2005):

$$\bar{q} \propto d_p^x \qquad \textbf{(Equation 5.7)}$$

Besides the three parameters described above, unipolar charging may be influenced by several other factors such as particle morphology, ion properties, particle dielectric constant, gas pressure, humidity and temperature (Kulkarni et al. 2011). **Figure 5.5** shows the average number of charges per particle for unipolar charging in environments with three different $N_i t$-products. Fitted values are according to **Equation 5.7**.

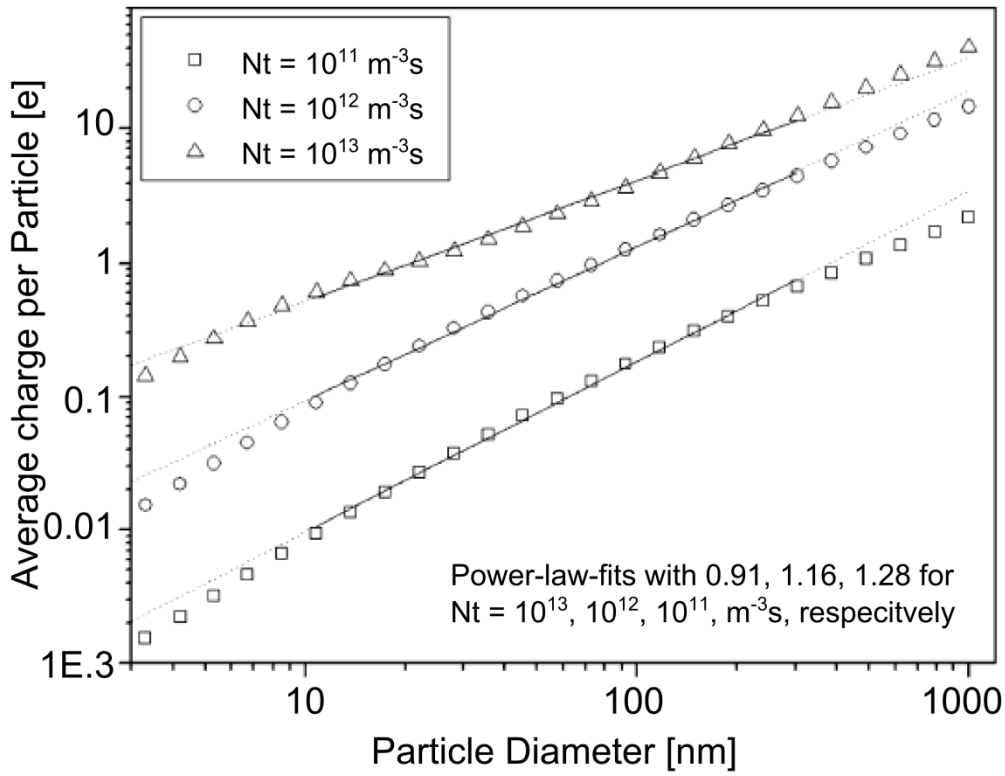

Figure 5.5. Charging levels and power-law fits for particles in conditions with three different $N_i t$-products. Adapted from Kulkarni (2011).

The advantage in the use of unipolar charging as opposed to bipolar charging is that it provides a higher charging state of the particles. This increases the measured signal per particle for electrometer type detectors and therefore also lowers the concentration detection limit. However, having a higher charging state of the aerosol also infers a broader charge distribution for each particle size, which complicates the correction for multiple charges per particle in the conversion from measured signal to other particle characteristics (Hoppel 1978). It is therefore important to properly determine such charger characteristics well. Other techniques besides pure

diffusion charging for achieving a known unipolar charge state of particles exist, often strong external electric fields to increase the particle-ion-interaction. Schematic overviews of three common types of unipolar chargers can be seen in **Figure 5.6**. The direct corona charger (**a**) is the simplest type of charger. It exposes the aerosol to a strong electric field during charging, with the downside of it causing particle losses. The indirect corona charger (**b**), uses a grounded grid to shield the electric field from the aerosol, reducing particle losses. The turbulent jet charger (**c**) produces its ions separately from the particles, and then mixes them. This means that practically no electric field is affecting the particles, but instead the secondary flow needed for the charger dilutes the aerosol. All three charger types are normally followed by an ion-trap to remove unattached ions.

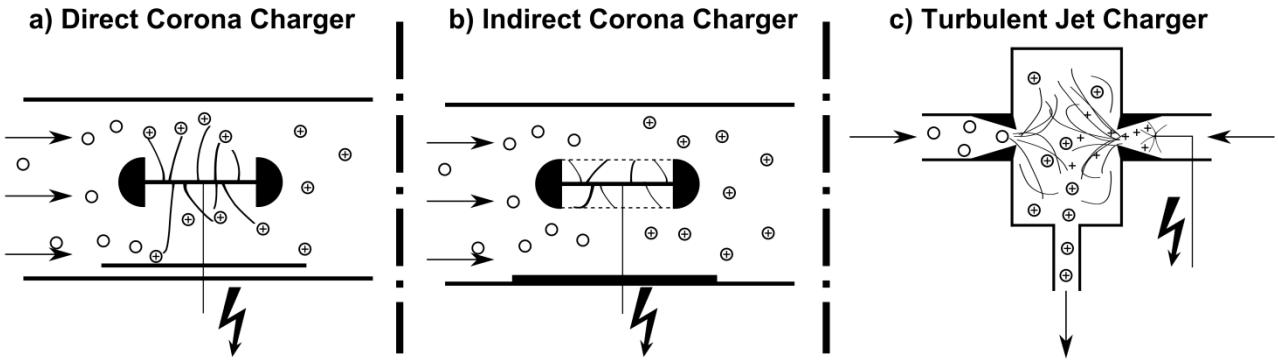

Figure 5.6. Schematic overview of three common types of unipolar chargers.

Several techniques using unipolar charging of particles are available in commercial instruments which measures particles' size distribution, number concentration, and LDSA concentration. The simplest measurement technique taking advantage of the use of unipolar charging is the Diffusion Charging Sensor (DCS, Jung and Kittelson 2005). In this type of instrument, the aerosol is charged through a unipolar diffusion charger, it passes through an ion trap to remove excess ions not attached to particles and is measured through a Faraday cage electrometer. The measured signal from the detector is thus integrated over all particle sizes and is proportional to both the particle number concentration and particle size. In essence the basic DCS technique is a simple way of measuring aerosol concentrations in real-time, without using radio-active material or working fluids. Commercial versions of the DCS exist in the form of the LQ1-DC (Matter engineering,

Germany, AG 2001) and the Electrical Aerosol Detector (EAD 3070A, TSI Inc., MN, USA, Medved et al. 2000). Even though the DCS measures electrical current, the results are often given in the form of 'total aerosol length', given as mm/cm^3, since the instrument response has a size-dependent response of approximately $\propto d_p^1$. Another metric that can be measured using the DCS technique is LDSA concentration, both in the form of alveolar deposited fraction (A) and tracheobronchial deposited fraction (TB). The reason for this is that in the ICRP lung deposition model (ICRP 1994), the fractions have approximate size-dependency of d_p^{-1} in the region of 20-500 nm (A) and 20-200 nm (TB), **Figure 4.1b**. Since surface area has an approximate quadratic size dependency, d_p^2 , a measurement with a d_p^1 response, such as the DCS, can be calibrated to measure the product of the surface area and deposition fraction (Fissan et al. 2007; Asbach et al. 2009). This method is the working principle of the Nanoparticle Surface Area Monitor (NSAM 3550, TSI Inc., MN, USA, (Fissan et al. 2007; Shin et al. 2007) which uses an opposed flow diffusion charger (Medved et al. 2000; Kaminski et al. 2012) and an adjustable ion trap to regulate the size-dependent response to measure LDSA concentration.

Another technique employing unipolar charging of particles is the Electrical-sensing Mobility Spectrometer (EMS), which shares many aspects with the DMA described in **Section 5.2.1**, in that the charged particles, alongside a sheath flow, are introduced to an electric field in-between two concentric cylinders and their resulting migrating velocity across the cylinder gap is used to determine their electrical mobility. Unlike the DMA, where a narrow range of mobility is selected through a gap in the outer cylinder, these techniques have a series of electrometers mounted on the outer cylinder, as shown in **Figure 5.7**, which simultaneously measure the current of the particles as they impact onto them. If the charging state of the particles is known, trajectories can be calculated to link electrometer number with particle size and subsequently measure current with particle concentration (Rohmann 1923; Whitby and Clark 1966; Tammet et al. 2002; Johnson et al. 2004).

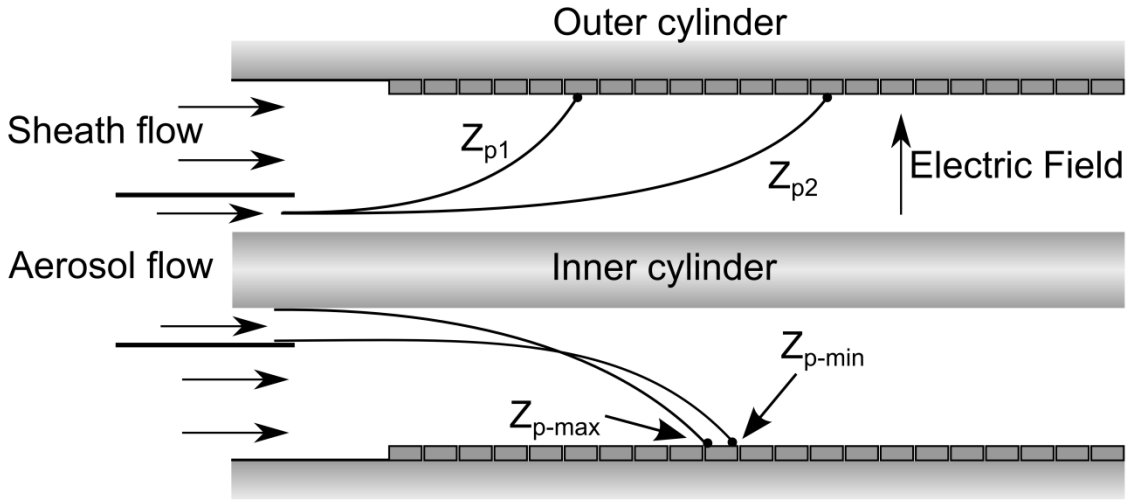

Figure 5.7 Schematic figure of an EMS. Upper half shows the trajectory of two particles with different electrical mobilities ($Z_{p1} > Z_{p2}$). Bottom half shows the upper and lower extremes in the range of mobilities that are detected by the same electrometer.

The advantage of the EMS technique is that it allows for much faster mobility distribution measurement, having time-resolutions down to less than a second. Disadvantages of the EMS technique include a higher limit of detection, due to the use of electrometer detection as compared to the commonly used CPC in a SMPS system. The detection limit of the EMS therefore becomes dependent on the particle charge, which in turn varies with particle size, **Equation 5.7**, with small particles having a higher limit of detection than larger particles. Since increasing particle size also broadens the charge distribution, the response from a specific electrometer will correspond to several mobility-equivalent combinations of particle size and charge. This in turn sets an upper size limit of the instrument, typically at 500-1000 nm. Commercial instruments of this type include the Fast Mobility Particle Sizer (FMPS model 3091, TSI Inc. Shoreview, MN, USA, TSI 2006), the Engine Exhaust Particle Sizer (EEPS model 3090, TSI Inc. Shoreview, MN, USA, Johnson et al. 2004), the Electrical Aerosol Spectrometer, (EAS, Tammet et al. 2002) and the Differential Mobility Spectrometer (DMS 500, Cambustion, UK, Reavell et al. 2002; Biskos et al. 2005).

An instrument of special concern in this thesis work is the FMPS, which uses dual unipolar diffusion chargers to charge the sampled particles. The particles first pass a negative corona diffusion charger to minimize the probability of highly positively charged particles, and then a positive corona diffusion charger to charge the particles positively to a known level. The particles are thereafter separated in an electric field according to their electrical mobility and detected by 22 electrometers positioned in a vertical column, **Figure 5.8**. The acceleration voltage between the inner and outer cylinder is varied in three steps along the column to enable a larger measurement range and minimize instrument size. The measured currents are then corrected for multiple charges and image charges and are then inverted from the 22 measured currents into 32 size channels ranging from 5.6 to 560 nm in electric mobility equivalent diameter. Since the output contains more size channels than actual measurements, some assumptions must be made in the data inversion algorithm, although these have not been disclosed by the manufacturer. The FMPS measures particle size distributions with a one-second time resolution. Intake sampling for the FMPS is done at 10 l/min through a pre-separating cyclone with a 50% cut-off at 1 µm ($PM_{1.0}$).

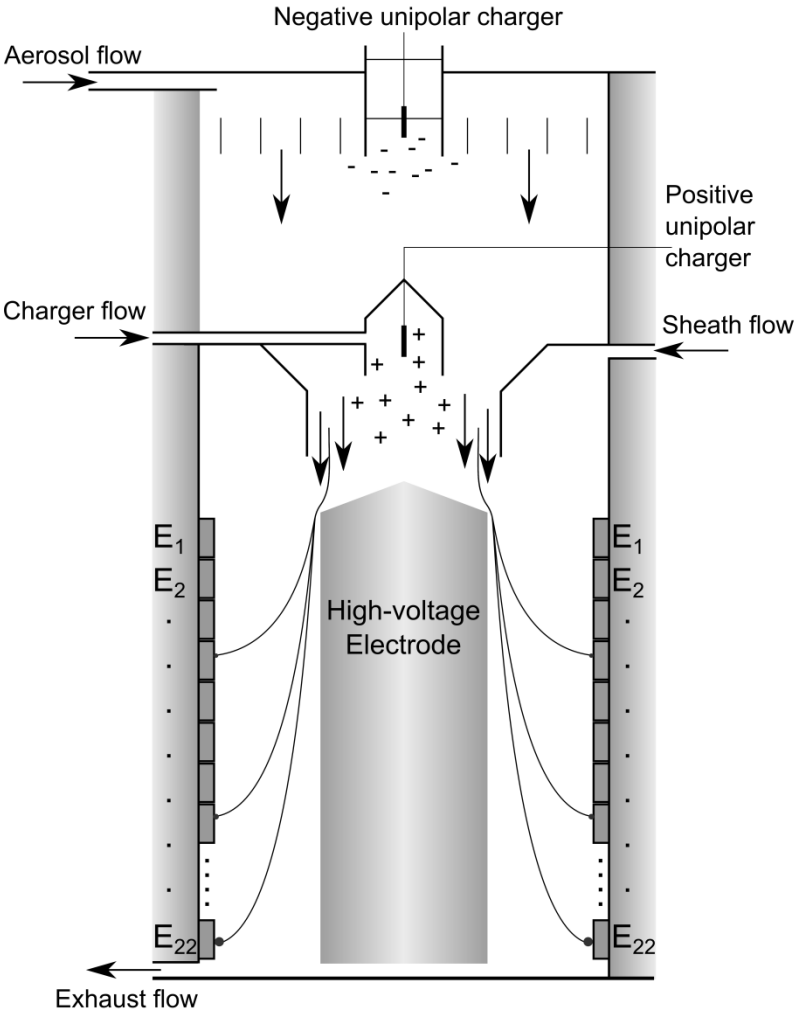

Figure 5.8 Schematic overview of the FMPS including trajectories of particles impacting on electrometers.

A similar instrument to the FMPS is the EEPS, which shares most of the design of the FMPS but measures size distributions at higher time resolutions, and therefore has a higher minimum detection limit in terms of concentration. The DMS500, while based on the same basic technique, has a larger size range extending up to 2.5 µm. This is accomplished by lowering the working pressure of the instrument to 250 mbar. Decreasing the working pressure increases the mean free path, which affects the particle slip (**Equation 5.4**), increases the particle mobility, and allows for size separation according to mobility in a larger size range.

With the need for light, portable instruments for measurement of aerosol characteristics, unipolar diffusion chargers have been developed to meet this demand (Qi et al. 2008; Park et al. 2010). Commercial, portable devices employing the technique of unipolar diffusion charging include NanoCheck (Grimm Aerosoltechnik) and the NanoTracer (Philips Aerasense, Marra et al. 2009), which both use the assumption of unimodal, log-normal size distributions to measure particle number concentration and mean particle size. The DiSCmini (Matter Aerosol, Fierz et al. 2011) measures particle number concentration, mean particle size and LDSA concentration. It uses a compact design, **Figure 5.9**, consisting of a unipolar diffusion charger, an ion trap, a diffusion stage and an electrical filter stage. The sampled aerosol is charged and excess un-attached ions are removed and are introduced to a set of metal screens, the diffusion stage, connected to an electrometer measuring the current from attaching particles. Since smaller particles have a larger Brownian motion, they are more likely to be captured in this stage. Finally the remaining particles are captured in the filter stage, where the resulting current is measured with an electrometer. Due to the size dependency in the first stage, the ratio between the two measured currents can be used with a calibration curve to determine the mean particle size. This particle size can then be used to calculate the number concentration from the combined currents, since the average charge per particle is known. Since the charger has an average charge-diameter dependency of approximately d_p^1, it can also be used to estimate the LDSA concentration, as described previously.

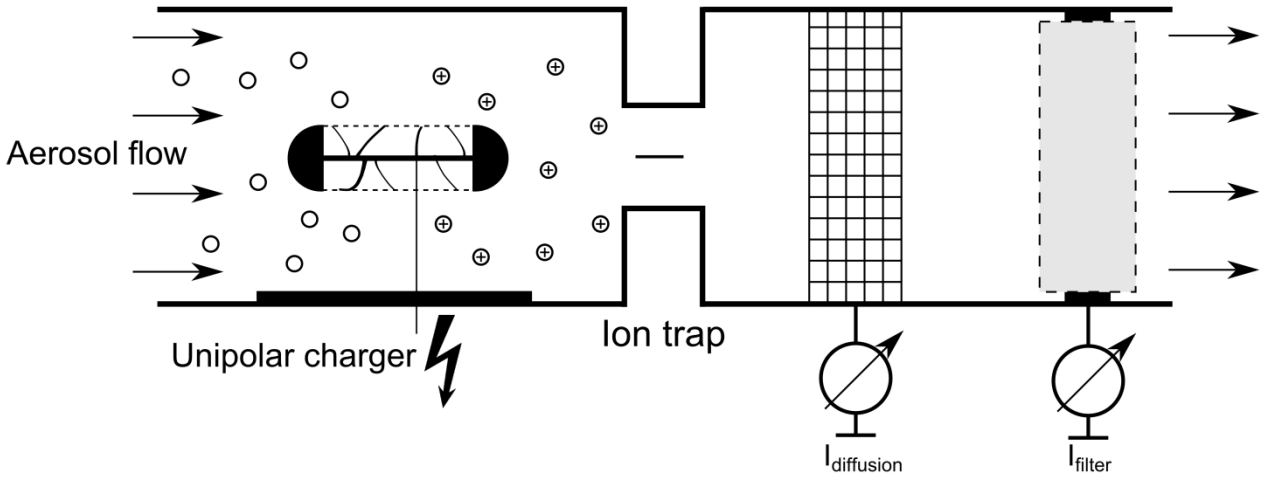

Figure 5.9 Schematic overview of the DiSCmini instrument consisting of a unipolar charger, an ion trap and two measurement stages.

5.3 Inertial classification

Inertial classifiers are a commonly used technique to separate particles based on their aerodynamic properties. The classified particle size using these techniques is the aerodynamic equivalent diameter, defined as the diameter of a spherical particle of unit density that has the same gravitational settling velocity as the particle of interest. The simplest form of inertial classification is through a so-called *body impactor*, which simply consists of a solid body placed in a moving aerosol stream. As the carrier gas is deflected by the body and flows around it, particles with a significantly higher density than the carrier gas will not be deflected as much due to their inertia. If the particle is large enough, it will strike the body. The influencing factors in this simple case are the velocity of the carrier gas, U, the size of the particle, d_p, the particle density, ρ_p, and the size of the body, d_b. The relationship as to whether the particle will strike the object is defined as the ratio of the particle's stopping distance to the physical dimensions of the object. This property is denoted as the Stokes' number, *Stk*, and defined as:

$$Stk = \frac{\rho_p C_C d_p^2 U}{18 \eta d_b} \qquad \textbf{(Equation 5.8)}$$

If *Stk* is larger than unity, the particle is likely to impact onto the object. The Stokes' number can be seen to be important not just in this simple case, but in all types of inertial collectors. A more commonly used type of inertial collector is the *conventional impactor*, which consists of one or more nozzles which accelerates the aerosol towards a collection plate (**Figure 5.10**).

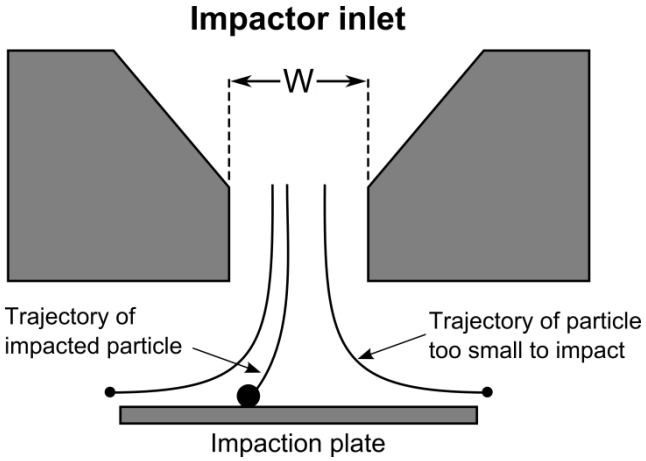

Figure 5.10. Schematic figure of a conventional impactor showing nozzle diameter, *W*, and the trajectories of an impacted and a non-impacted particle.

The Stokes' number for a conventional impactor with a single circular nozzle with diameter *W* is:

$$Stk = \frac{\rho_p C_C d_p^2 U}{9\eta W} \qquad \textbf{(Equation 5.9)}$$

The Stokes' number, or more commonly the square root of it, can be used to predict whether a particle will impact onto a collection plate or will follow the streamlines out of the impaction region. Inertial classifiers are therefore often characterized by the $\sqrt{Stk_{50}}$ value which corresponds to the particle size, where particles are collected at 50% efficiency. If this value is given for a conventional impactor, the corresponding cut-size will be:

$$d_{50} = \sqrt{\frac{9\eta W}{\rho_p C_C U}}\sqrt{Stk_{50}} \qquad \textbf{(Equation 5.10)}$$

Since it is often of interest to obtain a more size-resolved collection and not just a collection of particles larger than a certain size, conventional impactors are often used in series so that the aerosol passes from one impactor stage to next, with a decreasing d_{50} value. This serial setup of impactors is called a *cascade impactor*. To decrease the d_{50} value of each stage, increasingly smaller nozzle diameters are used, but to perform size-separation in the nanometer range, this might not be enough. It is therefore common to decrease the pressure, such as in the *low-pressure*

impactor, which increases the slip correction and allows for smaller d_{50} values (Berner et al. 1979; Hering et al. 1979; Hering and Marple 1986; Hillamo and Kauppinen 1991).

While cascade impactors are often used for time-integrated analysis after the sampling period, such as gravimetrical or microscopical analysis, a new method for time-resolved use of a cascade was developed by Keskinen et al. (1992). In this method, now commercialized as the Electrical Low Pressure Impactor (ELPI+, Dekati, Finland), electrical detection of impacted particles carrying a charge is measured simultaneously over all stages to provide real-time operation. **Figure 5.11** shows the instrument design, which consists of a unipolar corona charger which brings the aerosol particle to a known charge state. The particles are then classified according to their aerodynamic diameter in a multi-jet cascade impactor setup, were the induced current of the impacted particles is registered with electrometers at each stage. The cascade impactor consists of 14 impaction stages followed by a filter collection stage to measure the smallest size bin (Marjamaki et al. 2005).

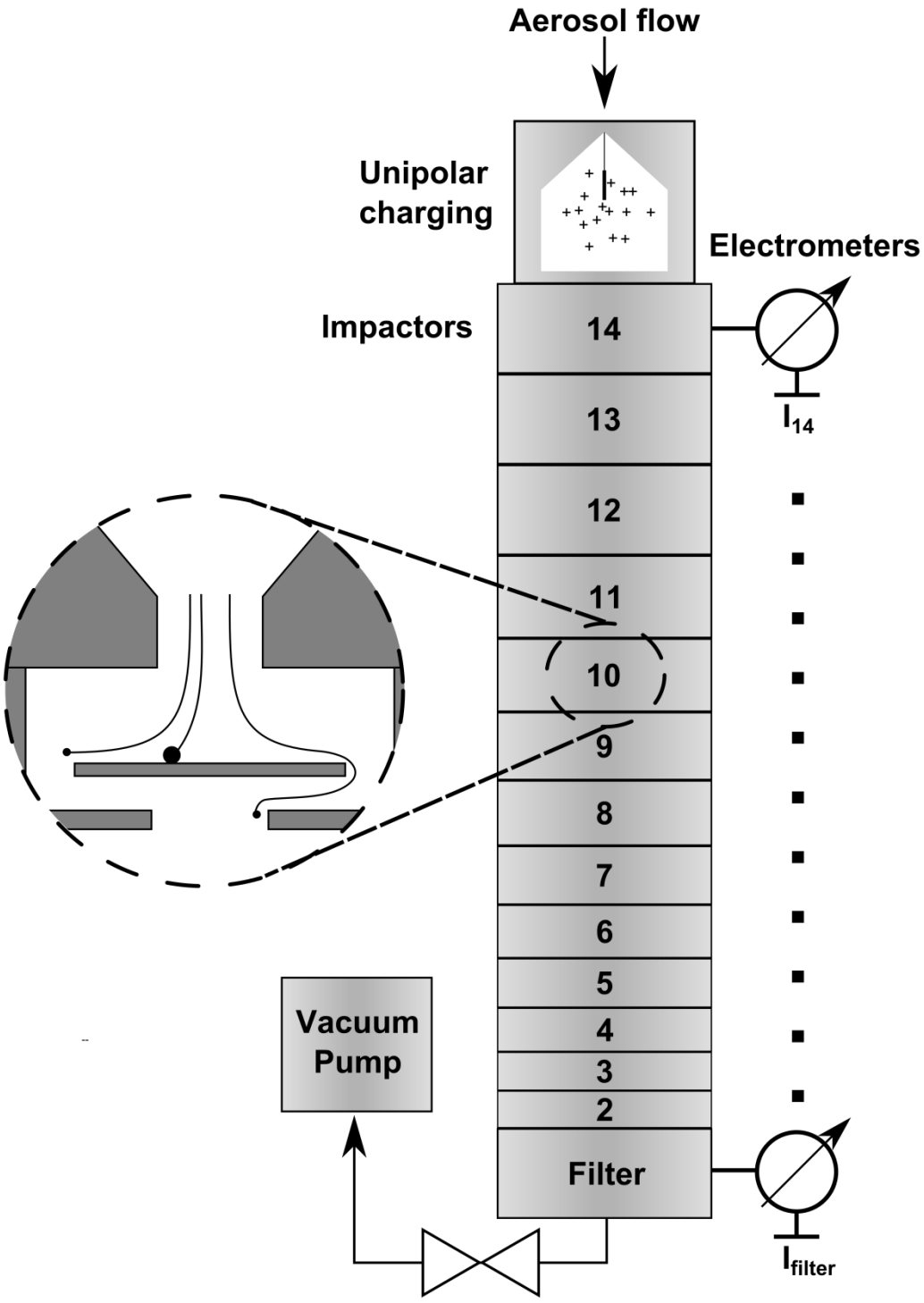

Figure 5.11 Schematic overview of the ELPI with a unipolar charge, 13 impaction stages and one filter stage, all connected to electrometers for measurement of current.

Another technique which uses the particle inertia to measure particle concentrations both size and time-resolved, is the Aerodynamic Particle Size (APS 3321, TSI Inc., MN, USA, (Agarwal et al. 1982). Unlike the previously described inertial techniques, the APS does not bend the gas-flow around a physical object, but rather accelerates it linearly and measures particle properties in a time-of-flight manner. In this instrument, an aerosol flow of 1 l/min is accelerated through two nozzles surrounded by a sheath flow. Directly after the acceleration, the aerosol passes two closely fitted laser beams. Light scattered from passing particles is detected as two pulses per particle by a photomultiplier. Since the aerodynamic and inertial properties of the particle determine to what extent it was able to follow the acceleration of the gas-flow, the time-of-flight between the two lasers can be calibrated against the aerodynamic equivalent size of the particle. The APS can measure aerodynamic particle sizes between 0.5 and 20 µm at a 1 second interval. Due to the risk of coincidence at high particle concentrations, the recommended maximum concentration is 1000 cm^{-3}.

5.4 Particle size & shape

The particles studied during measurements of ENMs in occupational settings are often emitted by processes that yield non-spherical particles, but rather various states of agglomerated and aggregated particles (Brouwer et al. 2009; Schneider and Jensen 2009). In addition to this, the particle shape can be changed due to various processes after the initial emission (Seipenbusch et al. 2008). Many of the techniques described in the previous sections observe a parameter of the particle and define a size for it based on the size of spherical particles that would act the same in its specific conditions. A measurement of a non-spherical particle therefore gives a size which is only fully relevant in conditions equal to those of the measurement principle. For example, DMA classification of agglomerate particles only represents the transportation of the agglomerate particles in electric fields. For all other purposes, the classified size will not be entirely correct. Depending on the type of particle morphology, density, and measurement principle, these effects can often be corrected for and/or neglected.

For electrical classification techniques such as the DMA and FMPS, there are two main effects of particle shape on the measured mobility equivalent diameter. The first effect comes from its effect on the drag force imposed on the particle. Several studies have been conducted on the effect of particle shape on electrical mobility for small clusters of spheres, aggregates/agglomerates and fibers (Schmidt-Ott 1988; Rogak and Flagan 1992; Rogak et al. 1993; Baron et al. 1994; Kousaka et al. 1996). Mobility of the particles was found to scale with the projected area of the particle for compact agglomerates, but for more open-structure agglomerates, it rather scales with total area of the particle. The second effect of particle shape is not a direct effect of the actual measurement technique but rather a change in the pre-conditioning of the charge state of the particle. For bipolar charging, only limited knowledge is available on the charging effect of agglomerate particles (Rogak and Flagan 1992; Maricq 2008; Ku et al. 2011; Xiao et al. 2012). Lall et al. (2008) suggests that, for agglomerates, the Boltzmann distribution can be a good approximation for the fraction of particles that carries *n* charges:

$$f(n)_{agg} = \frac{e}{\sqrt{\pi D_n kT}} exp\left(\frac{-n^2 e^2}{D_n kT}\right) \qquad \textbf{(Equation 5.11)}$$

where *k* is the Boltzmann constant, *T* is temperature and D_n is a charging equivalent diameter, i.e. describing the diameter of a sphere with the same charge as the agglomerate. For unipolar charging, the effects of agglomerates are more profound (Biskos et al. 2004; Gopalakrishnan et al. 2013). Shin et al. (2010) showed that for agglomerate particles, as particle structure becomes looser and particle size becomes larger, the mean number of charges per particle increases as compared to spherical particles of the same mobility diameter. **Figure 5.12** shows their results for both experimental and theoretical determination of mean charge per particle as a function of mobility size.

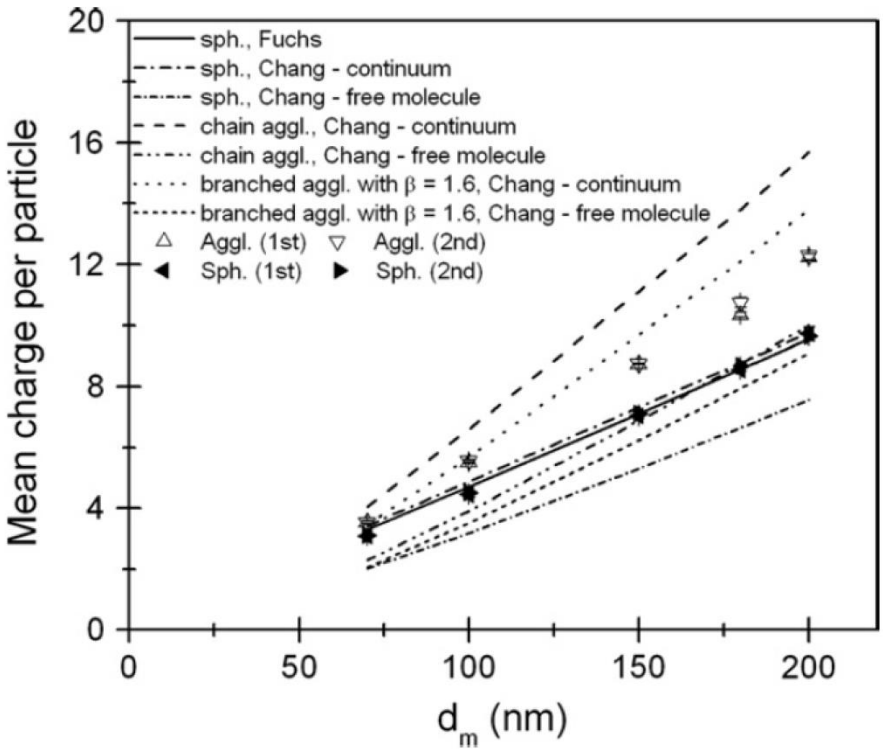

Figure 5.12. Experimental and theoretical determination of mean charge per particle as a function of mobility size. Reprinted with permission from Shin et al. (2010).

An increased mean number of charges per particle as compared to spherical particles will have a strong effect on instruments using the EMS techniques, as it has two effects.

- The first effect is that the force caused by the electric field, **Equation 5.1**, will be increased due to the increased number of charges per particle, n_e, and the trajectory of the particle will thus be steeper. The EMS-based instrument will therefore underestimate the size of such particles.
- The second effect comes from the fact that the particle concentration is measured based on particle charge using electrometers. An increased charge per particle will mean an overestimation of the number concentration.

There will also be a combinatory effect, since the conversion from measured current to number concentration is based on the measured particle size, i.e. the trajectory of the particle in the instrument. Since the size is underestimated, the difference between the expected size-specific

charge for a spherical particle, **Equation 5.7**, and the charge carried by the larger agglomerate will be even greater and the number concentration overestimated further. In other instruments using unipolar charging of particles only as a preconditioning for detection, such as DCS techniques and ELPI, the increased number of charges will not cause such a drastic overestimation in measured concentration, however it will be present.

The effect of particle shape on drag force is also an important effect for inertia-based measurement techniques such as impaction-based instruments (ELPI) and time-of-flight instruments (APS). The Stokes' law for drag force on moving particles is based on the assumption of spherical particles. To account for non-spherical particles, the *dynamic shape factor*, χ, is introduced and defined as:

$$\chi = \frac{F_D}{F_{Dve}} \qquad \textbf{(Equation 5.12)}$$

where F_D is the drag force on the non-spherical particle and F_{Dve} is the drag force on the particle's volume-equivalent sphere when traveling at the same velocity, *v*, as shown in **Figure 5.13**. The dynamic shape factor is therefore defined as 1 for spherical particles and above for all other geometries.

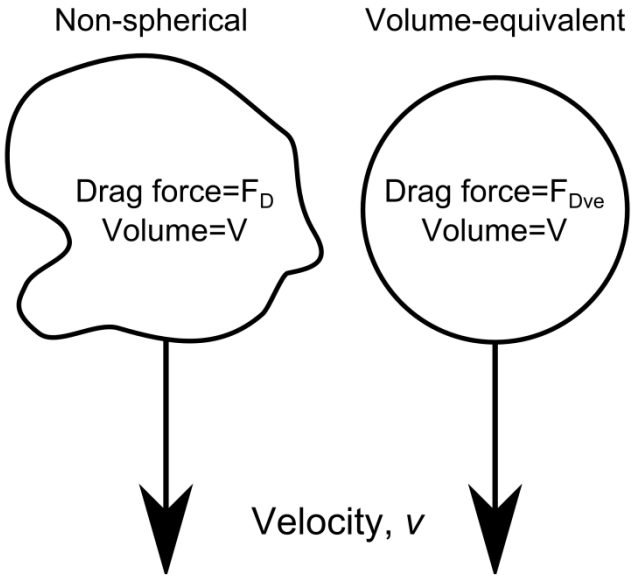

Figure 5.13. Non-spherical particle and its volume-equivalent sphere.

This means that, for inertia-based techniques measuring aerodynamic equivalent size based on the assumption of spherical particles, the aerodynamic size of an agglomerated particle will be overestimated as compared to a volume-equivalent sphere.

6 Summary of included articles

This section covers the results included in the thesis publications regarding exposure modeling (**Paper I**) and how external factors might influence the results (**Paper II**). Thereafter it covers two studies of instrument comparison with focus of the Fast Mobility Particle Size (**Paper III**) and the measurement of particle surface area through different real-time methods (**Paper IV**).

6.1 Dustiness and exposure assessment of pharmaceutical agents - Paper I

In the study described in **Paper I** investigate the feasibility of using dustiness data for simple modeling of exposure scenarios and for selection of the safest to use material from four similar candidates. The small rotating drum was used to determine the gravimetrical respirable dustiness of four pharmaceutical agents that were candidates for production. The aerosol generated by the small rotating drum was also used to assess penetration of realistic powder dust particles through damaged industrial-grade ventilation duct HEPA-filters.

In order to assess the potential exposure caused by handling the pharmaceutical powders, numerical solutions were calculated for a simple NF/FF mass-balance model for a realistic working scenario (further details in **Paper I**) using:

$$V_{NF}\frac{\mathrm{d}C_{NF}}{\mathrm{d}t} = \varepsilon_i - C_{NF}\cdot Q_{NF} + C_{FF}\cdot Q_{NF} \qquad \textbf{(Equation 6.1)}$$

$$V_{FF}\frac{\mathrm{d}C_{FF}}{\mathrm{d}t} = C_{NF}\cdot Q_{NF} - C_{FF}\cdot Q_{NF} - C_{FF}\cdot Q_{FF} \qquad \textbf{(Equation 6.2)}$$

In Equations 6.1 and 6.2, C is the concentration and *Q* is the flow in and out of the respective NF and FF volumes, *V*, and ε_i is the mass emission rate. This rate is based on a measured dustiness index coupled with a scaling factor, *h*, to take into account the type of powder handling performed in the specific scenario. The results of this assessment are shown in **Figure 6.1**.

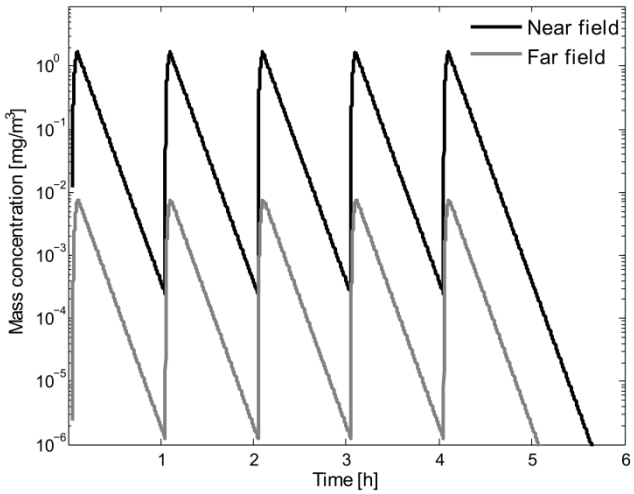

Figure 6.1. Modeled mass concentrations for near-field and far-field during a work day with a realistic working scenario, using equations from the ART exposure model.

The study demonstrated the use of dustiness data in mass-balance modeling for simple and fast assessment of exposure potential based on a specific material dustiness. Measured data, see **Paper I** for more details, and modeled scenarios were used to prioritize the most suitable pharmaceutical candidate based on exposure potential, dustiness kinetics and size measurements. While all four materials were candidates for the same product, the risk of worker exposure varied strongly (up to 10 times) between them. The study also looked into the Particle Generation Rate (PGR) of the materials during dustiness testing. It showed that while three of the powders were aerosolized at a fairly constant rate, one of them stood out with a high initial rate of emission and quick decrease in emission potential, **Figure 6.2.**

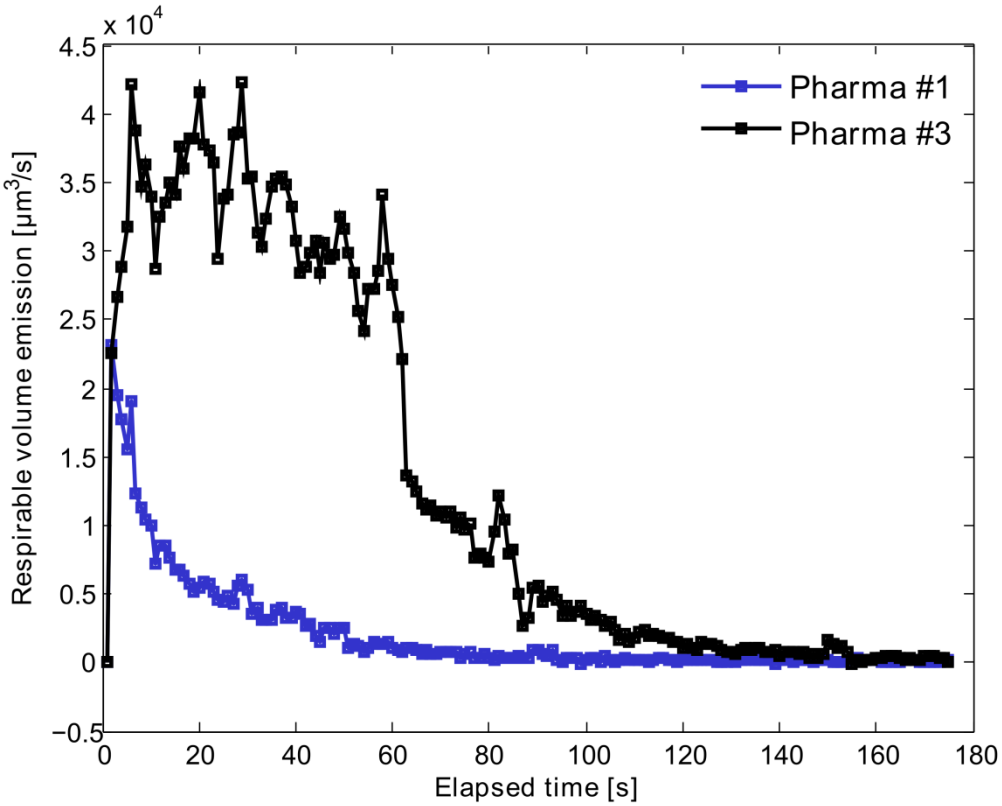

Figure 6.2 Respirable volumetric particle generation rate during rotating-drum testing of two pharmaceutical powders.

In the testing of particle penetration through three degrees of damaged HEPA filters, the highest particle-number penetration ratios were found for 70–80 nm size particles and reached 1 between the two highest damage levels. The penetration ratio for 300–560 nm sized particles reached 0.01 to 0.03 at the two highest damage levels, but would be most significant by weight.

6.2 Changes in dustiness due to external conditions - Paper II

The study covered in **Paper II** focuses on the effects of various storage conditions on powder dustiness and how these may influence, and add uncertainty to, exposure modeling. Gravimetrical

respirable dustiness was determined for five different metal oxides at three different humidities (30, 50 and 70%RH), with and without uniaxial loading.

The results showed a general trend of increasing dustiness index with decreased humidity (**Figure 6.3**). The most severe effect was seen for TiO_2, where the dustiness index increased 439 times when the humidity was changed from 50 to 30%RH. The effect of uniaxial loading was less clear, but generally it decreased the dustiness index.

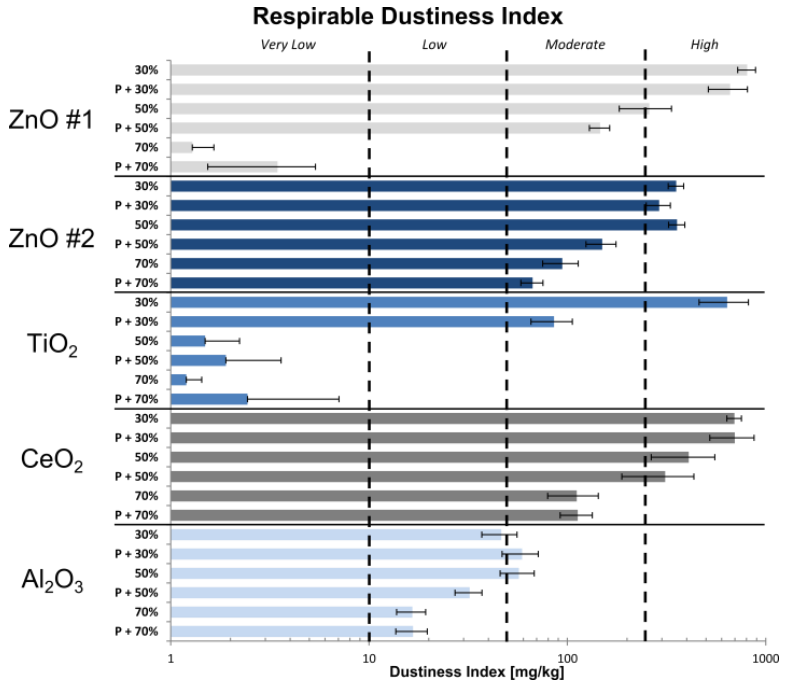

Figure 6.3. Dustiness indices of five different nanomaterials tested in six different conditions.

Tests of water uptake of the powders after seven days of incubation in the respective humidity conditions showed a very high uptake of water for the TiO_2 as compared to the other materials. This, in addition to the HNO_3 stabilization of the TiO_2 that may be lost at 30%RH, is something that may well explain the more drastic change in dustiness index for the material.

Tests done in the study on the effect of dustiness changes on the control-banding model NanoSafer produced, using the normal EN:15051 standard of 50%RH test for TiO_2 and a realistic working scenario (details in **Paper II**), the lowest level of exposure ranking. If the 30%RH conditions were assumed instead, and the powder had been stored at these conditions with the

resulting increase in dustiness index, then the correct ranking, based on NanoSafer, would instead be the highest possible level of exposure. The study showed the importance of relative humidity and the need to consider storage and humidity under use-conditions in future, both for minimization of potential exposure and for accurate exposure modeling.

6.3 Comparability of instruments for controlled test particles - Paper III

This study focused on the performance of the Fast Mobility Particle Sizer (FMPS) and its ability to correctly size and count spherical quasi-monodisperse aerosols. The FMPS is a fairly commonly used instrument in exposure measurements due to its high time resolution, but its measurement reliability has previously not been determined. In the study, 39 different size distributions of Di-Ethyl-Hexyl-Sebacat (DEHS) particles were measured on with the FMPS, SMPS and ELPI. The resulting fitted Geometric Mean Diameters (GMD) for each instrument are shown in **Figure 6.4**.

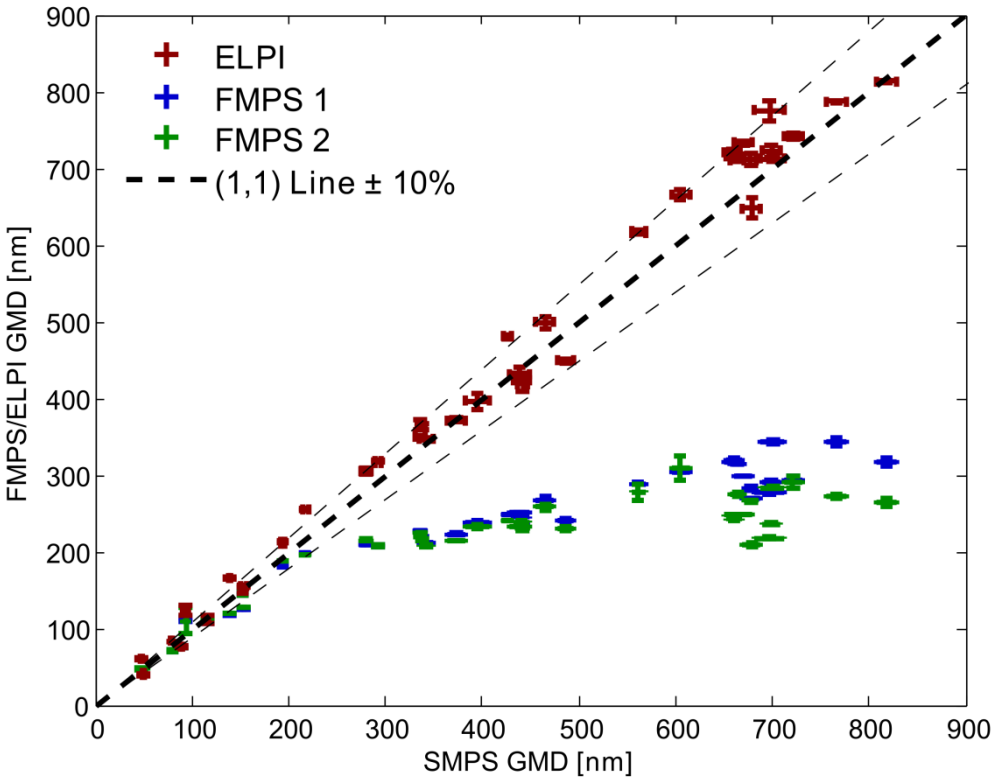

Figure 6.4. Fitted GMDs from FMPSs and ELPI plotted against GMDs from SMPS.

From these results it is clear that the FMPS is unable to reliably measure the size of spherical particles with a size above 200nm. Furthermore, there appears to be an ambiguous response for particles above this size, making a correction algorithm impossible. Effects were also seen on the measured particle number concentration for the particles which were misclassified. As the particles were interpreted as smaller than their actual size, the charge carried by them did not correspond to the actual number concentration, but was overestimated. The study also characterized the unipolar charger used in the FMPS and determined the relationship between particle size and mean number of charges per particle. Using this, the resulting particle mobility as a function of particle size could be calculated (**Figure 6.5**).

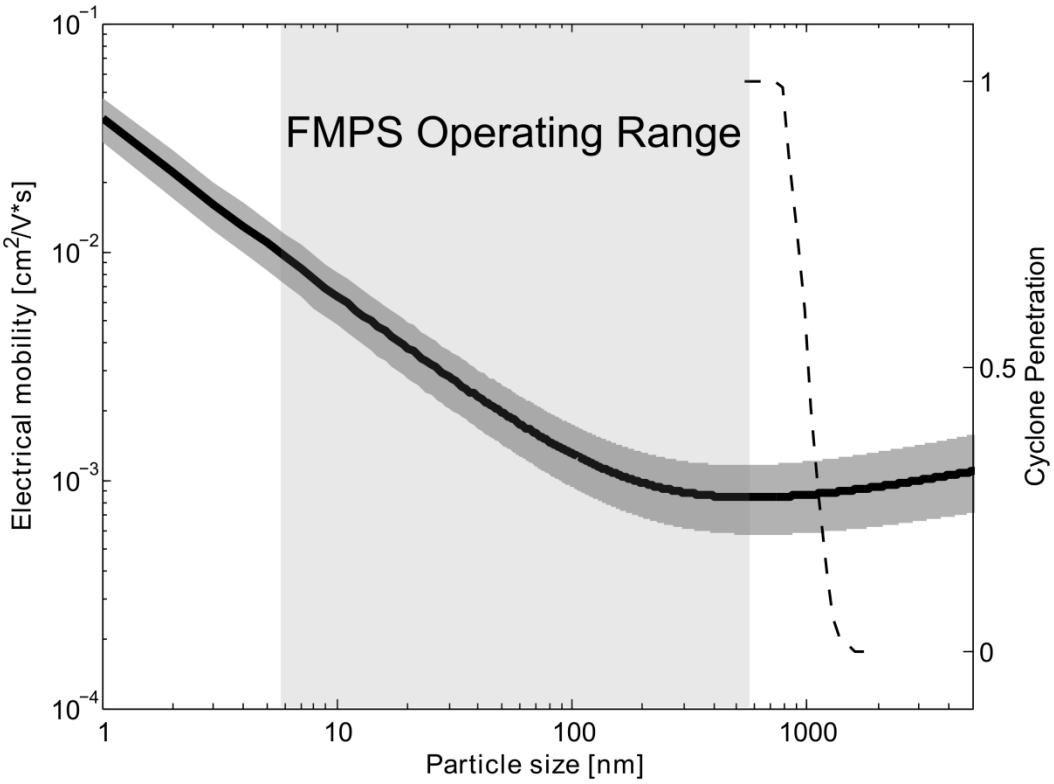

Figure 6.5. Calculated electrical mobility as a function of particle size. Dark shaded area denotes 95% confidence bounds based on fitting. Light shaded area denotes the size range of the FMPS. Dashed line indicates penetration through FMPS inlet cyclone pre-separator.

From **Figure 6.5** it is clear that while the curve minimum is outside the measurement range, (Z_{min}=577 nm), it becomes practically impossible to separate particles in the upper particle size

range due to the small difference in particle trajectories, based on their electrical mobility, and the physical size of an electrometer. Furthermore, since the minimum is below the cut-off diameter of the pre-separating cyclone, larger particles may still interfere with the measurements.

6.4 Comparability of instrument response and calculated surface area for powder dust - Paper IV

The work done within this study concerned the feasibility of measuring Lung Deposited Surface Area (LDSA) concentrations of powder dusts using real-time instruments and monitors. With LDSA becoming more accepted as a biologically relevant metric for toxicity of ENMs, new modeling approaches and regulatory exposure assessment might well come to include this metric. It is therefore important that reliable methods exist for real-time measurement of LDSA concentrations. The comparison between different LDSA concentration measurements (direct measurements with NSAM and Aerotrak, recalculation from size distributions assuming spherical shape with FMPS and ELPI) of spherical particles as well as agglomerated dust particles generated from the small rotating drum is shown in **Figure 6.6**.

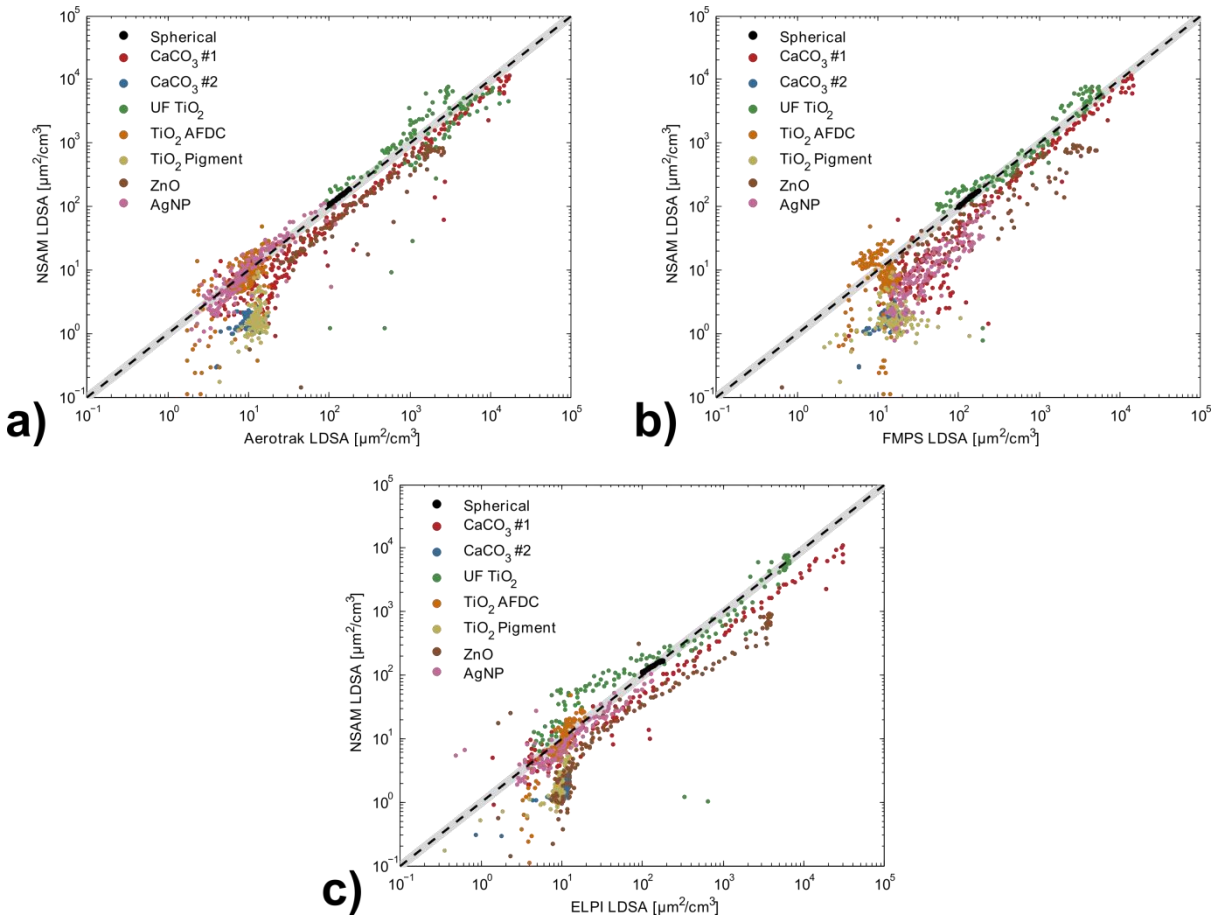

Figure 6.6. Comparison of alveolar deposited surface area measured by NSAM and (a) Aerotrak, (b) FMPS, and (c) ELPI. Gray area denotes ±20 % uncertainty.

The measurements showed that, for spherical particles, all four instruments agree well (R^2 > 0.97, Ratio 0.98-0.99), but for agglomerates the results become more material and method-dependent. In general, the conversion from size distribution worked fairly well for high LDSA concentration (ELPI-NSAM R^2=0.87 - 0.93 Ratio 1.12-5.19, FMPS-NSAM R^2=0.89 - 0.97 Ratio 0.77-4.38) but poorer for the low LDSA-concentration materials.

Comparison of respirable surface area converted from size distributions from ELPI and FMPS was compared to respirable surface area from gravimetrical filter sampling coupled with material density and Specific Surface Area (SSA). The values measured by the ELPI generally correlated well with the values for filter-based calculations (R^2 0.98, Ratio 1.17), but a large difference was seen for the Ag nanoparticles, probably due to its high density and low SSA. The corresponding values

for the FMPS did not have a general trend towards approaching the gravimetrical value (Ratio 0.23).

The observed lack of data agreement between the different types of state-of-the-art measurement equipment is important and the apparent discrepancies encourage the need for further metrological research.

7 Discussion

Results from the study in **Paper I** will possibly need to be re-evaluated in the light of the results from **Paper II** and **Paper III**. The mass-balance modeling based on dustiness results at a relative humidity of 50%RH may not be predictive of material exposure potential if the humidity conditions differ in the workplace. Therefore, more specific assessments of exposure need to consider the relative humidity of the workplace and storage conditions of the materials, especially when working with hygroscopic powders such as the materials tested in this study. All trends for the relationship between dustiness and relative humidity found in **Paper II** point toward an increased dustiness and exposure level in such scenarios, though the magnitude of this increase is material-specific and unknown in this case. Furthermore, results from **Paper III** can be assumed to have implications on the measurements of size distributions using the FMPS conducted in the studies in **Paper I & II**. In the first study, the particle size distributions were, however, backed by measurements of collected particles by Atomic Force Microscopy (AFM). However, due to propriety reasons from the producer of the pharmaceutical powders, these AFM results have not been released for publication. The magnitude of how these effects may have affected the measured penetration through the damaged filters is unclear, but it may well affect both the most penetrating particle size and penetration ratios. In **Paper II,** the size distributions are not so strongly backed up by microscopy work, and based on the results from **Paper III**, the characteristic size mode around 150-200 nm might be an artefact of the FMPS measurement technique. This would not, however, have any implications on the major conclusions of the work, as these are based on the gravimetrical measurements.

The study of Particle Generation Rate (PGR) of the pharmaceutical powders during dustiness testing in **Paper I** raises some interesting questions. This is something which is usually not taken into consideration in mass-balance modeling, but might have an important effect, depending on the scenario studied. Currently, the source term used for modeling assumes that particles are released at a constant rate during the rotating dustiness testing, which is approximately true for three of the powders studied. One of these, however, released almost all particles during the initial stage of the drum rotation. If constant emission rate is assumed for this, then the peak

emission rate of the material, which is relevant for pouring of powder material, is underestimated. This would in turn underestimate the potential exposure as given by the models. It is therefore of importance that PGR is taken into account in future development of exposure models, especially for scenarios with a single agitation of the material, such as pouring.

The results from the study in **Paper II** should have large implications for exposure assessments and control-banding modeling that use dustiness indices as a primary source term. The large effect of humidity is source of uncertainty in exposure and control-banding modeling, which could lead to severe under-use of personal protection equipment by workers and under-dimensioning of local ventilation. The results therefore also indicate that relative humidity should be included in exposure assessment and control banding tools using modeling based on powder dustiness.

The results from **Paper III** highlight a possible major source of error in exposure measurements when using size classification techniques based on unipolar charging, with the FMPS as a specific case. The error could lead to either an under- or overestimation of a deposited dose in the respiratory systems, through two different mechanisms of error.

- As shown in **Paper III**, the underestimation of particle size leads to an overestimation of particle concentration as compared to measurements with a CPC. This would then cause an overestimation of exposure in terms of particle number concentration.
- The deposited dose could be underestimated if the particles are incorrectly sized to 200-300 nm where the alveolar, tracheobronchial and total lung deposition all have a local minimum. Even if the number concentration is underestimated due to assumption of incorrect size in the conversion from current to number, recalculated mass concentrations from the measured size distribution could still be underestimated due to the underestimation in size. If both mass concentration and deposition fraction are underestimated, the assessment of exposure will be severely incorrect.

For non-spherical particles, such as aggregates and agglomerates, the effect shown in **Paper III** would most likely be more severe. As was described in **Section 5.4**, agglomerates can carry more charge than spherical particles of the same particle size. Even more relevant, the increase in mean charge per particle with increasing particle size is steeper. This would result in a minimum within the measurement and a definite ambiguous signal-to-size conversion. Measurements of non-

spherical particles with the FMPS could therefore possibly lead to highly incorrect assessments of exposure.

Measured LDSA concentrations in **Paper IV** show that techniques using ion attachment to the particles and direct measurement of LDSA concentration, e.g. NSAM, have a highly material-dependent relation to those of converted size distribution measurements from FMPS and ELPI. With LDSA concentration ratios varying from 0.8 to 10 for FMPS-NSAM and 1 to 6.2 for ELPI-NSAM, a calibration factor would be hard to determine, even in cases of good data correlation. This of course has implications on the uncertainty in exposure assessment based on the techniques. The study also showed that dust surface area converted from ELPI data generally correlate well ($R^2 > 0.98$, Ratio 1.17) with the surface area of the generated dust particles, based on gravimetrical and BET measurements. Further validations of this method are needed, but it shows promise as a method for assessing airborne surface area. If LDSA concentration is to become an important metric in regulatory exposure assessments and new modeling approaches, a method of choice has to be decided upon or developed, as current techniques do not have the appropriate comparability and material-dependent correlations.

8 Conclusion & Perspectives

This thesis work has aimed to improve the knowledge in the field of measurement of airborne engineered nanomaterials in order to perform assessments of worker exposure to ENMs. It also aimed to improve our understanding of the potential use and challenges in the use of dustiness data for material ranking, as a source term in exposure modeling, and to highlight potential misclassifications of worker exposure if important parameters, such as relative humidity during storage, are neglected.

The results from **Paper III** demonstrates that a specific instrument based on the EMS technique, the Fast Mobility Particle Sizer, incorrectly measures particle sizes of spherical particles with a GMD above 200 nm. For these particles, it underestimates the particle size and overestimates the number concentration. Therefore, measured size distributions with particle modes above 150 nm should not be deemed reliable as they might arise from misclassification of larger size particles. This effect is likely to be more severe for non-spherical particles, such as the agglomerates and aggregates often found after aerosolization of ENMs. The effect was also shown for non-spherical particles generated by dustiness testing, but further studies of more controlled agglomerate aerosols are needed to assess the severity of the effect.

Based on **Paper I & II**, future work is needed if dustiness is to become a more reliable source term for exposure assessment and control band models. More information on the influence of relative humidity is needed, both for assessment of the current standard for dustiness testing and for modeling. **Paper II** showed very high changes (439 times increase with 20%RH decrease) in dustiness with changes of ±20%RH. The current standard allows for ±10%RH error in the air used for pre-conditioning and testing. It is likely that big variations can be observed within that margin but further studies are needed in order to prove that a modification of the standard is necessary.

The results also show that in the future, if dustiness is used as a source term for exposure modeling, the pre-conditioning for dustiness testing has to be performed at the same humidity as the modeled scenario. This is something that none of the current control-banding models takes into account. As a minimum effect of this study, control-banding models should state that the

given results are only valid if the powder material is stored at the conditions listed in the EN15051 standard. The Particle Generation Rate during the rotating dustiness test should also be taken into account for further model developments to ensure that peak emission rates are not underestimated.

Results from **Paper IV** shows that for occupational exposure limits to be based on biologically more relevant factors, such as LDSA concentration and particle number concentration, further development of the reliability and comparability of instruments measuring these parameters is needed. While particle number concentrations can be measured reliably (CPC) and particle size distributions can be determined at a lower time resolution, assuming stable concentrations, methods for size distribution measurements with time resolution down to one second remain too unreliable. Techniques based on unipolar charging, such as EMS techniques and ELPI, may work well for specific conditions, as shown in **Paper III**, but are too dependent on information on particle morphology to be used as monitoring instruments in occupational exposure settings. In order to obtain legislative exposure measurements, either new techniques need to be developed to cope with the challenges posed by ENMs, or a single technique needs to be chosen as a standard. As it stands today, the most dependable technique is likely to be a time-integrating, size-selective sampling coupled with offline techniques for determination of surface-area concentrations. This might, however, miss acute exposures and should not be seen as an optimal technique for exposure assessment.

Achieving reliable size distribution measurements at high time resolution could either be achieved by improving the time resolution of SMPS systems, something which instrument manufacturers are currently attempting, or by improving the reliability of systems with a current high temporal resolution. One way forward in this could be the use dual setups with different charging types, i.e. different size dependency for the number of charges per particle. This could possibly be used to gain information on the agglomeration state of the aerosol and the reliability of the instrument.

9 Acknowledgements

The research for this thesis was carried out at the Department of Micro- and Nanotechnology at the Technical University of Denmark (DTU) as well as at the National Research Centre for the Working Environment (NRCWE). I express my gratitude to both institutes for providing me with the working facilities.

I am grateful to my supervisor, Associate Professor Kristian Mølhave, for his constantly positive discussions and feedback, his almost overwhelming pool of great ideas and suggestions for future work, and for providing me with a truly multidisciplinary environment to carry out my work in. I wish to thank Senior Researchers Keld A. Jensen and Ismo K. Koponen at NRCWE for supervising me and spending so much of their time helping me and answering my questions on a daily basis.

I thank the people at NRCWE for not only creating a great work atmosphere, but also for providing the opportunities to relax and enjoy activities not related to work. I also thank the Molecular Windows group at DTU, which I have had the pleasure of being a part of during my Ph.D. work.

The studies presented in this thesis would not have been possible without the collaboration and efforts of all my co-authors. I thank them for their expertise, help and support during the various studies. I also wish to thank all the people who have helped with practical support during my work, especially Technician Signe H. Nielsen at NRCWE for taking parts of the workload during some of the more tedious experiments. The Aerosol group at Lund University, especially Dr. Joakim Pagels and Dr. Anders Gudmundsson, for allowing me to use their facilities and guiding me during my measurements there.

My gratitude also goes to my friends who have grown up with me, supported me and reminded me that life is more than work. Finally, I warmly thank my family; my parents for their unwavering support throughout life, you have granted me the building blocks to reach this far. My brother for being an inspiration and providing great discussions, both within science and outside of it. Maria for always brightening my days and supporting me throughout this work. Thank you.

10 References

Abbott LC, Maynard AD (2010) Exposure Assessment Approaches for Engineered Nanomaterials. Risk Anal 30:1634–1644. doi: 10.1111/j.1539-6924.2010.01446.x

Adachi M, Kousaka Y, Okuyama K (1985) Unipolar and Bipolar Diffusion Charging of Ultrafine Aerosol-Particles. J Aerosol Sci 16:109–123. doi: 10.1016/0021-8502(85)90079-5

AG (2001) Matter Engineering AG. Operating Manual of LQ1-DC.

Agarwal J, Remiarz R, Quant F, Sem G (1982) Real-Time Aerodynamic Particle-Size Analyzer. J Aerosol Sci 13:222–223.

Agarwal J, Sem G (1980) Continuous-Flow, Single-Particle-Counting Condensation Nucleus Counter. J Aerosol Sci 11:343–&. doi: 10.1016/0021-8502(80)90042-7

Ahn K, Liu B (1990) Particle Activation and Droplet Growth-Processes in Condensation Nucleus Counter .1. Theoretical Background. J Aerosol Sci 21:249–261. doi: 10.1016/0021-8502(90)90008-L

Aitken J (1888) On the number of dust particles in the atmosphere. Proc R Soc Edin 35:1–19.

Allen M, Raabe O (1985) Slip Correction Measurements of Spherical Solid Aerosol-Particles in an Improved Millikan Apparatus. Aerosol Sci Technol 4:269–286. doi: 10.1080/02786828508959055

Almeida SM, Pio CA, Freitas MC, et al (2005) Source apportionment of fine and coarse particulate matter in a sub-urban area at the Western European Coast. Atmos Environ 39:3127–3138. doi: 10.1016/j.atmosenv.2005.01.048

Anderson HR (2009) Air pollution and mortality: A history. Atmos Environ 43:142–152. doi: 10.1016/j.atmosenv.2008.09.026

Arndt R, Packroff R, Gorner B, et al (2005) An easy-to-use workplace control scheme for hazardous substances - A guidance for small and medium enterprises to comply with the new German Ordinance on hazardous substances for hazardous chemical agents without an occupational exposure limit value. Gefahrstoffe Reinhalt Luft 65:13–+.

Asbach C, Fissan H, Stahlmecke B, et al (2009) Conceptual limitations and extensions of lung-deposited Nanoparticle Surface Area Monitor (NSAM). J Nanoparticle Res 11:101–109.

Baron P, Deye G, Fernback J (1994) Length Separation of Fibers. Aerosol Sci Technol 21:179–192. doi: 10.1080/02786829408959707

Baron P, Maynard A, Foley M (2002) Evaluation of aerosol release during the handling of unrefined single walled carbon nanotube material.

Berner A, Lurzer C, Pohl F, et al (1979) Size Distribution of the Urban Aerosol in Vienna. Sci Total Environ 13:245–261. doi: 10.1016/0048-9697(79)90105-0

Biskos G, Mastorakos E, Collings N (2004) Monte-Carlo simulation of unipolar diffusion charging for spherical and non-spherical particles. J Aerosol Sci 35:707–730. doi: 10.1016/j.jaerosci.2003.11.010

Biskos G, Reavell K, Collings N (2005) Unipolar diffusion charging of aerosol particles in the transition regime. J Aerosol Sci 36:247–265. doi: 10.1016/j.jaerosci.2004.09.002

Breum NO (1999) The rotating drum dustiness tester: Variability in dustiness in relation to sample mass, testing time, and surface adhesion. Ann Occup Hyg 43:557–566.

Bricard J, Delattre P, Madelaine G, Pourprix M (1976) Detection of ultra-fine particles by means of a continuous flux condensation nuclei counter. Fine Part B H Liu Ed N Y Acad 566–580.

Brouwer D (2010) Exposure to manufactured nanoparticles in different workplaces. Toxicology In Press, Corrected Proof:-.

Brouwer D, Berges M, Virji MA, et al (2012) Harmonization of Measurement Strategies for Exposure to Manufactured Nano-Objects; Report of a Workshop. Ann Occup Hyg 56:1–9. doi: 10.1093/annhyg/mer099

Brouwer DH, Links IHM, Vreede S a. FD, Christopher Y (2006) Size Selective Dustiness and Exposure; Simulated Workplace Comparisons. Ann Occup Hyg 50:445–452. doi: 10.1093/annhyg/mel015

Brouwer D, van Duuren-Stuurman B, Berges M, et al (2009) From workplace air measurement results toward estimates of exposure? Development of a strategy to assess exposure to manufactured nano-objects. J Nanoparticle Res 11:1867–1881.

BS EN:15051 (2006) EN15051 Workplace Atmospheres: Measurement of the Dustiness of Bulk Materials - Requirements and Reference Test Methods.

Burdett G, Bard D, Kelly A, Thorpe A (2013) The effect of surface coatings on the dustiness of a calcium carbonate nanopowder. J Nanoparticle Res 15:1311. doi: 10.1007/s11051-012-1311-9

Burtscher H, Scherrer L, Siegmann H, et al (1982) Probing Aerosols by Photoelectric Charging. J Appl Phys 53:3787–3791. doi: 10.1063/1.331120

Chen DR, Pui DYH, Hummes D, et al (1998) Design and evaluation of a nanometer aerosol differential mobility analyzer (Nano-DMA). J Aerosol Sci 29:497–509. doi: 10.1016/S0021-8502(97)10018-0

Cherrie JW, Schneider T (1999) Validation of a New Method for Structured Subjective Assessment of Past Concentrations. Ann Occup Hyg 43:235–245.

Cooper D, Reist P (1973) Neutralizing Charged Aerosols with Radioactive Sources. J Colloid Interface Sci 45:17–26. doi: 10.1016/0021-9797(73)90239-7

Cunningham E (1910) On the velocity of steady fall of spherical particles through fluid medium. Proc R Soc Lond Ser -Contain Pap Math Phys Character 83:357–365. doi: 10.1098/rspa.1910.0024

Dadvand P, Parker J, Bell ML, et al (2013) Maternal Exposure to Particulate Air Pollution and Term Birth Weight: A Multi-Country Evaluation of Effect and Heterogeneity. Environ Health Perspect 121:367–373. doi: 10.1289/ehp.1205575

Davies C (1945) Definitive Equations for the Fluid Resistance of Spheres. Proc Phys Soc Lond 57:259–270. doi: 10.1088/0959-5309/57/4/301

Dockery D, Pope C, Xu X, et al (1993) An Association Between Air-Pollution and Mortality in 6 United-States Cities. N Engl J Med 329:1753–1759. doi: 10.1056/NEJM199312093292401

Dolez P (2015) Nanoengineering: Global Approaches to Health and Safety Issues. Elsevier Science B.V.

Donaldson K, Schinwald A, Murphy F, et al (2013) The Biologically Effective Dose in Inhalation Nanotoxicology. Acc Chem Res 46:723–732. doi: 10.1021/ar300092y

Donaldson K, Stone V, Clouter A, et al (2001) Ultrafine particles. Occup Env Med 58:211–6, 199.

Donaldson K, Stone V, Tran CL, et al (2004) Nanotoxicology. Occup Environ Med 61:727–728.

Duffin R, Tran L, Brown D, et al (2007) Proinflammogenic effects of low-toxicity and metal nanoparticles in vivo and in vitro: Highlighting the role of particle surface area and surface reactivity. Inhal Toxicol 19:849–856. doi: 10.1080/08958370701479323

ECHA (2012) Guidance on information requirements and chemical safety assessment. Chapter R.14: Occupational exposure estimation. Version 2.1.

ECOTOC (2012) ECETOC TRA version 3: Background and Ratio-nale for the Improvements – Technical Report No. 114. Euro-pean Centre for Ecotoxicology and Toxicology of Chemicals,Brussels.

EEA (2010) The European environment state and outlook 2010, (http://www.eea.europa.eu/soer). European Environment Agency (EEA).

EU (2011) Regulation No. 1169/2011 of the European Parliament and Council of 25 October 2011 on the provision of food information to consumers.

Evans DE, Turkevich LA, Roettgers CT, et al (2013) Dustiness of Fine and Nanoscale Powders. Ann Occup Hyg 57:261–277.

Fierz M, Houle C, Steigmeier P, Burtscher H (2011) Design, Calibration, and Field Performance of a Miniature Diffusion Size Classifier. Aerosol Sci Technol 45:1–10. doi: 10.1080/02786826.2010.516283

Fierz M, Scherrer L, Burtscher H (2002) Real-time measurement of aerosol size distributions with an electrical diffusion battery. J Aerosol Sci 33:1049–1060. doi: 10.1016/S0021-8502(02)00057-5

Filippov A (1993) Charging of Aerosol in the Transition Regime. J Aerosol Sci 24:423–436. doi: 10.1016/0021-8502(93)90029-9

Fissan H, Hummes D, Stratmann F, et al (1996) Experimental comparison of four differential mobility analyzers for nanometer aerosol measurements. Aerosol Sci Technol 24:1–13. doi: 10.1080/02786829608965347

Fissan H, Neumann S, Trampe A, et al (2007) Rationale and principle of an instrument measuring lung deposited nanoparticle surface area. J Nanoparticle Res 9:53–59. doi: 10.1007/s11051-006-9156-8

Fissan H, Ristig S, Kaminski H, et al (2014) Comparison of different characterization methods for nanoparticle dispersions before and after aerosolization. Anal Methods 6:7324–7334. doi: 10.1039/c4ay01203h

Flagan RC (1998) History of electrical aerosol measurements. Aerosol Sci Technol 28:301–380. doi: 10.1080/02786829808965530

Flagan RC (2008) Differential Mobility Analysis of Aerosols: A Tutorial. Kona Powder Part J 26:254–268.

Fuchs NA (1963) On the stationary charge distribution on aerosol particles in a bipolar ionic atmosphere. Geofis Pura E Appl 56:185–193. doi: 10.1007/BF01993343

Fuchs NA, Sutugin AG (1965) Coagulation rate of highly dispersed aerosols. J Colloid Sci 20:492–500. doi: 10.1016/0095-8522(65)90031-0

Future Markets (2011) Nanomaterials Production 2002-2016: Production Volumes, Revenues and End User Market Demand. Future Markets Inc. ID: 1924269.

Gamero-Castano M, de la Mora JF (2000) A condensation nucleus counter (CNC) sensitive to singly charged sub-nanometer particles. J Aerosol Sci 31:757–772. doi: 10.1016/S0021-8502(99)00555-8

Goehler D, Stintz M, Hillemann L, Vorbau M (2010) Characterization of Nanoparticle Release from Surface Coatings by the Simulation of a Sanding Process. Ann Occup Hyg 54:615–624. doi: 10.1093/annhyg/meq053

Golanski L, Gaborieau A, Guiot A, et al (2011) Characterization of abrasion-induced nanoparticle release from paints into liquids and air. J Phys Conf Ser 304:012062. doi: 10.1088/1742-6596/304/1/012062

Gomez V, Levin M, Saber AT, et al (2014) Comparison of Dust Release from Epoxy and Paint Nanocomposites and Conventional Products during Sanding and Sawing. Ann Occup Hyg 58:983–994. doi: 10.1093/annhyg/meu046

Gopalakrishnan R, Thajudeen T, Ouyang H, Hogan CJ (2013) The unipolar diffusion charging of arbitrary shaped aerosol particles. J Aerosol Sci 64:60–80. doi: 10.1016/j.jaerosci.2013.06.002

Grassian VH (2008) When Size Really Matters: Size-Dependent Properties and Surface Chemistry of Metal and Metal Oxide Nanoparticles in Gas and Liquid Phase Environments. J Phys Chem C 112:18303–18313. doi: 10.1021/jp806073t

Hagendorfer H, Lorenz C, Kaegi R, et al (2010) Size-fractionated characterization and quantification of nanoparticle release rates from a consumer spray product containing engineered nanoparticles. J Nanoparticle Res 12:2481–2494. doi: 10.1007/s11051-009-9816-6

Han BW, Shimada M, Okuyama K, Choi M (2003) Classification of monodisperse aerosol particles using an adjustable soft X-ray charger. Powder Technol 135:336–344. doi: 10.1016/S0032-5910(03)00167-0

Heim M, Kasper G, Reischl GP, Gerhart C (2004) Performance of a new commercial electrical mobility spectrometer. Aerosol Sci Technol 38:3–14. doi: 10.1080/02786820490519252

Heitbrink W, Todd W, Cooper T, Obrien D (1990) The Application of Dustiness Tests to the Prediction of Worker Dust Exposure. Am Ind Hyg Assoc J 51:217–223. doi: 10.1202/0002-8894(1990)051<0217:TAODTT>2.0.CO;2

Hering S, Friedlander S, Collins J, Richards L (1979) Design and Evaluation of a New Low-Pressure Impactor .2. Environ Sci Technol 13:184–188. doi: 10.1021/es60150a009

Hering SV, Marple VA (1986) Low pressure and microorifice impactors. In Cascade Impactors: Sampling & Data Analysis, James P. Lodge and Tai L. Chan (eds.).

Hering SV, Stolzenburg MR, Quant FR, et al (2005) A laminar-flow, water-based condensation particle counter (WCPC). Aerosol Sci Technol 39:659–672. doi: 10.1080/02786820500182123

Hillamo R, Kauppinen E (1991) On the Performance of the Berner Low-Pressure Impactor. Aerosol Sci Technol 14:33–47. doi: 10.1080/02786829108959469

Hinds WC (1999) Aerosol Technology: Properties, Behavior and Measurements of Airborne Particles, 2nd ed. John Wiley & Sons, New York

Hogan AW, Gardner G (1968) A nucleus counter of increased sensitivity. J Rech Atm 3:59–61.

Hoppel WA (1978) Determination of the Aerosol Size Distribution from the Mobility Distribution of the Charged Fraction of Aerosols. J Aerosol Sci 9:41–54.

Hoppel WA, Frick GM (1986) Ion—Aerosol Attachment Coefficients and the Steady-State Charge Distribution on Aerosols in a Bipolar Ion Environment. Aerosol Sci Technol 5:1–21. doi: 10.1080/02786828608959073

Hornsby KE, Pryor SC (2014) A Laboratory Comparison of Real-Time Measurement Methods for 10-100-nm Particle Size Distributions. Aerosol Sci Technol 48:571–582. doi: 10.1080/02786826.2014.901488

Hsu LY, Chein HM (2007) Evaluation of nanoparticle emission for TiO2 nanopowder coating materials. J Nanoparticle Res 9:157–163.

Hussein M, Madl P, Khan A (2011) Lung deposition predictions of airborne particles and the emergence of contemporary diseases Part-I. theHealth 2:51–59.

Hussein T, Wierzbicka A, Londahl J, et al (2015) Indoor aerosol modeling for assessment of exposure and respiratory tract deposited dose. Atmos Environ 106:402–411. doi: 10.1016/j.atmosenv.2014.07.034

ICRP (1994) Human respiratory tract model for radiological protection.

ISO (2013) Nanotechnologies -- Vocabulary -- Part 6: Nano-object characterization. ISO/TS 80004-6.

ISO (2007) ISO/TR 27628: Workplace atmospheres - Ultrafine, nanoparticle and nanostructured aerosols - Inhalation exposure characterization and assessment.

Jacobsen NR, Moller P, Jensen KA, et al (2009) Lung inflammation and genotoxicity following pulmonary exposure to nanoparticles in ApoE(-/-) mice. Part Fibre Toxicol 6:2. doi: 10.1186/1743-8977-6-2

Jayjock MA, Armstrong T, Taylor M (2011) The Daubert Standard as Applied to Exposure Assessment Modeling Using the Two-Zone (NF/FF) Model Estimation of Indoor Air Breathing Zone Concentration as an Example. J Occup Environ Hyg 8:D114–D122. doi: 10.1080/15459624.2011.624387

Jensen ACØ (2015) Exposure Assessment of Particulate Matter from Abrasive Treatment of Carbon and Glass Fibre-Reinforced Epoxy-Composites – Two Case Studies. Aerosol Air Qual Res. doi: 10.4209/aaqr.2015.02.0086

Jensen KA, Koponen IK, Clausen PA, Schneider T (2009) Dustiness behaviour of loose and compacted Bentonite and organoclay powders: What is the difference in exposure risk? J Nanoparticle Res 11:133–146.

Johnson T, Caldow R, Pocher A, et al (2004) An Engine Exhaust Particle Sizer Spectrometer for Transient Emission Particle Measurements, SAE Technical Paper No. 2004-01-1341. Warren, PA: Society for Automotive Engineers.

Jung HJ, Kittelson DB (2005) Characterization of aerosol surface instruments in transition regime. Aerosol Sci Technol 39:902–911. doi: 10.1080/02786820500295701

Jung T, Burtscher H, Schmidtott A (1988) Multiple Charging of Ultrafine Aerosol-Particles by Aerosol Photoemission (ape). J Aerosol Sci 19:485–490. doi: 10.1016/0021-8502(88)90023-7

Kaminski H, Kuhlbusch TAJ, Fissan H, et al (2012) Mathematical Description of Experimentally Determined Charge Distributions of a Unipolar Diffusion Charger. Aerosol Sci Technol 46:708–716. doi: 10.1080/02786826.2012.659360

Kaminski H, Kuhlbusch TAJ, Rath S, et al (2013) Comparability of mobility particle sizers and diffusion chargers. J Aerosol Sci 57:156–178. doi: 10.1016/j.jaerosci.2012.10.008

Keller A, Fierz M, Siegmann K, et al (2001) Surface science with nanosized particles in a carrier gas. J Vac Sci Technol -Vac Surf Films 19:1–8. doi: 10.1116/1.1339832

Keskinen J, Pietarinen K, Lehtimaki M (1992) Electrical Low-Pressure Impactor. J Aerosol Sci 23:353–360. doi: 10.1016/0021-8502(92)90004-F

Knutson EO, Whitby KT (1975) Aerosol classification by electric mobility: Apparatus, theory, and applications. J Aerosol Sci 6:443–451.

Koivisto AJ, Jensen ACØ, Levin M, et al (2015) Testing the near field/far field model performance for prediction of particulate matter emissions in a paint factory. Environ Sci Process Impacts 17:62–73. doi: 10.1039/c4em00532e

Koivisto AJ, Palomaki JE, Viitanen A-K, et al (2014) Range-Finding Risk Assessment of Inhalation Exposure to Nanodiamonds in a Laboratory Environment. Int J Environ Res Public Health 11:5382–5402. doi: 10.3390/ijerph110505382

Koponen IK, Jensen KA, Schneider T (2009) Sanding dust from nanoparticle-containing paints: Physical characterisation. J Phys Conf Ser 151:012048–.

Koponen IK, Jensen KA, Schneider T (2011) Comparison of dust released from sanding conventional and nanoparticle-doped wall and wood coatings. J Expo Sci Environ Epidemiol 21:408–418. doi: 10.1038/jes.2010.32

Kousaka Y, Endo Y, Ichitsubo H, Alonso M (1996) Orientation-specific dynamic shape factors for doublets and triplets of spheres in the transition regime. Aerosol Sci Technol 24:36–44. doi: 10.1080/02786829608965350

Kousaka Y, Endo Y, Muroya Y, Fukushima N (1992) Development of a High Flow Rate Mixing Type CNC and its Application to Cumulative Type Electrostatic Particle Size Analysis. Aerosol Res 219–229.

Kousaka Y, Niida T, Okuyama K, Tanaka H (1982) Development of a Mixing Type Condensation Nucleus Counter. J Aerosol Sci 13:231–240. doi: 10.1016/0021-8502(82)90064-7

Kreyling WG, Semmler-Behnke M, Moller W (2006) Ultrafine particle-lung interactions: Does size matter? J Aerosol Med-Depos Clear Eff Lung 19:74–83. doi: 10.1089/jam.2006.19.74

Kristensen HV, Jensen KA, Koponen IK, et al (2010) Nanopartikler i arbejdsmiljøet - Viden og inspiration om håndtering af nanomaterialer. . Industriens Branchearbejdsmiljøråd, Branchearbejdsmiljørådet for Undervisning og Forskning samt Universitets og Bygningsstyrelsen. Copenhagen, Denmark

Ku BK, Deye GJ, Kulkarni P, Baron PA (2011) Bipolar diffusion charging of high-aspect ratio aerosols. J Electrost 69:641–647. doi: 10.1016/j.elstat.2011.08.006

Kuempel ED, Geraci CL, Schulte PA (2012) Risk Assessment and Risk Management of Nanomaterials in the Workplace: Translating Research to Practice. Ann Occup Hyg 56:491–505. doi: 10.1093/annhyg/mes040

Kuhlbusch TAJ, Asbach C, Fissan H, et al (2011) Nanoparticle exposure at nanotechnology workplaces: A review. Part Fibre Toxicol 8:22. doi: 10.1186/1743-8977-8-22

Kuhlbusch T a. J, Fissan H (2006) Particle characteristics in the reactor and pelletizing areas of carbon black production. J Occup Environ Hyg 3:558–567. doi: 10.1080/15459620600912280

Kuhlbusch T a. J, Neumann S, Fissan H (2004) Number size distribution, mass concentration, and particle composition of PM1, PM2.5, and PM10 in bag filling areas of carbon black production. J Occup Environ Hyg 1:660–671. doi: 10.1080/15459620490502242

Kulkarni P, Baron PA, Willeke K (2011) Aerosol Measurement: Principles, Techniques, and Applications, Third Edition.

Kulkarni P, Namiki N, Otani Y, Biswas P (2002) Charging of particles in unipolar coronas irradiated by in-situ soft X-rays: enhancement of capture efficiency of ultrafine particles. J Aerosol Sci 33:1279–1296. doi: 10.1016/S0021-8502(02)00067-8

Kulkarni P, Wang J (2006) New fast integrated mobility spectrometer for real-time measurement of aerosol size distribution: II. Design, calibration, and performance characterization. J Aerosol Sci 37:1326–1339. doi: 10.1016/j.jaerosci.2006.01.010

Lall AA, Rong W, Madler L, Friedlander SK (2008) Nanoparticle aggregate volume determination byelectrical mobility analysis: Test of idealized aggregate theory using aerosol particle mass analyzer measurements. J Aerosol Sci 39:403–417. doi: 10.1016/j.jaerosci.2007.12.010

Lee HM, Kim CS, Shimada M, Okuyama K (2005) Bipolar diffusion charging for aerosol nanoparticle measurement using a soft X-ray charger. J Aerosol Sci 36:813–829. doi: 10.1016/j.jaerosci.2004.10.011

Leskinen J, Joutsensaari J, Lyyranen J, et al (2012) Comparison of nanoparticle measurement instruments for occupational health applications. J Nanoparticle Res 14:718. doi: 10.1007/s11051-012-0718-7

Levin M, Koponen IK, Jensen KA (2014) Exposure Assessment of Four Pharmaceutical Powders Based on Dustiness and Evaluation of Damaged HEPA Filters. J Occup Environ Hyg 11:165–177. doi: 10.1080/15459624.2013.848038

Liden G (2006) Dustiness testing of materials handled at workplaces. Ann Occup Hyg 50:437–439.

Li L, Chen D-R (2011) Aerosol Charging Using Pen-Type UV Lamps. Aerosol Air Qual Res 11:791–801. doi: 10.4209/aaqr.2011.07.0103

Lim SS, Vos T, Flaxman AD, et al (2012) A comparative risk assessment of burden of disease and injury attributable to 67 risk factors and risk factor clusters in 21 regions, 1990-2010: a systematic analysis for the Global Burden of Disease Study 2010. Lancet 380:2224–2260.

Maricq MM (2008) Bipolar diffusion charging of soot aggregates. Aerosol Sci Technol 42:247–254. doi: 10.1080/02786820801958775

Marjamaki M, Lemmetty M, Keskinen J (2005) ELPI response and data reduction - I: Response functions. Aerosol Sci Technol 39:575–582. doi: 10.1080/027868291009189

Marquart H, Heussen H, Le Feber M, et al (2008) “Stoffenmanager”, a web-based control banding tool using an exposure process model. Ann Occup Hyg 52:429–441. doi: 10.1093/annhyg/men032

Marra J, Voetz M, Kiesling H-J (2009) Monitor for detecting and assessing exposure to airborne nanoparticles. J Nanoparticle Res 12:21–37. doi: 10.1007/s11051-009-9695-x

Maynard AD, Aitken RJ (2007) Assessing exposure to airborne nanomaterials: Current abilities and future requirements. Nanotoxicology 1:26–41. doi: 10.1080/17435390701314720

Maynard AD, Baron PA, Foley M, et al (2004) Exposure to carbon nanotube material: Aerosol release during the handling of unrefined single-walled carbon nanotube material. J Toxicol Environ Health-Part A 67:87–107.

Maynard AD, Kuempel ED (2005) Airborne nanostructured particles and occupational health. J Nanoparticle Res 7:587–614.

McClellan R (2000) Particle interactions in the respiratory tract. Particle-Lung interactions, In Gehr P, Heyder J (Eds).

Medved A, Dorman F, Kaufman SL, Pocher A (2000) A New Corona Based Charger For Aerosol Particles. J Aerosol Sci 31:616–617.

Mills JB, Park JH, Peters TM (2013) Comparison of the DiSCmini Aerosol Monitor to a Handheld Condensation Particle Counter and a Scanning Mobility Particle Sizer for Submicrometer Sodium Chloride and Metal Aerosols. J Occup Environ Hyg 10:250–258. doi: 10.1080/15459624.2013.769077

Modesto-Lopez LB, Kettleson EM, Biswas P (2011) Soft X-ray charger (SXC) system for use with electrospray for mobility measurement of bioaerosols. J Electrost 69:357–364. doi: 10.1016/j.elstat.2011.04.014

Nasterlack M, Zober A, Oberlinner C (2008) Considerations on occupational medical surveillance in employees handling nanoparticles. Int Arch Occup Environ Health 81:721–726. doi: 10.1007/s00420-007-0245-5

Nazarenko Y, Lioy PJ, Mainelis G (2014) Quantitative assessment of inhalation exposure and deposited dose of aerosol from nanotechnology-based consumer sprays. Environ Sci-Nano 1:161–171. doi: 10.1039/c3en00053b

Nazarenko Y, Zhen H, Han T, et al (2012) Potential for Inhalation Exposure to Engineered Nanoparticles from Nanotechnology-Based Cosmetic Powders. Environ Health Perspect 120:885–892. doi: 10.1289/ehp.1104350

Nel A (2005) Air pollution-related illness: Effects of particles. Science 308:804–806. doi: 10.1126/science.1108752

Norgaard AW, Jensen KA, Janfelt C, et al (2009) Release of VOCs and Particles During Use of Nanofilm Spray Products. Environ Sci Technol 43:7824–7830. doi: 10.1021/es9010468

Oberdorster G (2001) Pulmonary effects of inhaled ultrafine particles. Int Arch Occup Env Health 74:1–8.

Oberdorster G (2000) Toxicology of ultrafine particles: in vivo studies. Philos Trans R Soc Lond Ser - Math Phys Eng Sci 358:2719–2739. doi: 10.1098/rsta.2000.0680

Oberdorster G, Maynard A, Donaldson K, et al (2005) Principles for characterizing the potential human health effects from exposure to nanomaterials: elements of a screening strategy. Part Fibre Toxicol 2:8–.

Okuyama K, Kousaka Y, Motouchi T (1984) Condensational Growth of Ultrafine Aerosol-Particles in a New Particle-Size Magnifier. Aerosol Sci Technol 3:353–366. doi: 10.1080/02786828408959024

Park D, Kim Y-H, Lee S-G, et al (2010) Development and performance test of a micromachined unipolar charger for measurements of submicron aerosol particles having a log-normal size distribution. J Aerosol Sci 41:490–500. doi: 10.1016/j.jaerosci.2010.02.007

Plinke MAE, Leith D, Boundy MG, Loffler F (1995) Dust Generation from Handling Powders in Industry. Am Ind Hyg Assoc J 56:251–257.

Politis M, Pilinis C, Lekkas TD (2008) Ultrafine Particles (ufp) and Health Effects. Dangerous. Like No Other Pm? Review and Analysis. Glob Nest J 10:439–452.

Pollak LW, Metnieks AL (1958) New calibration of photoelectric nucleus counters. Geofis Pura Appl 41:201–210.

Pope CA 3rd (2000) Review: Epidemiological basis for particulate air pollution health standards. Aerosol Sci Technol 32:4–14.

Pope CA, Burnett RT, Thun MJ, et al (2002) Lung cancer, cardiopulmonary mortality, and long-term exposure to fine particulate air pollution. JAMA 287:1132–1141.

Price HD, Stahlmecke B, Arthur R, et al (2014) Comparison of instruments for particle number size distribution measurements in air quality monitoring. J Aerosol Sci 76:48–55. doi: 10.1016/j.jaerosci.2014.05.001

Pui D, Fruin S, Mcmurry P (1988) Unipolar Diffusion Charging of Ultrafine Aerosols. Aerosol Sci Technol 8:173–187. doi: 10.1080/02786828808959180

Qi C, Chen D-R, Greenberg P (2008) Performance study of a unipolar aerosol mini-charger for a personal nanoparticle sizer. J Aerosol Sci 39:450–459. doi: 10.1016/j.jaerosci.2008.01.003

Qi C, Chen D-R, Pui DYH (2007) Experimental study of a new corona-based unipolar aerosol charger. J Aerosol Sci 38:775–792. doi: 10.1016/j.jaerosei.2007.05.005

Quadros ME, Marr LC (2010) Environmental and Human Health Risks of Aerosolized Silver Nanoparticles. J Air Waste Manag Assoc 60:770–781. doi: 10.3155/1047-3289.60.7.770

Reavell K, Hands T, Collings N (2002) A Fast Response Particulate Spectrometer for Combustion Aerosols. SAE International, Warrendale, PA

Rich TA (1955) A photo-electric nucleus counter with size discrimination. Geofis Pura E Appl 31:60–65. doi: 10.1007/BF01999586

Rich TA (1961) A continuous recorder for condensation nuclei. Geofis Pura E Appl 50:46–52. doi: 10.1007/BF02000625

Roco MC (2005) Environmentally responsible development of nanotechnology. Environ Sci Technol 39:106A–112A. doi: 10.1021/es053199u

Roco MC, Harthorn B, Guston D, Shapira P (2011) Innovative and responsible governance of nanotechnology for societal development. J Nanoparticle Res 13:3557–3590.

Roduner E (2006) Size matters: why nanomaterials are different. Chem Soc Rev 35:583–592. doi: 10.1039/b502142c

Rogak S, Flagan R (1992) Bipolar Diffusion Charging of Spheres and Agglomerate Aerosol-Particles. J Aerosol Sci 23:693–710. doi: 10.1016/0021-8502(92)90037-V

Rogak S, Flagan R, Nguyen H (1993) The Mobility and Structure of Aerosol Agglomerates. Aerosol Sci Technol 18:25–47. doi: 10.1080/02786829308959582

Rohmann H (1923) Method for measuring the size of floating particles. Z Phys 17:253–265. doi: 10.1007/BF01328683

Romay F, Pui D (1992) On the Combination Coefficient of Positive-Ions with Ultrafine Neutral Particles in the Transition and Free-Molecule Regimes. Aerosol Sci Technol 17:134–147. doi: 10.1080/02786829208959566

RosellLlompart J, Loscertales IG, Bingham D, delaMora JF (1996) Sizing nanoparticles and ions with a short differential mobility analyzer. J Aerosol Sci 27:695–719. doi: 10.1016/0021-8502(96)00016-X

Saber AT, Jacobsen NR, Jackson P, et al (2014) Particle-induced pulmonary acute phase response may be the causal link between particle inhalation and cardiovascular disease. Wiley Interdiscip Rev-Nanomedicine Nanobiotechnology 6:517–531. doi: 10.1002/wnan.1279

Sadik OA, Zhou AL, Kikandi S, et al (2009) Sensors as tools for quantitation, nanotoxicity and nanomonitoring assessment of engineered nanomaterials. J Environ Monit 11:1782–1800.

Schmidt-Ott A (1988) In situ measurement of the fractal dimensionality of ultrafine aerosol particles. Appl Phys Lett 954 – 956. doi: 10.1063/1.99239

Schneider T, Brouwer DH, Koponen IK, et al (2011) Conceptual model for assessment of inhalation exposure to manufactured nanoparticles. J Expo Sci Environ Epidemiol 21:450–463.

Schneider T, Jensen K (2009) Relevance of aerosol dynamics and dustiness for personal exposure to manufactured nanoparticles. J Nanoparticle Res -.

Schneider T, Jensen KA (2008) Combined Single-Drop and Rotating Drum Dustiness Test of Fine to Nanosize Powders Using a Small Drum. Ann Occup Hyg mem059–.

Schulte PA, Murashov V, Zumwalde R, et al (2010) Occupational exposure limits for nanomaterials: state of the art. J Nanoparticle Res 12:1971–1987.

Seipenbusch M, Binder A, Kasper G (2008) Temporal Evolution of Nanoparticle Aerosols in Workplace Exposure. Ann Occup Hyg 52:707–716. doi: 10.1093/annhyg/men067

Sgro LA, de la Mora JF (2004) A simple turbulent mixing CNC for charged particle detection down to 1.2 nm. Aerosol Sci Technol 38:1–11. doi: 10.1080/02786820490247560

Shimada M, Han BW, Okuyama K, Otani Y (2002) Bipolar charging of aerosol nanoparticles by a soft X-ray photoionizer. J Chem Eng Jpn 35:786–793. doi: 10.1252/jcej.35.786

Shin WG, Pui DYH, Fissan H, et al (2007) Calibration and numerical simulation of nanoparticle surface area monitor (TSI model 3550 NSAM). J Nanoparticle Res 9:61–69. doi: 10.1007/s11051-006-9153-y

Shin WG, Wang J, Mertler M, et al (2010) The effect of particle morphology on unipolar diffusion charging of nanoparticle agglomerates in the transition regime. J Aerosol Sci 41:975–986. doi: 10.1016/j.jaerosci.2010.07.004

Siegel RW, Hu E, Cox DM, et al (1999) Nanostructure Science and Technology. Springer Netherlands, Dordrecht

Sinclair D, Hoopes GS (1975) A continuous flow condensation nucleus counter. J Aerosol Sci 6:1–7.

Skala GF (1963) A New Instrument for the Continuous Measurement of Condensation Nuclei. Anal Chem 35:702–706. doi: 10.1021/ac60199a007

Stolzenburg M, Mcmurry P (1991) An Ultrafine Aerosol Condensation Nucleus Counter. Aerosol Sci Technol 14:48–65. doi: 10.1080/02786829108959470

Tammet H, Mirme A, Tamm E (2002) Electrical aerosol spectrometer of Tartu University. Atmospheric Res 62:315–324. doi: 10.1016/S0169-8095(02)00017-0

Tielemans E, Warren N, Fransman W, et al (2011) Advanced REACH Tool (ART): Overview of Version 1.0 and Research Needs. Ann Occup Hyg 55:949–956. doi: 10.1093/annhyg/mer094

Tischer M, Bredendiek-Kaemper S, Poppek U, Packroff R (2009) How Safe is Control Banding? Integrated Evaluation by Comparing OELs with Measurement Data and Using Monte Carlo Simulation. Ann Occup Hyg 53:449–462. doi: 10.1093/annhyg/mep037

Tsai C-J, Lin G-Y, Liu C-N, et al (2012) Characteristic of nanoparticles generated from different nano-powders by using different dispersion methods. J Nanoparticle Res 14:777. doi: 10.1007/s11051-012-0777-9

Tsai SJ, Ada E, Isaacs J, Ellenbecker M (2008) Airborne nanoparticle exposures associated with the manual handling of nanoalumina and nanosilver in fume hoods. J Nanoparticle Res -.

TSI (2006) Fast Mobility Particle Sizer Spectrometer; Operation and Service Manual, TSI Incorporated, Shoreview, MN, USA.

Van Broekhuizen P, van Broekhuizen F, Cornelissen R, Reijnders L (2012) Workplace exposure to nanoparticles and the application of provisional nanoreference values in times of uncertain risks. J Nanoparticle Res 14:770. doi: 10.1007/s11051-012-0770-3

Van Duuren-Stuurman B, Vink SR, Verbist KJM, et al (2012) Stoffenmanager Nano Version 1.0: A Web-Based Tool for Risk Prioritization of Airborne Manufactured Nano Objects. Ann Occup Hyg -.

Vanhanen J, Mikkila J, Lehtipalo K, et al (2011) Particle Size Magnifier for Nano-CN Detection. Aerosol Sci Technol 45:533–542. doi: 10.1080/02786826.2010.547889

Wang S, Flagan R (1990) Scanning Electrical Mobility Spectrometer. Aerosol Sci Technol 13:230–240. doi: 10.1080/02786829008959441

Whitby K, Clark W (1966) Electric Aerosol Particle Counting and Size Distribution Measuring System for 0.015 to 1 Mu Size Range. Tellus 18:573–&.

Wiedensohler A (1988) An Approximation of the Bipolar Charge-Distribution for Particles in the Sub-Micron Size Range. J Aerosol Sci 19:387–389. doi: 10.1016/0021-8502(88)90278-9

Winklmayr W, Reischl G, Lindner A, Berner A (1991) A New Electromobility Spectrometer for the Measurement of Aerosol Size Distributions in the Size Range from 1 to 1000 Nm. J Aerosol Sci 22:289–296. doi: 10.1016/S0021-8502(05)80007-2

Wohlleben W, Brill S, Meier MW, et al (2011) On the Lifecycle of Nanocomposites: Comparing Released Fragments and their In-Vivo Hazards from Three Release Mechanisms and Four Nanocomposites. Small 7:2384–2395. doi: 10.1002/smll.201002054

Xiao K, Swanson JJ, Pui DYH, Kittelson DB (2012) Bipolar Diffusion Charging of Aggregates. Aerosol Sci Technol 46:794–803. doi: 10.1080/02786826.2012.667585

Yun KM, Lee SY, Iskandar F, et al (2009) Effect of X-ray energy and ionization time on the charging performance and nanoparticle formation of a soft X-ray photoionization charger. Adv Powder Technol 20:529–536. doi: 10.1016/j.apt.2009.07.002

Zhang M, Wexler AS (2006) Cross flow ion mobility spectrometry: Theory and initial prototype testing. Int J Mass Spectrom 258:13–20. doi: 10.1016/j.ijms.2006.05.012

Zhang S, Akutsu Y, Russell L, et al (1995) Radial Differential Mobility Analyzer. Aerosol Sci Technol 23:357–372. doi: 10.1080/02786829508965320

Zhang Z, Liu B (1990) Dependence of the Performance of Tsi 3020 Condensation Nucleus Counter. Aerosol Sci Technol 13:493–504. doi: 10.1080/02786829008959464

Zimmerman N, Pollitt KJG, Jeong C-H, et al (2014) Comparison of three nanoparticle sizing instruments: The influence of particle morphology. Atmos Environ 86:140–147. doi: 10.1016/j.atmosenv.2013.12.023

Paper I

Journal of Occupational and Environmental Hygiene, 11: 165–177
ISSN: 1545-9624 print / 1545-9632 online

DOI: 10.1080/15459624.2013.848038

Exposure Assessment of Four Pharmaceutical Powders Based on Dustiness and Evaluation of Damaged HEPA Filters

Marcus Levin,[1,2] Ismo K. Koponen,[2] and Keld A. Jensen[2]

[1]Department of Micro- and Nanotechnology, Technical University of Denmark, Lyngby, Denmark
[2]Danish NanoSafety Centre, National Research Center for Working Environment (NRCWE), Copenhagen, Denmark

In this study, we show the different dustiness characteristics of four molecular pharmaceutical powder candidates and evaluate the performance of HEPA filters damaged with three different pinhole sizes and exposed to dust using real industrial powders in a miniaturized EN15051 rotating drum dustiness tester. We then demonstrate the potential use of such data using first-order exposure modeling to assess the potential worker exposure and transmission of active powder ingredients into ventilation systems. The four powders had highly variable inhalable dustiness indices (1,036 – 14,501 mg/kg). Dust particle size-distributions were characterized by three peaks; the first occurred around 60–80 nm, the second around 250 nm, and the third at 2–3 μm. The second and third peaks are often observed in dustiness test studies, but peaks in the 60–80 nm range have not been previously reported. Exposure modeling in a 5 times 20 kg powder pouring scenario, suggests that excessive dust concentrations may be reached during use of powders with the highest dustiness levels. By number, filter-damage by three pinhole sizes resulted in damage-dependent penetration of 70–80 nm-size particles, but by volume and mass the penetration is still dominated by particles larger than 100 nm. Whereas the exposure potential was evident, the potential dust concentrations in air ducts following the pouring scenario above were at pg/m³ levels. Hence, filter penetration at these damage levels was assumed to be only critical, if the active ingredients were associated with high hazard or unique product purity is required.

[Supplementary materials are available for this article. Go to the publisher's online edition of Journal of Occupational and Environmental Hygiene *for the following free supplemental resource: An example of a typical particle number time-series of a complete dustiness test. It provides information on the HEPA-filter used including a scanning electron microscopy image of it. It also provides APS-measurements of particles penetrating the damaged HEPA-filter.]*

Keywords pharmaceuticals, dustiness, rotating drum, HEPA filter, filter damage, exposure assessment

Address correspondence to: Keld Alstrup Jensen, Danish NanoSafety Centre, National Research Center for Working Environment, Lersø Park Alle 105, DK-2100 Copenhagen, Denmark; e-mail: kaj@nrcwe.dk

INTRODUCTION

Powder handling is a major activity in many productions, including the food and drug industries. Pre-evaluation of the technical applicability and suitability of powders can be made by using tests—e.g., flowability, hygroscopicity, and dispersibility. The potential for worker exposure during powder handling can be assessed using results from dustiness testing. In fact, the pharmaceutical industry was among the first to use this concept.[1] Today, several dustiness methods exist[2] or are under consideration. So far, only one dustiness standard (EN15051)—including two dustiness methods, namely the rotating drum and the continuous drop method—has been established.[3] In the past few years, interest in dustiness testing and its application for establishment of release potentials and use in control banding tools has increased.[4–15] Further use of dustiness data for modeling of time-resolved exposure levels for risk assessment has also been proposed and demonstrated.[11,16–18]

The use of active ingredients in the food and drug industries usually requires high-level dust control to ensure production of high-purity products, but also protection of their workers from exposure down to even ng/m³ levels.[19–23] Exposure to specific food and drug ingredients may cause different adverse effects such as development of caries,[24] sensitization,[20,25,26] and asthma,[27] as well as other chronic respiratory and systemic effects.[19,26,28] Therefore introduction of new or modified biologically active ingredients may require careful evaluation of the potential occupational exposure, cross-contamination, and environmental release.

High demand for exposure control may be particularly necessary in the transition into nano-food and nano-medicine.[29,30] Particulate nanomaterials may be dustier than conventional powders and generally release finer dust with a dominant concentration peak in the 100–300 nm-size range.[9,10] Similar phenomena may also be true for molecular powder ingredients, where the monomers normally are in the

lower nm range. However, nanomaterial powders may not always be dustier then the "non-nano" bulk counterpart.[6,15] Different production methods and intrinsic physico-chemical characteristics such as primary particle size, shape, roughness, hygroscopicity, and stickiness of the powder particles may affect dustiness due to aggregation, soft bridging, or other mechanisms of agglomeration.[31] Several food and pharmaceutical powder ingredients consist of greasy/oily or highly hygroscopic particles. Therefore such powders may aggregate, resulting in coarser dust and reduced dustiness than would be expected from the primary characteristics of the compounds.

Regular dust control of low hazard exposures is often facilitated by local exhaust ventilation and room air ventilation, which may be recirculated. High-level dust control is achieved by other means such as containment and isolation. HEPA filters are the typical choice in high-efficiency exposure and emission control systems as well as in factory ventilation systems and their particle filtration efficiencies for undamaged filters are being well documented.[32–35] However, experience shows that HEPA filters are often damaged over time because of factors including—unintended overload, pressure shocks, ageing, chemical and physical damage, and the initial damage level being not easily identifiable.[36,37] The effects of filter damage appear to be rarely studied, but it is an important issue in factories working with possibly toxic compounds or producing different products which cannot tolerate cross-contamination of active ingredients. Therefore, assessments of powders may also require assessment of the dust transfer in ventilation systems and risk of cross-contamination.

A recent study investigated the penetration of 4–30 nm-size Cu nanoparticles through three types of HEPA filters (A: 4.5 μm fiber diameter, 0.060 solidity, 1.6e5 cm^{-1} airflow resistance; B: 3.3 μm fibers, 0.065 solidity, 4.2e5 cm^{-1} airflow resistance; C: 1.3 μm fiber diameter, 0.078 solidity, 35.4e5 cm^{-1} airflow resistance) damaged by perforation using 0.4, 1.32, and 2.0 mm needles, respectively.[38] Particle size- and needle-diameter-dependent increased penetrations were observed for filters A and B, but not for filter C with the finest fiber size. In all three cases, the maximum penetration remained at particle sizes coarser than the largest particle size (30 nm) in the test.

Previous filter penetration studies for μm- and sub-μm-size range particles appears to have been completed mainly on face masks, where fitting is a major issue and the increase in penetration with increasing percent leakages in ULPA filters has been shown for the most penetrating particle size.[39] Studies have shown that the level of nanoparticle penetration is both structure- and material-dependent in various HEPA filter mediums.[32,40] Consequently, it is likely of great importance to test filter performances and effects of filter leaks using dusts from materials to which they will be challenged in the intended use. Such data could ensure that effects of specific dust size-ranges and other potentially relevant properties are covered in the test. However, such tests—e.g., of highly expensive pharmaceutical powders of limited quantities—may be difficult and costly following standard procedures. Therefore, faster and less-consuming procedures may be interesting for first assessments.

The objectives of this study were to:

1. investigate the dustiness characteristics of a group of molecular pharmaceutical powders and to demonstrate the potential use of the rotating drum dustiness test for evaluating the performance of damaged filters to realistic dusts from commercial powders with high cost and/or limited availability
2. demonstrate the potential use of the dustiness characteristics (dustiness levels, size distributions, and particle generation rate) and first-order modeling for assessment and scaling of the potential occupational exposure level using case-specific contextual information, and
3. demonstrate the use of first-order modeling and particle penetration data for damaged HEPA filters to estimate the potential transmission efficiency of active powder ingredients into company ventilation systems.

METHODS

Sample Materials

Samples included four different pharmaceutical active powder ingredients (hereafter called Pharma#1 to 4), which were all candidates for the same product. The four powders were dried molecular (primary molecule in the 1–100 nm range) active ingredients received as powders. All materials were hygroscopic and water-soluble organic compounds and therefore had a specific density close to 1 g/cm^3. The powders were stored in sealed bags at $-18^{\circ}C$ until use to prevent interaction with humid air during storage. The powders had slightly different macroscopic appearances. Pharma#1, 2, and 4 were all loose, fine-grained (flour-like) powders, whereas Pharma#3 consisted of mm-size granules. Pharma#2-4 were new alternatives to the existing product, Pharma#1. Their bulk (pour) densities were very low to low (0.16 (Pharma#4), 0.40 (Pharma#3 and Pharma#1), and 0.47 g/cm^3 (Pharma#2)) and determined by weighing the samples (n = 3; Type R162 P; Sartorius GmbH, Göttingen, Germany) immediately before dustiness testing using carefully pre-weighed 18.7 cm^3 stainless steel cups.

Dustiness Testing with Online Dust Size-distribution Measurements

All dustiness tests were completed using a down-scaled EN15051 rotating drum.[9] The small drum was 5.9 L with 3 symmetrically placed lifter vanes for powder agitation during rotation. A standard air-velocity through the drum was maintained at 11 L/min, using 50% RH-adjusted HEPA-filtered laboratory room air (Figure 1). Inhalable dust was collected at 9 L/min on 90 mm OD Cellulose-Nitrate filters (pore size = 0.8 μm) mounted in a filter cone at the end of the sampling line. The collection efficiency followed the calm-air curve from Dai et al.[41] as calculated by Schneider and Jensen.[9] The

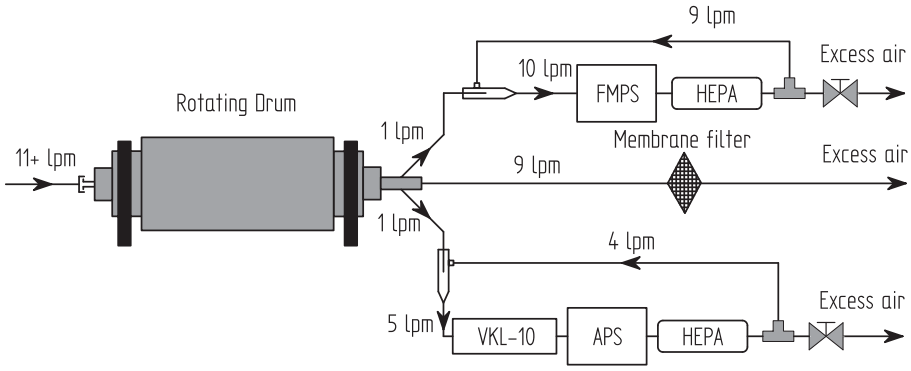

FIGURE 1. Schematic overview of the test and measurement setup used for dustiness testing.

particle number size distributions of the dusts were measured from the same sampling line using a Fast Mobility Particle Sizer (FMPS) (TSI model 3091, TSI Inc., Shoreview, Minn.) and an Aerodynamic Particle Sizer, (APS) (TSI, model 3021), respectively. The dust to the APS and the FMPS was sampled at 1 L/min and diluted with HEPA-filtered air. In the FMPS sampling tube, 9 L/min was added directly through a T-connection to meet the volume flow of the FMPS. For the APS, 4 L/min makeup air was first added through a mixing cone and further diluted using a VKL-10 diluter (Palas, GmbH, Karlsruhe, Germany) to reach 50 times dilution to ensure that the APS concentrations did not exceed 1000 particles/cm^3 (See Schneider and Jensen[9] for a full description of the setup).

All weighing, done after the cellulose-nitrate filters were conditioned at 20°C and 50% RH for at least 24 h, was done using a Sartorius microbalance (Type R162 P; Sartorius GmbH, Göttingen, Germany). For calculation of the gravimetric dustiness indices (mg dust/kg powder), the weighing data were corrected for both handling and conditional variations using blind filters as controls. Based on these data the quantification limit for weighing was 0.73 mg, calculated as three times the standard deviation of the blind filters.

Each dustiness test was done in triplicate, preceded with a "saturation" run for coating all inner surfaces of the test system with dust to prevent severe wall loss in the experiment. Each run was performed by loading the rotating drum with ca. 6 g powder on the upper side of a lifter vane positioned at bottom position, closing the drum, and conditioning the powder for 180 seconds in the 50% RH, 11 L/min airflow. The conditioning period was also used for collection of background measurements. After powder conditioning, the drum was rotated 180° to complete an alternative single drop test and stopped for another 180 seconds. Then the drum was rotated again to complete the rotation drum test at 11 rpm for 60 seconds, after which data were recorded for an additional 60 seconds, to collect the residual dust in the system. See Figure S1 for a typical test time series as measured with FMPS and APS.

Particle Penetration through Damaged HEPA Filters

Particle filter penetration was tested on 25-mm ID H14 class HEPA filter sheets (Camfill Farr, Søborg, Denmark) subjected to three damage levels (ca. 0.25, 0.6, and 1 area percent) using Pharma#1 powder. Undamaged filter sheets were tested for reference. The damage levels were induced by symmetrically piercing the filters 13 times using 0.10, 0.25, and 0.36 mm OD Pt needles, respectively (see Figure S2). The tested HEPA filter medium (ca. 0.4 mm thick; 8.2587 μg/cm^3) was made of nonwoven glass fibers with diameters ranging from a few hundred nm to around 6 μm (see Figure S2). According to the manufacturer, the pressure drop was up to 6 mbar and the filter efficiency was 99.975% for 0.3 μm particles. The tested H14 filter was supplied by an anonymous industrial partner and is used in a wide range of industrial powder, food, and pharmaceutical production facilities.

Figure 2 illustrates the experimental setup for the particle filter penetration measurements and includes parallel measurement with two FMPS' and one APS. One FMPS measured dust directly from the sampling line, diluted 1:9 as done for normal dustiness testing. The other FMPS and the APS measured in parallel 1:9 and 1:49 diluted air directly after passage through 25 mm ID flow-through filter mounts. Comparison between the two FMPS instruments showed episodic concentration variations of up to 15% for individual channels. However, use of multi-channel data averaged over the experimental time spans enables identification and elimination of sudden changes in instrument performance.

The filter mounts and filter-support grids were made of stainless steel and an O-ring used to fix the filter on the inlet side was made of Teflon. Air-tight assembly was ensured by a screw-lock assembling the top and bottom side of the filter mount. The 1 L/min volume-flow through the filter mount resulted in a filter face velocity of 3.4 cm/s. This is 22.5% higher than recommended (2.775 cm/s) and may result in a slight downward shift in the most-penetrating particle size.[42,43]

The normal dustiness testing experiments were completed using ca. 6 grams of powder for each damage level, with the sampling durations. First, initial background measurements

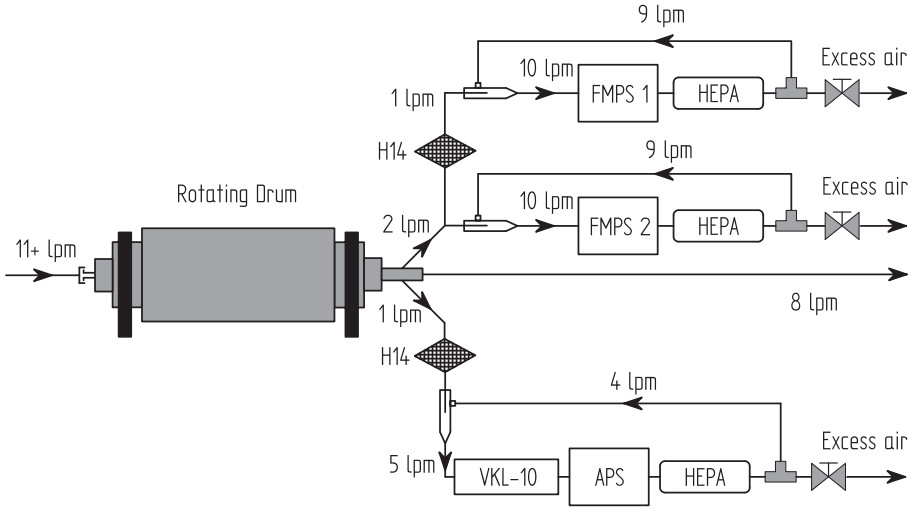

FIGURE 2. Schematic overview of the test and measurement setup used for measurements of filter penetration.

were made for 180 seconds followed by 180 seconds of rotation and another 180 seconds of data recording after rotation. The extended duration was chosen to ensure a high filter loading and an extended measurement time of the filter performance.

The strategy and setup for filter testing does not resemble the existing standard (EN 1822-1:2009) for testing of flat filter mediums.[44] Most importantly, the exposed filter area was about 20% of the standard 100 cm^2 and the number of repeats was three instead of five. Even though the standard permits the use of two separate instruments for data recording, one upstream of the filter and one downstream, it does not mention the FMPS and favors the use of a single instrument alternating between the two. This method is, however, not possible in our case, because the test aerosol is usually not delivered from the rotating drum at a uniform rate. Moreover, the particle release from the damaged filters may occur in short bursts due to caking and additional filter rupture with time, which can only be measured with high time-resolution instruments.

Data Treatment

The calculation of particle number size-distribution and total particle concentrations for the dustiness tests were done taking into account flow rates through the drum and dilution. The Particle Generation Rate (PGR), at time i, was calculated according to Equation 1 as first described in Jensen et al.[6] and Schneider and Jensen[9]

$$PGR_i = \frac{k}{\Delta t}\left(C_i - C_{i-1}e^{-\frac{\Delta t}{\tau}}\right) \quad \textbf{(1)}$$

In Equation 1

k is the volume of the dustiness drum, Δt is the time interval (1 s),

C is the volume concentration

τ is a measured time constant which has previously been shown to be 20 seconds.[9]

For calculation of penetration through damaged H14 filters, only data from 16 FMPS channels with midpoints ranging from 60.4 to 523.3 nm were used as the remaining channels were too noisy for such a comparison. The penetration ratio, P, was calculated for each size bin, D_p, and measurement run using the particle concentrations, N as shown in Equation 2. Quantification for larger particles was not possible due to availability of only one APS, but transmitted particles were detected (See Figure S3).

$$P_{Dp} = \frac{\sum_{t=0}^{180} N_{FMPS1,Dp}}{\sum_{t=0}^{180} N_{FMPS2,Dp}} \quad \textbf{(2)}$$

In Equation 2, the time, t, is counted from the beginning of the rotation part of the test. An average penetration for each size bin and filter type was thereafter calculated.

Statistics

A paired three-tail T-test was applied to assess the similarity between the different dustiness measurements using the default statistics in Microsoft Excel 2003 SP3. Differences at p-values below 0.05 were assumed to be statistically significant; values between 0.05 and 0.1 were assumed borderline significant, and data with p-values larger than 0.1 were considered statistically similar. Error bars and error values in tables and figures denote one standard deviation.

Assessment of Exposure Potential and Accidental Dust Transmission Into Air Ducts

The emission potential and potential near- (NF) and far-field (FF) worker exposure was estimated using the equations from the Advanced REACH Tool (ART),[45] implemented in MatLab (version R2012b) and the dustiness data. The dustiness indexes (mg/kg) were used to calculate the amount of dust (mg) that potentially could be aerosolized per mass unit of powder handled. The use of dustiness data as input data for exposure

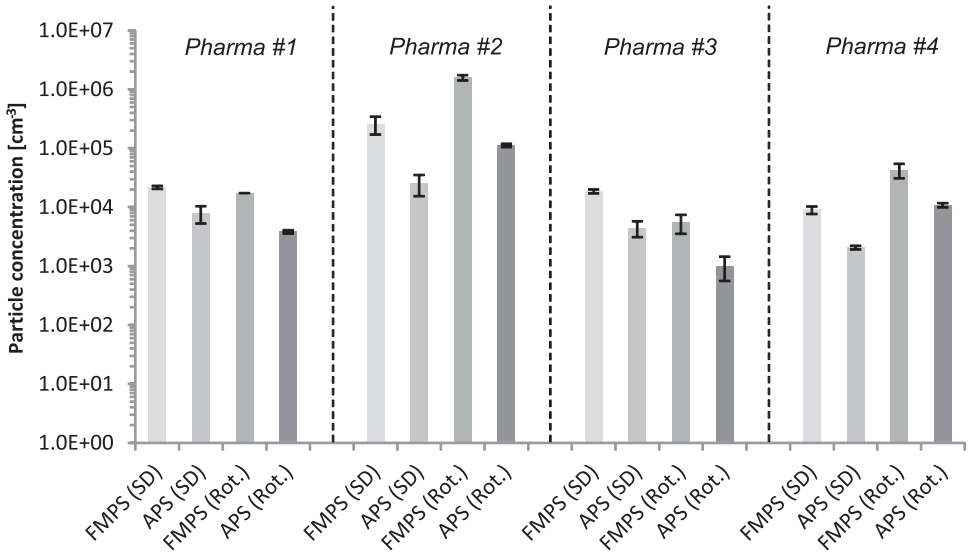

FIGURE 3. 10 sec: average peak number concentrations during the single drop (SD) and rotation (Rot.). Error bars denote one standard deviation.

assessment is implemented in ART and for nanomaterials has also previously been discussed, for example in Schenider and Jensen et al.[9] The assumption is that the dustiness level given by the rotating dustiness drum correlates with the dust release potential during powder handling. This relation is given by the handling factor, h, set to 0.3 in this study as recommended for pouring activities by Cherrie and Schneider.[46] The NF was defined as a virtual cube of 2 m^3 surrounding the activity and the FF is the remaining air volume in the room. The work situation simulated consisted of five 3-min episodes of pouring 20 kg powder into a dissolver over a total work-period of 8 hr. The work-room was 10 × 4 × 3 m^3 and had a ventilation rate of 10 h^{-1}. Assessments of worker exposure were made for all powders using Equations 3 and 4 for NF and FF mass concentrations, C, respectively.

$$V_{NF} \cdot \frac{dC_{NF}}{dt} = \varepsilon_i - C_{NF} \cdot Q_{NF} + C_{FF} \cdot Q_{NF} \quad \textbf{(3)}$$

$$V_{FF} \cdot \frac{dC_{FF}}{dt} = C_{NF} \cdot Q_{NF} - C_{FF} \cdot Q_{NF} - C_{FF} \cdot Q_{FF} \quad \textbf{(4)}$$

In Equation 3 and 4,

V is the volume
Q is the flow in and out of the respective NF and FF volumes
ε_i is the particle emission rate.

Similarly, the accidental dust transmission into the ventilation air ducts through damaged HEPA filters was assessed for Pharma#1 assuming that the sizes and number of particles released per mass of handled powder was the same as in the dustiness test. The number and size distribution of fine particles potentially penetrating the damaged HEPA filters could be assessed from the HEPA filter penetration curves, assuming that the particle size distribution in the FMPS range remained unchanged during transport from the source to the filter. Finally, the total mass passing the HEPA filter during an 8-hr workday and mass concentration in the duct airflow was calculated assuming spherical particle shape and unity density of the dust particles.

RESULTS AND DISCUSSION

Total Concentrations

Figure 3 gives an overview of the peak emission number concentrations emitted from 6 g of test material, using both single drop and a rotation test using the FMPS and the APS, respectively. The values are calculated as 10-sec averages from the highest release period in each of the three runs except for Pharma#1, where only two valid tests were performed. In both single drop and rotation tests, the FMPS concentrations are about 2 to 15 times higher than APS concentrations, demonstrating that dustiness in number concentrations is dominated by particles under 560 nm.

Size Distributions

Figure 4 shows 5-sec averages of the particle number size distribution spectra at the initial single drop burst as well as at the initial peak and at the end of the rotation test for each of the powders, respectively. Because, the FMPS and APS measures the mobility equivalent and aerodynamic equivalent particle sizes, respectively, the size distributions are not to be considered a continuous spectra. However, if we assume that the particle-effective densities are close to the specific densities of the powders (ca. 1 g/cm^3) differences between the two types of diameters can be considered small. Both single-drop and rotating drum tests produced trimodal particle size distributions for all four powders tested. Two main peak sizes are located at around 250 nm and 2 μm, respectively. The third mode is observed as a "shoulder" below the 250 nm mode, with

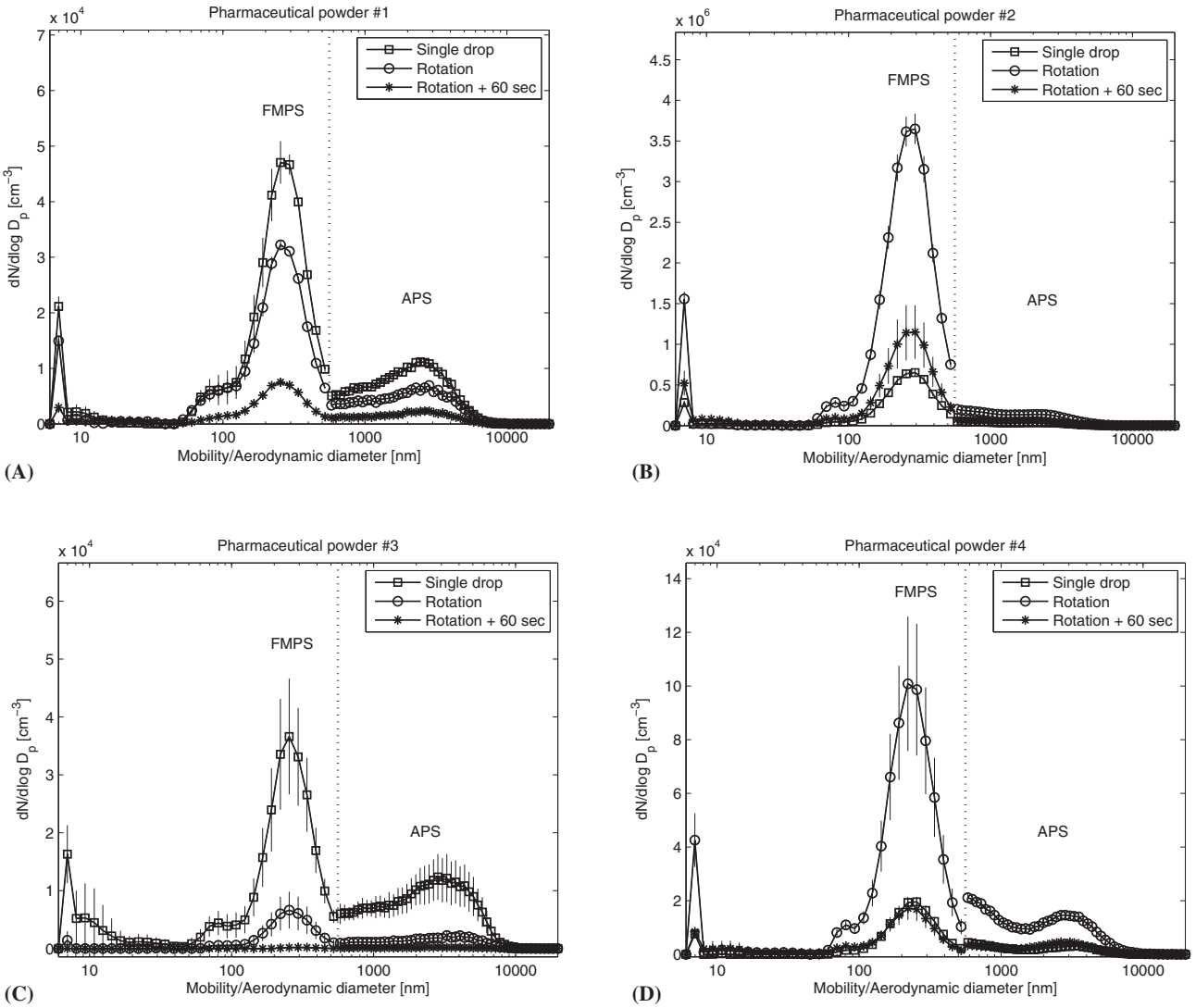

FIGURE 4. Plot of 5-sec averaged particles number size distributions of dust generated by single drop (peak concentration) and rotating drum (peak concentration and 60 sec thereafter) dustiness testing: a) Pharma#1, b) Pharma#2 (note the expanded scale as compared to a, c, and d), c) Pharma#3, d) Pharma#4. Error bars denote one standard deviation.

peak sizes between 60 and 80 nm. Peaks located at the 7 nm channel are considered phantom peaks and not measurements of actual primary particles. Similar phantom peaks have been observed before.[6]

From the particle number and number size distribution plots, Pharma#2 is clearly dustier than the other powders. The shape of the dust size distribution spectra of Pharma#1, 2, and 3 is almost similar between the 2 μm modes and the lower size limit of the APS. In Pharma#4 the APS spectrum is different, showing increasing numbers with decreasing size, which results in an apparent independent size-mode at around 700 nm. It is possible, however, that this could be a continuation of the mode seen within the FMPS range.

Completing a three-modal, log-normal fitting of the particle size distributions, according to Makela et al.,[47] we calculated the position and number of particles in each size mode at the peak concentration for each powder during the rotating drum dustiness testing (Table I). In accordance with the visual observation, the fitting identifies the two main modes with geometric mean diameters (GMD) of roughly 250 nm and at 2–2.5 μm. Particles between these two modes did not have modal structure. The third mode is the smallest mode with fitted positions between 66 and 86 nm. By number, all dusts are highly dominated by sub-μm to nm-size particles with the μm mode making 9.7 (Pharma#2) to 37.6% (Pharma#3) by number of the dust (Table I). All four powders showed statistically significantly different modal distributions with only Pharma#1 and Pharma#3 having statistically similar peak positions for peak 1 ($\sim$90 nm) and peak 2 ($\sim$260 nm).

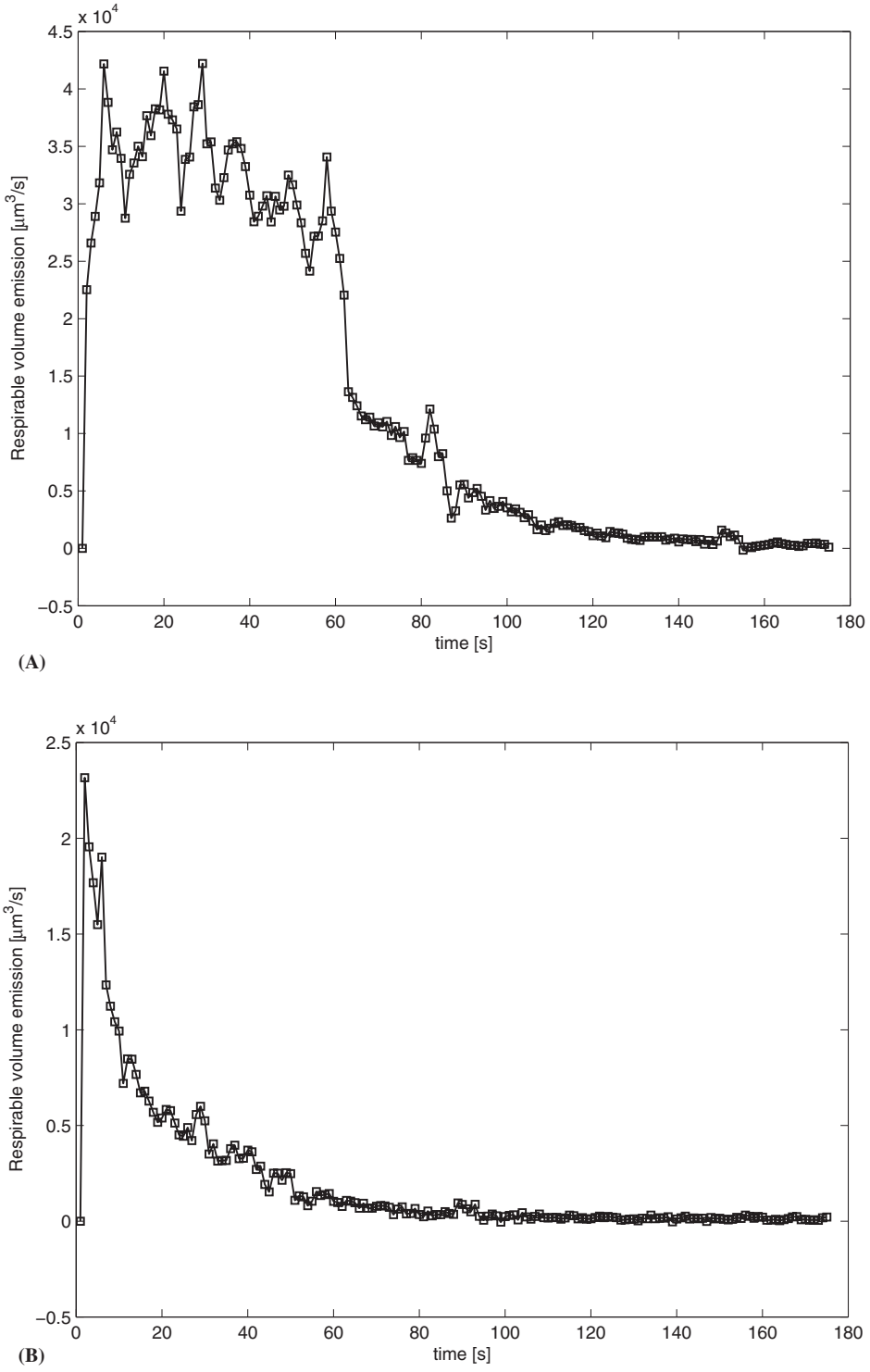

FIGURE 5. Particle generation rate during rotating drum testing of: **a)** Pharma#1. **b)** Pharma#3.

Particle Generation Rate

The PGR was calculated for the equivalent spherical volume data and is therefore dominated by contributions from particles above 1 μm. Two different general PGR evolution patterns were observed for these Pharma powders. For Pharma#1, #2, and #4, the PGR initially increases and then remains more or less constant over the entire rotation time (Figure 5a). The granular Pharma#3 showed a different PGR with a rapid initial

TABLE I. Size Modes and Modal Particle Numbers Calculated Using Log-Normal Fitting

	Mode 1	Mode 2	Mode 3
Pharma#1			
ρ	1.25	1.48	1.83
GMD [μm]	$8.57{\cdot}10^{-2}$	$2.58{\cdot}10^{-1}$	2.22
N [cm^{-3}]	$1.25{\cdot}10^{3}$	$1.33{\cdot}10^{4}$	$4.30{\cdot}10^{3}$
Pharma#2			
ρ	1.06	1.45	2.25
GMD [μm]	$6.60{\cdot}10^{-2}$	$2.70{\cdot}10^{-1}$	2.31
N [cm^{-3}]	$2.36{\cdot}10^{4}$	$1.49{\cdot}10^{6}$	$1.62{\cdot}10^{5}$
Pharma#3			
ρ	1.13	1.41	1.98
GMD [μm]	$7.89{\cdot}10^{-2}$	$2.61{\cdot}10^{-1}$	2.52
N [cm^{-3}]	$6.46{\cdot}10^{1}$	$2.47{\cdot}10^{3}$	$1.53{\cdot}10^{3}$
Pharma#4			
ρ	1.09	1.44	1.54
GMD [μm]	$7.04{\cdot}10^{-2}$	$2.33{\cdot}10^{-1}$	2.94
N [cm^{-3}]	$7.19{\cdot}10^{2}$	$3.98{\cdot}10^{4}$	$7.02{\cdot}10^{3}$

GMD denotes the geometric mean diameter, N the modal particle concentration, and ρ the geometric standard deviation of the mode.

burst followed by an almost exponential decay to zero during the remaining period of the rotation test (Figure 5b). Both PGR evolution patterns have been previously reported for inorganic (mineral) powders.[6,9] The rapid decay of PGR for Pharma#3, in addition to low dustiness by particle numbers, might suggest less total exposure potential if the powder work process involves repeated agitation.

Dustiness Levels

Figure 6 presents the mass-based dustiness index and the total number of particles emitted during the single drop event and the rotation. The mass-based dustiness indices varied significantly with Pharma#2 (14,501 $\pm$ 1,720 mg/kg) and #4 (10,013 $\pm$ 709 mg/kg) having the highest dustiness indices. Pharma#2 also shows a much higher number of fine particles in the FMPS size range than the other powders, but a greater number of particles were also generated in the APS size-ranges. Pharma#1 and #4 show roughly the same number concentrations in FMPS measurements, but the ca. five times greater number of APS-size particles in rotation tests with Pharma#4 can explain the higher mass-based dustiness index of Pharma#4.

Comparison with the EN15051 dustiness ranking showed that Pharma#1 and #3 have moderate inhalable dustiness levels and Pharma#2 and #4 have high levels. To further put the results into perspective, Figure 7 compares the dustiness indices of the pharmaceutical powder ingredients with dustiness indices of 13 other powders previously studied on the same system.[6,9,48,49] This comparison shows that the inhalable dustiness levels of Pharma#2 and #4 surpass the values of all other powders previously reported for this system. The inhalable dustiness of Pharma#1 and #3 ranks at intermediate levels, but these levels are nonetheless still in the upper 50% of the previously tested powders.

Performance of Damaged HEPA Filters

Figure 8 shows the particle size-dependent penetration for the three different damage levels tested in the H14 class HEPA filter segments. Filter damage resulted in decreased filter performance and all three damage levels resulted in maximum penetration of particle sizes around 70 nm and a minimum plateau between 200 and 560 nm. The penetration ratio for the

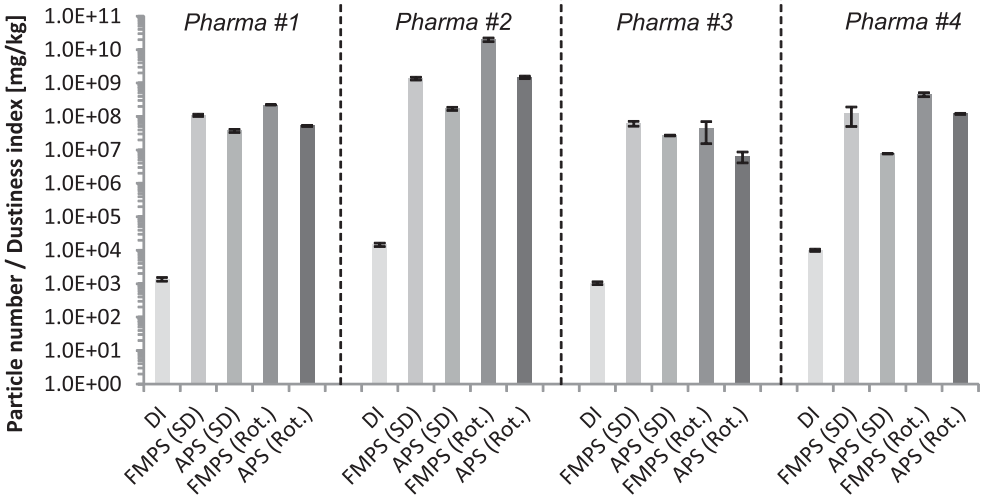

FIGURE 6. Mass-based dustiness indices (DI) and total emitted particles during single drop (SD) and rotation (Rot.) for the four pharmaceutical powders. Error bars denote one standard deviation.

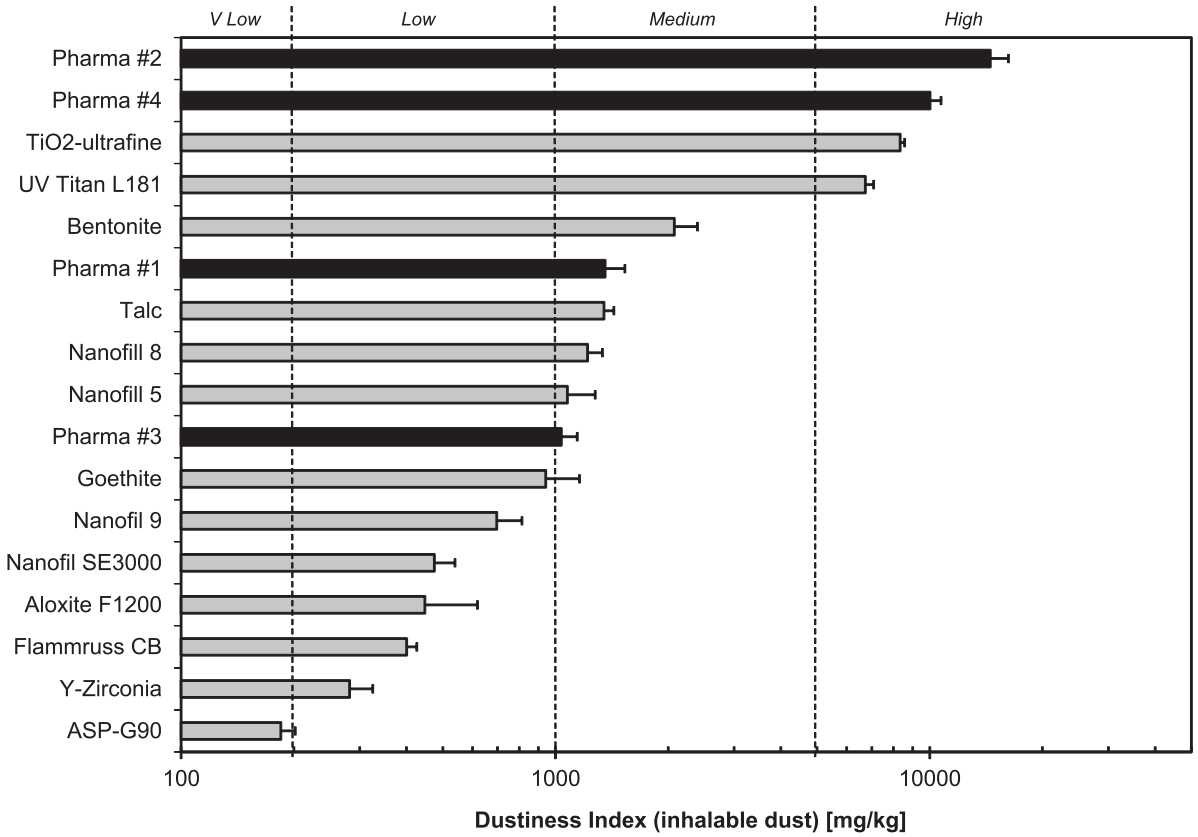

FIGURE 7. Comparison of inhalable dustiness indices for powders measured using the small rotating drum method and sampling of inhalable fraction (calm air). Limit values for EN15051 ranking of powder dustiness are shown. Inserted dustiness classes are from the EN15051 standard. Error bars denote one standard deviation.

most penetrating particle size varied from 0.03 to 1 at 0.10 and 0.36 mm pinholes, respectively. Our measurements of undamaged filters rendered particle concentrations below the detection limit for the FMPS and suggest that the undamaged filters live up to its requirements.

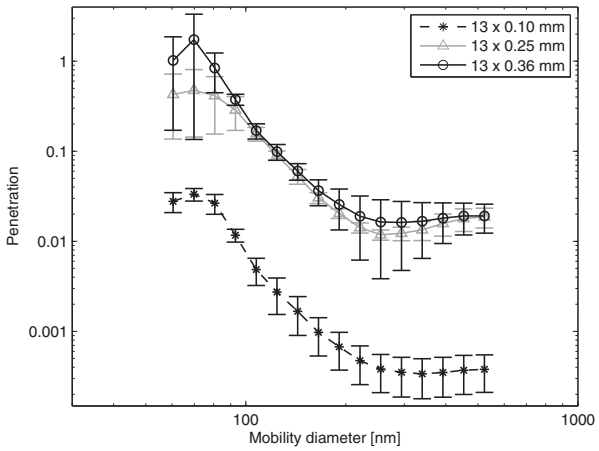

FIGURE 8. Size-dependent particle penetration for H14 filters with three different levels of applied pinhole damage. Data for the undamaged filter are not shown due to particle counts below the minimum detection limit. Error bars denote one standard deviation.

A plausible reason for the observed particle penetration profiles would be that the relatively large pinholes caused the airflow facing the filter to lose its laminar behavior ($Re<500$ without pinholes) and gain an increased flow through the pinholes. Whereas smaller particles (60–80 nm) can follow the bend in airflow towards these holes, the larger particles (>120 nm) are more likely to follow their initial path and impact the undamaged filter surface. In addition, the particle penetration did not always occur continuously over time, but, instead, in one or several bursts. This phenomenon may be due to dust buildup on the filter during sampling, from which lumps of dust are released again through the damage holes in episodic events and/or events of filter rupture. This observation has implications for the procedures by which filter evaluations should be performed. There may be several types of damage to the filter during usage and the pinhole damage used within this study represents but one of these possible damage types.

Independent from the different potential penetration mechanisms, decreased filter performance was observed for even small damage levels (0.25 to 1 area%) with 13 sub-mm-size pinholes as compared to producer specifications of particles penetration through undamaged filter. Consequently, such

TABLE II. Modeled Acute and Daily Levels of Exposure (mg/m^3) to Inhalable Dust in the Near-Field and Far-Field Work Area

Sample	Pharma#1	Pharma#2	Pharma#3	Pharma#4
Acute (15 min) near-field	0.700	7.474	0.534	5.161
Acute (15 min) far-field	0.003	0.035	0.002	0.024
8-hr average near-field	0.227	2.427	0.173	1.675
8-hr average far-field	0.001	0.012	0.001	0.008

filter damage is potentially critical in "sensitive" productions. We could not quantify the penetration for the coarser APS-size particles without a parallel data set with use of two similar instruments. However, damage-dependent levels of penetration were observed and the resulting APS size distributions are shown in Figure S3.

Assessment of Exposure Risk

Despite the fact that dustiness levels provide direct information on the relative potential for exposure, first order modeling of the potential exposure levels may provide better data for exposure assessment, because the exposure depends on several contextual conditions.[18] In agreement with the dustiness ranking, ART[16] modeling showed highest exposure levels of inhalable dust for Pharma#2 and lowest for Pharma#4 (Table II). The acute (15 min) NF exposure levels were predicted to be 7.5 mg/m^3 (Pharma#2), 5.2 mg/m^3 (Pharma#4), 0.7 mg/m^3 (Pharma#1), and 0.5 mg/m^3 (Pharma#3) mg/m^3. Hence, the potential NF exposure level of Pharma 2 exceeds the 6 mg/m^3 acute exposure limit for total organic dust established by the Danish Working Environment Authority. The maximum potential 8-hr daily exposure was 2.4 and 0.012 mg/m^3 in the NF and FF, respectively. Naturally, the modeled exposure concentrations should be considered conservative estimates, because the ART model neglects such factors as particle agglomeration, wall loss, and gravimetric sedimentation. However, the modeled data give context-specific ranking and suggest that if the powders have high toxicity, even the estimated μg/m^3 exposure levels in the FF may require further risk management. In any case, based on dustiness data and assessed exposure levels, Pharma#3 or alternatively Pharma#1 are the most favorable powder ingredients. Considering also the PGR (Figure 5), the lower release rate during repeated agitation observed for the granular Pharma#3 might additionally make this material preferable to Pharma#1.

Assessment of Filter Penetration

Considering the estimated exposure levels above, it is clear that extensive load of total dust may also reach the workplace ventilation systems. Whereas undamaged filters will have a high degree of filtration efficiency, we demonstrated that even small levels of damage result in considerable decrease in filter efficiency for small particles. By numbers, the penetration ratio of particles reaches close to 1 for particles around 70–80 nm, but only around 0.01 at the range where the studied pharmaceutical powders have their maximum peak concentrations (Figure 8). Hence, the observed particle penetration in damaged HEPA filters may be of concern.

Again using the ART exposure model with the particle number dustiness levels acquired for Pharma#1 in the rotating drum test, calculations suggest that the NF and FF peak concentrations would reach $4.0 \cdot 10^6$ #/m^3 and $1.8 \cdot 10^4$ #/m^3 (Figure 9). Modeling also predicted that almost all particles would be ventilated out approximately 1.5 hr after the final handling incident. However, this may not be the case using the dustier Pharma#2 and #4 in the model. Handling of these powders would result in an approximately 77.8 (Pharma#2) and 2.1 (Pharma#4) times higher number concentrations than Pharma#1 in the first event.

Knowing the number of particles generated during handling allows us to calculate the accumulated size distribution penetrating the ventilation filters for each of the three damage levels (Figure 10). The number size distribution has a peak penetration at 70 nm and a lower plateau stretching between 100 and 300 nm (Figure 10a). The corresponding spherical equivalent volume size distribution also shows a peak at approximately 70 nm, but it is clear that by volume the coarser penetrating

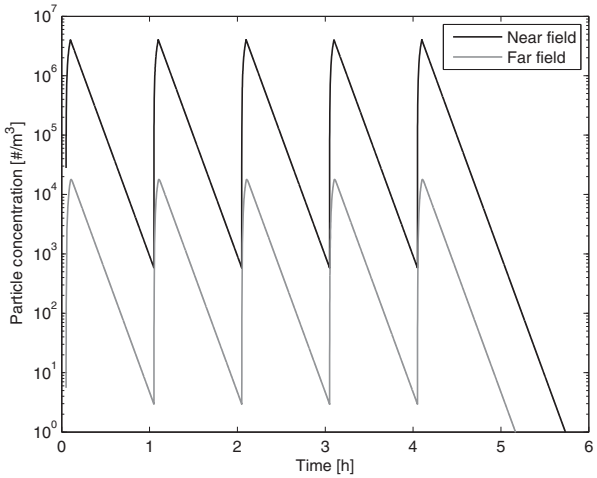

FIGURE 9. Simulated particle concentration for near-field and far-field using equations from the ART exposure model. See text for further explanation.

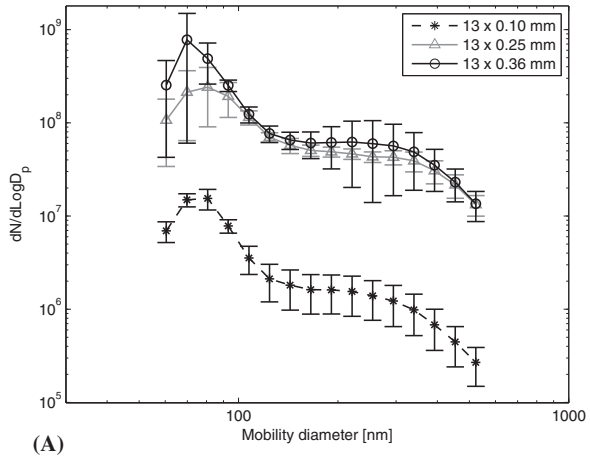

FIGURE 10. a) Accumulated size distribution of Pharma#1 particles penetrating H14 filter during work situation simulation; b) Volume size-distribution of particles penetrating the H14 filter at the three different damage levels, respectively. Error bars denote one standard deviation.

particles still outweigh the nano-size particles (Figure 10b). For Pharma 1, this results in a primary volume peak size at 200 nm or above.

The accumulated FMPS range volume-size-distribution allows us to estimate the dust concentration in the air duct and the total amount of process-generated powder penetrating the damaged H14 filter (Table III). In this calculation, we use the volume-flow of 1200 m^3/h given by the air-exchange in the work scenario and assume unit density, spherical size of the dust particles, and no particle loss between the source and the air duct or during transmission from the air duct. The results show that for Pharma#1, a total of $9.3{\cdot}10^{-6}$ to $4.3{\cdot}10^{-4}$ mg of dust may be transmitted through the air duct in the FMPS size range per day in the work scenario (Table III). Considering the volume flow in the work scenario, this would amount to air duct concentrations ranging from $1.3{\cdot}10^{-9}$ to $6.0{\cdot}10^{-8}$ mg/m^3 at the lowest and highest damage levels, respectively (Table III). These concentrations are not dramatic, but may still not be acceptable for factories dealing with biologically highly active substances. A shift to one of the very dusty powders (e.g., Pharma#2 with an almost 78 times higher number concentrations) and/or larger scale use would increase the accidental air duct transmission considerably. Modeling was only possible for the fine FMPS size ranges. Penetration of coarser particles was observed (Figure S3) and transmission of even a low number concentration of these coarse particles would increase the mass concentration considerably.

CONCLUSION

The main objectives of this study were to: 1) investigate the dustiness characteristics of four molecular pharmaceutical powders with focus on whether they might release nano-size dust particles and whether differences in the emission characteristics occur between different molecular powder ingredients with similar intended use; 2) investigate the potential use of the rotating drum dustiness test system for evaluation of the performance of pristine and damaged filters compared to realistic workplace particles; and 3) demonstrate the use of dustiness levels as an input parameter for exposure modeling and product selection taking specific contextual conditions into consideration.

The inhalable dustiness indices of the four powders were all statistically significant different: Pharma#2 (14,501 mg/kg) > Pharma#4 (10,013 mg/kg) > Pharma#1 (1,358 mg/kg) > Pharma#3 (1,036 mg/kg). Pharma#2 and #4 were the dustiest materials tested so far with this method. Moreover, the tested powders had a nanoparticle size mode between 66 and 86 nm, which has not been observed before in rotating drum dustiness testing. Additional typically observed size modes were found at 230 to 270 nm and a secondary peak between 2.2 and

TABLE III. Calculated Penetrated Mass and Air Duct Mass Concentration of Pharma#1 Particles Penetrating H14 Filter During Work Situation Simulation

Filter damage	Penetrated mass [mg]	Mass concentration [mg/m^3]
13 × 0.10 mm	$9.3{\cdot}10^{-6}$ ($\pm$ $4.1{\cdot}10^{-6}$)	$1.3{\cdot}10^{-9}$ ($\pm$ $5.7{\cdot}10^{-10}$)
13 × 0.25 mm	$3.6{\cdot}10^{-4}$ ($\pm$ $8.6{\cdot}10^{-5}$)	$5.0{\cdot}10^{-8}$ ($\pm$ $1.2{\cdot}10^{-8}$)
13 × 0.36 mm	$4.3{\cdot}10^{-4}$ ($\pm$ $2.2{\cdot}10^{-4}$)	$6.0{\cdot}10^{-8}$ ($\pm$ $3.1{\cdot}10^{-8}$)

Note: Error values denote one standard deviation.

2.9 μm. The granular Pharma#3 had a lower dustiness level and released most of the dust in an acute burst, as compared to the other powders.

The rotating dustiness drum test set can facilitate performance evaluation of damaged filters challenged to realistic workplace particles using high size- and time-resolution monitors for quantification. However, there are limitations due to a relatively poor detection limit for small nanoparticles using the FMPS. In the H14 HEPA filter tested, the highest particle number penetration ratios were found for 70–80 nm-size particles and reached 1 between the two highest damage levels. The penetration ratio for 300–560 nm-size particles reached 0.01 to 0.03 at the two highest damage levels, but would be most significant by weight.

First-order exposure modeling of pouring 20 kg powder five times during an 8-hr work shift showed risk of excessive inhalable dust exposure to the pharmaceutical powder ingredients. Near-field dust concentrations exceeded acute occupational exposure limits for ordinary total organic dust for the dustiest powder. Estimates of the potential dust transmission after penetration through damaged HEPA filters suggest that air duct concentrations only reach pg/m^3 concentrations in the FMPS size-range. Hence, at the tested damage levels, accidental release and risk of cross-contamination only appear critical for highly dusty powders or high-volume productions.

This study demonstrates the potential use of dustiness and filter testing for elaborated exposure assessment for early risk management. We demonstrate the ability to assess worker safety by dustiness data combined with first-order modeling, which showed that different powder candidates for similar use can have widely different dustiness characteristics and estimated exposure levels. The results reveal that H14 filter penetration of particles is likely to occur at filter damage levels similar to those found in actual in-use ventilation systems. Depending on the nature of the active ingredients, the estimated concentrations could give rise to a significant daily mass transfer through air ducts. Therefore, accidental air duct dust transfer could also be a source of cross-contamination of powders and occupational particle exposure. In the specific work scenario presented in this article, the granular Pharma#3 and the in-use fine Pharma#1 powder were the powder candidates associated with the lowest risk of exposure and transmission into damaged HEPA-filtered ventilation systems.

ACKNOWLEDGMENTS

This work was conducted as part of the Strategic Research effort at the National Research Centre for the Working Environment and the Danish Centre for Nanosafety (20110092173/3) from the Danish Working Environment Research Foundation. For the experimental part we gratefully acknowledge constructive discussion and access to sample material from an anonymous industrial partner and the skilled assistance from our technician S.H. Nielsen. We also thank Dr. K.I. Kling (NRCWE) for SEM-imaging of the HEPA filter.

REFERENCES

1. **Boundy, M., D. Leith, and T. Polton:** Method to evaluate the dustiness of pharmaceutical powders. *Ann. Occup. Hyg. 50*(*5*):453–458 (2006).
2. **Hamelmann, F., and E. Schmidt:** Methods for dustiness of industrial powders. *China Particuology 03*(*01n02*):90–93 (2005).
3. **British Standards Institute and British Standards Institution:** *Workplace Atmospheres: Measurement of the Dustiness of Bulk Materials - Requirements and Reference Test Methods.* London**:** British Standards Institution, 2006.
4. **Ibaseta, N., and B. Biscans:** Ultrafine aerosol emission from the free fall of TiO2 and SiO2 nanopowders. *Kona-Powder and Particle 25*:190–204 (2007).
5. **Dahmann, D., and C. Monz:** Determination of dustiness of nanostructured materials. *Gefahrstoffe Reinhaltung der Luft 71*(*11–12*):481–487 (2011).
6. **Jensen, K.A., I.K. Koponen, P.A. Clausen, and T. Schneider:** Dustiness behaviour of loose and compacted bentonite and organoclay powders: What is the difference in exposure risk? *J. Nanoparticle Res. 11*(*1*):133–146 (2009).
7. **O'Shaughnessy, P.T., M. Kang, and D. Ellickson:** A novel device for measuring respirable dustiness using low-mass powder samples. *J. Occup. Environ. Hyg. 9*(*3*):129–139 (2012).
8. **Pensis, I., J. Mareels, D. Dahmann, and D. Mark:** *Comparative Evaluation of the Dustiness of Industrial Minerals According to European Standard EN 15051* [Standard], 2006. *Ann. Occup. Hyg. 54*(*2*):204–216 (2010).
9. **Schneider, T., and K.A. Jensen:** Combined single-drop and rotating drum dustiness test of fine to nanosize powders using a small drum. *Ann. Occup. Hyg. 52*(*1*):23–34 (2008).
10. **Tsai, C.J., C.H. Wu, M.L. Leu, et al.:** Dustiness test of nanopowders using a standard rotating drum with a modified sampling train. *J. Nanoparticle Res. 11*(*1*):121–131 (2009).
11. **Jensen, K.A., A.T. Saber, I.K. Koponen, H.V. Kristensen and H. Wallin. Nanosafer:** A flexible web-based control-banding tool for precautionary risk evaluating of dust exposure to manufactured nanomaterials in the work-place.
12. **Paik, S.Y., D.M. Zalk, and P. Swuste:** Application of a pilot control banding tool for risk level assessment and control of nanoparticle exposures. *Ann. Occup. Hyg. 52*(*6*):419–428 (2008).
13. **Tielemans, E., D. Noy, J. Schinkel, et al.:** Stoffenmanager Exposure Model: Development of a quantitative algorithm. *Ann. Occup. Hyg. 52*(*6*):443–454 (2008).
14. **Van Duuren-Stuurman, B., S.R. Vink, K.J.M. Verbist, et al.:** Stoffenmanager nano version 1.0: A web-based tool for risk prioritization of airborne manufactured nano objects. *Ann. Occup. Hyg. 56*(*5*):525–541 (2012).
15. **Evans, D.E., L.A. Turkevich, C.T. Roettgers, G.J. Deye, and P.A. Baron:** Dustiness of fine and nanoscale powders. *Ann. Occup. Hyg. 57*(*2*):261–277 (2013).
16. **Cherrie, J.W., A.T. Gillies, A. Sleeuwenhoek, et al.:** Modelling exposure to pharmaceutical agents. *J. Phys. Conf. Ser. 151*(*012063*) (2009).
17. **Mc Donnell, P.E., J.W. Cherrie, A. Sleeuwenhoek, A. Gilles, and M.A. Coggins:** Refinement and validation of an exposure model for the pharmaceutical industry. *J. Environ. Monitor. 13*(*3*):641–648 (2011).
18. **Schneider, T., D.H. Brouwer, I.K. Koponen, et al.:** Conceptual model for assessment of inhalation exposure to manufactured nanoparticles. *J. Exposure Sci. Environ. Epidemiol. 21*(*5*):450–463 (2011).
19. **Binks, S.P.:** Occupational toxicology and the control of exposure to pharmaceutical agents at work. *Occup. Med.-Oxford 53*(*6*):363–370 (2003).
20. **Larsen, A.I., C.R. Johnsen, J. Frickmann, and S. Mikkelsen:** Incidence of respiratory sensitisation and allergy to enzymes among employees in an enzyme producing plant and the relation to exposure and host factors. *Occup. Environ. Med. 64*(*11*):763–768 (2007).

21. **Michaels, D., and C. Monforton:** Scientific evidence in the regulatory system: Manufacturing uncertainty and the demise of the formal regulatory system. *J. Law & Policy 13*:17–41 (2005).
22. **Watrous, R.M.:** Health hazards of the pharmaceutical industry. *Br. J. Indus. Med. 4*(*2*):111–125 (1947).
23. **Wollowitz, S.:** Managing high-potency active pharmaceutical ingredients-A drug sponsor's guide. *Drug Develop. Res. 71*(*7*):420–428 (2010).
24. **Touger-Decker, R., and C. van Loveren:** Sugars and dental caries. *Amer. J. Clin. Nutr. 78*(*4*):881S–892S (2003).
25. **Johnsen, C.R., T.B. Sorensen, A.I. Larsen, et al.:** Allergy risk in an enzyme producing plant: A retrospective follow up study. *Occup. Environ. Med. 54*(*9*):671–675 (1997).
26. **Vanhanen, M., T. Tuomi, U. Tiikkainer, et al.:** Sensitisation to enzymes in the animal feed industry. *Occup. Environ. Med. 58*(*2*):119–123 (2001).
27. **Gorski, P., and S. Ulinski:** Effect of occupational exposure to opiates on the respiratory system. *Intern. J. Occup. Med. Environ. Health 9*(*3*):245–253 (1996).
28. **Heron, R.J.L., and F.C. Pickering:** Health effects of exposure to active pharmaceutical ingredients (APIs). *Occup. Med.-Oxford 53*(*6*):357–362 (2003).
29. **Hubbs, A.F., R.R. Mercer, S.A. Benkovic, et al.:** Nanotoxicology-A pathologist's perspective. *Toxicologic Pathol. 39*(*2*):301–324 (2011).
30. **Murashov, V.:** Occupational exposure to nanomedical applications. *Wiley Interdisciplinary Reviews-Nanomed. Nanobiotech. 1*(*2*):203–213 (2009).
31. **Schneider, T., and K. Jensen:** Relevance of aerosol dynamics and dustiness for personal exposure to manufactured nanoparticles. *J. Nanoparticle Res.* (2009).
32. **Golanski, L., A. Guiot, F. Rouillon, J. Pocachard and F. Tardif:** Experimental evaluation of personal protection devices against graphite nanoaerosols: fibrous filter media, masks, protective clothing, and gloves. *Human Experiment. Toxicol. 28*(*6–7*):353–359 (2009).
33. **Rengasamy, A., Z.P. Zhuang, and M.S. BerryAnn:** Respiratory protection against bioaerosols: Literature review and research needs. *Am. J. Infect. Control 32*(*6*):345–354 (2004).
34. **Rengasamy, S., and B.C. Eimer:** Nanoparticle penetration through filter media and leakage through face seal interface of N95 filtering facepiece respirators. *Ann. Occup. Hyg. 56*(*5*):568–580 (2012).
35. **Tsai, C.S.J., M.E. Echevarria-Vegar, G.A. Sotiriou, et al.:** Evaluation of environmental filtration control of engineered nanoparticles using the Harvard Versatile Engineered Nanomaterial Generation System (VENGES). *J. Nanopart. Res. 14*(*5*):812 (2012).
36. **Dubey, S.C., H.V. Murughar, R.K. Kaushik, and D.D. Kulkarni:** The efficiency of HEPA filters in the air-handling system of a bio-containment laboratory in India. *Appl. Biosaf. 14*(*3*):121–126 (2009).
37. **First, M.W.:** Aging of HEPA filters in service and storage. *J. Am. Biological Saf. Assoc. 1*(*1*):52–62 (1996).
38. **Mouret, G., D. Thomas, S. Chazelet, J.C. Appert-Collin, and D. Bemer:** Penetration of nanoparticles through fibrous filters perforated with defined pinholes. *J. Aerosol Sci. 40*(*9*):762–775 (2009).
39. **Brochot, C., N. Michielsen, S. Chazelet, and D. Thomas:** Measurement of protection factor of respiratory protective devices toward nanoparticles. *J. Occup. Hyg. 56*(*5*):595–605 (2012).
40. **Boskovic, L., I.E. Agranovski, I.S. Altman, and R.D. Braddock:** Filter efficiency as a function of nanoparticle velocity and shape. *J. Aerosol Sci. 39*(*7*):635–644 (2008).
41. **Dai, Y.T., Y.J. Juang, Y.Y. Wu, P.N. Breysse, and D.J. Hsu:** In vivo measurements of inhalability of ultralarge aerosol particles in calm air by humans. *J. Aerosol Sci. 37*(*8*):967–973 (2006).
42. *Code of Nuclear Air and Gas Treatment*, ASME AG-1, Article FC-4110 (b), New York: American Society of Mechanical Engineers. 2003.
43. *Code of Nuclear Air and Gas Treatment*, ASME AG-2, Article FC-5120, New York: American Society of Mechanical Engineers. 2013.
44. **Comite Europeen de Normalisation (CEN):** *B. B. EN1822-1:2009 High Efficiency Air Filters (EPA, HEPA and ULPA). Part 1: Classification, Performance, Testing, and Marking*. CEN, 2009.
45. **Cherrie, J.W., L. MacCalman, W. Fransman, et al.:** Revisiting the effect of room size and general ventilation on the relationship between near- and far-field air concentrations. *Ann. Occup. Hyg. 55*(*9*):1006–1015 (2011).
46. **Cherrie, J.W., and T. Schneider:** Validation of a new method for structured subjective assessment of past concentrations. *Ann. Occup. Hyg. 43*(*4*):235–245 (1999).
47. **Makela, J.M., I.K. Koponen, P. Aalto, and M. Kulmala:** One-year data of submicron size mods of tropospheric background aerosol in southern Finland. *J. Aerosol Sci. 31*(*5*):595–611 (2000).
48. **Clausen, P.A., N.R. Jacobsen, K.A. Jensen, et al.:** NANOPLAST: Nano-technological materials and products in the plastics industry: Exposure assessment and toxicological properties. *Mod. Polymeric Mat. Environ. Applic. 4*(*2*):53–60 (2010).
49. **Saber, A.T., K.A. Jensen, K.A. Hougaard, et al.:** NANOKEM: Nanoparticles in the paint and lacquer industry. Exposure and toxic properties. *Mod. Polymeric Mat. Environ. Applic. 4*(*2*):111–120 (2010).

Paper II

J Nanopart Res (2015)17:337
DOI 10.1007/s11051-015-3139-6

RESEARCH PAPER

Influence of relative humidity and physical load during storage on dustiness of inorganic nanomaterials: implications for testing and risk assessment

Marcus Levin · Elena Rojas · Esa Vanhala · Minnamari Vippola · Biase Liguori · Kirsten I. Kling · Ismo K. Koponen · Kristian Mølhave · Timo Tuomi · Danijela Gregurec · Sergio Moya · Keld A. Jensen

Received: 30 September 2014 / Accepted: 3 August 2015

Abstract Dustiness testing using a down-scaled EN15051 rotating drum was used to investigate the effects of storage conditions such as relative humidity and physical loading on the dustiness of five inorganic metal oxide nanostructured powder materials. The tests consisted of measurements of gravimetrical respirable dustiness index and particle size distributions. Water uptake of the powders during 7 days of incubation was investigated as an explanatory factor of the changes. Consequences of these varying storage conditions in exposure modelling were tested using the control banding and risk management tool NanoSafer. Drastic material-specific effects on powder respirable dustiness index were observed with the change in TiO_2 from 30 % RH (639 mg/kg) to 50 % RH (1.5 mg/kg). All five tested materials indicate a decreasing dustiness index with relative humidity increasing from 30 to 70 % RH. Test of powder water uptake showed an apparent link with the decreasing dustiness index. Effects of powder compaction appeared more material specific with both increasing and decreasing dustiness indices observed as an effect of compaction. Tests of control banding exposure models using the measured dustiness indices in three different exposure scenarios showed that in two of the tested materials, one 20 % change in RH changed the exposure banding from the lowest level to the highest. The study shows the importance of powder storage conditions prior to tests for classification of material dustiness indices. It also highlights the importance of correct storage information and relative humidity and expansion of the dustiness test conditions specifically, when using dustiness indices as a primary parameter for source strength in exposure assessment.

Electronic supplementary material The online version of this article (doi:10.1007/s11051-015-3139-6) contains supplementary material, which is available to authorized users.

M. Levin (✉) · K. Mølhave
Department of Micro and Nanotechnology, Technical University of Denmark, 2800 Kongens Lyngby, Denmark
e-mail: mle@nrcwe.dk

M. Levin · B. Liguori · K. I. Kling · I. K. Koponen · K. A. Jensen
National Research Centre for the Working Environment, Lersø Parkallé 105, 2100 Copenhagen, Denmark

E. Rojas · D. Gregurec · S. Moya
CIC biomaGUNE, Paseo Miramón 182 C, 20009 San Sebastián, Gipuzkoa, Spain

E. Vanhala · M. Vippola · T. Tuomi
Finnish Institute of Occupational Health, Topeliuksenkatu 41 A, 00250 Helsinki, Finland

M. Vippola
Department of Materials Science, Tampere University of Technology, Korkeakoulunkatu 6, 33720 Tampere, Finland

B. Liguori
Department of Environmental Engineering, Technical University of Denmark, 2800 Kongens Lyngby, Denmark

Published online: 13 August 2015

Keywords Dustiness · Rotating drum · Exposure assessment · Powder storage · Occupational health · Nanotechnology

Introduction

Handling of powders in workplaces is known to be associated with risk of dust release and may result in important occupational exposure levels (Brouwer 2010; Kuhlbusch et al. 2011). The production stage and powder handling is also the activity that causes the highest risk of occupational exposure to manufactured nanomaterials (Borm et al. 2006; Hämeri et al. 2009). To enable precautionary exposure management, different test methods have been established, which allows relative ranking of powders regarding their propensity to release dust; i.e. dustiness (Hamelmann and Schmidt 2005). Some dustiness test methods are fully standardized, such as the rotating drum and the continuous drop methods that were established in EN15051 (BS EN:15051 2006; Liden 2006). Currently new methods are underway under the CEN-NEN Mandate M437 to establish nano-specific dustiness test methods and measurement protocols, also considering the two test methods in EN15051(Witschger et al. 2014).

To enable comparability in ranking, the standard dustiness methods are carefully harmonized regarding the mechanical design of the test systems, sampling design, as well as the conditions and measurement metrics to be used for quantification. In EN15051, the storage and experimental test conditions are set to room temperature and a relative humidity of 50 ± 10 %. However, workplace conditions are usually not controlled that well and in fact powder storage and handling is likely to take place under conditions relative far from the ideal testing conditions. Moreover, powders may be stored in different ways such as in small packs, drums, bags on palettes, big bags and silos, where the packed material may have been closed under vacuum or not. Consequently, powders may also be stored at great ranges in % RH and at high pressure gradients from top to bottom in a stack or silo. It is currently unclear how extensive such differences in humidity and storage pressure may affect different powders regarding their dustiness levels and dust characteristics.

Due to the general low number of workplace exposure measurement data, reliable early phase risk assessment becomes more and more important (Aitken et al. 2011). Therefore, a better understanding of the uncertainties and recommendations for improvements of critical tests and input parameters needs to be identified as soon as possible to ensure that the precautionary approaches are still reliable and can consider worst case scenarios. Some REACH tools and new control banding-like tools are currently available for such conservative evaluations of which several use dustiness data as an indicator for the potential exposure or source strength (Liguori et al. Submitted; Brouwer 2012).

A previous study (Jensen et al. 2009) showed different effects on dustiness levels after 5 min of uniaxial low-pressure compaction (3.54 ± 0.14 kg/cm^2) on a loose bentonite and granulated organoclay. The dustiness of the granulated organoclay increased after the uniaxial pressure load, whereas it was reduced in the case of the loose bentonite powders. Granulation is usually applied to improve the appearance, flow, mixing properties, of the powders as well as to decrease powder dustiness (Freitag and Kleinebudde 2003; Tardos 2005; Nishii and Horio 2007). It can be inferred that brief compaction of the bentonite in the study by Jensen et al. (2009) underwent some type of granulation, whereas the granulated organoclay was de-agglomerated resulting in reduced and increased dustiness, respectively.

Differences in the relative humidity (% RH) during powder storage may also change the characteristics of the emitted dust (Jensen et al. 2009). Intergranular fusion (caking) due to grain-particle-boundary dissolution–precipitation processes in partially water-soluble powder materials may occur in sufficiently humid air and durations of storage (Szepvolgyi et al. 2001; Gbureck et al. 2005; Brockel et al. 2006). Such processes may initially result in agglomerates of softly bridged particles and finally formation of aggregates.

While results from dustiness testing initially were intended for relative ranking of the substance emission potential, recent research investigates its potential use in control banding and time-resolved exposure modelling (Paik et al. 2008; Tielemans et al. 2008; Cherrie et al. 2009; Schneider et al. 2011; Van Duuren-Stuurman et al. 2012; Levin et al. 2014). Reliable use of standard dustiness indices for control banding and exposure modeling requires that the powders are not affected by their storage history and use conditions, or that the tests are conducted at the same conditions as

the storage and use. The limited documentation that is currently available suggests that a wider range in conditions during dustiness testing may be necessary. Previous studies did reveal important variation in dustiness with humidity for pharmaceutical powders, which are known to be hygroscopic and more susceptible to changes (Pujara 1997).

The primary aims of this study were

(1) To investigate to what degree the dustiness levels and dust characteristics of slightly water-soluble and insoluble inorganic powders and different chemical surface modifications may be affected during storage at low, medium and high relative humidity without and with a physical pressure-load.
(2) To assess the consequences of the results for risk assessment and management by comparison of assessment results using dustiness data from standard and non-standard incubation conditions.

All dustiness tests were conducted using the down-scaled EN15051 rotating dustiness drum which already has been used in a range of studies (Schneider and Jensen 2008; Jensen et al. 2009; Singh et al. 2011; Rasmussen et al. 2013, 2014; Levin et al. 2014) and currently is under evaluation as a standard method for dustiness testing of nanomaterial powders (Witschger et al. 2014).

The potential impact of the results on risk assessment was discussed using the obtained dustiness data in the NanoSafer control banding and risk management tool (http://nanosafer.i-bar.dk/, Kristensen et al. 2010) comparing the deviation from assessment results from standard and non-standard incubation conditions.

Methods and materials

Sample materials

Five different commercial inorganic nanostructured materials with slightly different primary particle sizes, morphologies, negligible to low water-solubilities, and some with and without chemical surface modifications were investigated within the study (Table 1). The powders originate from the EU FP7 project HINAMOX in which the current study was planned to increase understanding on the potential variability in exposure potentials during different storage conditions for these specific powders.

All test materials were received as powders and stored in air-tight containers until the time of experiments. The nanomaterials were previously reported to vary in particle size-ranges and states of aggregation (Table 1) (data from Pérez-Campaña et al. 2012, 2013). The average primary particle size varied from a few nm to 36 nm, but the size distributions were generally wide and polydispersive. Only ZnO #1 had a nearly monodispersive size distribution. The primary particles were mainly aggregated in all samples. One of the samples, TiO_2, was surface-modified during production using HNO_3,

Although all of the sample materials are generally considered very low- to in-soluble, literature data state solubility of ZnO between 4.88 and 7.40 mg/L (Xia et al. 2008; Reed et al. 2012; Li et al. 2012). Schmidt and Vogelsberger (2006) investigated solubility of TiO_2 and found that three commercially available nanosized TiO_2 had a solubility of 250 nmol/L (19.97 mg/L) at pH 1.5. The study also concluded that TiO_2 solubility increases with decreasing pH of medium and material primary particle size. This is of great importance as the TiO_2 sample in this study is stabilized by HNO_3, which is expected to render the surface to become highly hydroscopic. However, the effect may also include chemical destabilization and increased solubility. No literature values on solubility were found for CeO_2 and Al_2O_3.

The specific surface areas of the bulk nanopowders were measured using the BET (Brunauer–Emmett–Teller) nitrogen adsorption method. The materials were degassed for 72 h at 25 °C and subsequently analysed using Quantachrome Nova 4200 multipoint BET.

Surface analysis of the powders by X-ray photoelectron spectroscopy (XPS) was performed in a SPECS SAGE HR 100 system spectrometer on as-received powders. The X-ray source for TiO_2 was Mg Kα (non-monochromatic, operated at 12.5 kV and 250 W). For other powders, experiments are performed with an Al Kα source (non-monochromatic, operated at 12.5 kV and 300 W). The take-off angle was fixed at 90° and the measurements were conducted at a pressure of ~10–6 Pa. Survey spectra

Table 1 Key physicochemical characteristics of the test nanomaterials

Sample	Source	Primary size (nm)	Characteristics	Specific surface area (m2/g)	Surface elemental composition (XPS)	Surface modification	Density (g/cm3)	S_o (mg/L)
ZnO #1	Plasmachem GmbH	13.2 ± 5.4	Monodisperse, aggregated, spherical	26.2	16.9 % C, 50.9 % O, 32.2 % Zn	NA	5.61	4.88–7.40
ZnO #2	Degussa/Quimidroga	36.1 ± 18.1	Polydisperse, aggregated	21.9	20.7 % C, 43.8 % O, 35.5 % Zn	NA	5.61	4.88–7.40
Al_2O_3	Plasmachem GmbH	13.6 ± 8.4	Polydisperse, aggregated	76.3	5.5 % C, 46.1 % O, 48.4 % Al	NA	3.95	NA
CeO_2	Degussa/Quimidroga	13.0 ± 12.1	Polydisperse	56.7	22.1 % C, 60.8 % O, 17.0 % Ce	NA	7.2	NA
TiO_2	Plasmachem	1–10	Aggregated	173.1	21.5 % C, 42.2 % O, 36.3 % Ti	HNO_3 stabilized	4.23	NA

were obtained with a pass energy of 30 eV. Detailed spectra were acquired for C 1s, O 1s and metal regions (Ti 2p, Zn 2p, Ce 2s and Al 2p) with a pass energy of 15 eV. Spectra were analysed with the CasaXPS 2.3.15dev87 software. The analysis consisted of satellite removal, Shirley background subtraction, calibration of the binding energies to the C 1s C–C peak at 285 eV, and peak fitting with Gaussian–Lorentzian line shapes to determine the atomic percentages and chemical states of elements contained in each powder. The results from XPS characterisation are presented in Table 1.

Total carbon is assigned to adventitious carbon (Barr and Seal 1995), a carbonaceous material found on the surface of most samples exposed to air. Stoichiometric ratio (O/metal) is calculated from oxygen assigned to the metal oxide and the total metal contribution. Titanium analysis results with 85 % of Ti IV, while 15 % is assigned to Ti III or lower oxidation states, which explains the O/Ti ratio of 1.2. In the case of both zinc powders, the O/Zn ratio is 1 as expected, with a slightly higher amount of adventitious carbon for ZnO #2 powder. In the Ce 3d spectra, peaks are assigned to two oxidation states: Ce IV and Ce III (Engelhard et al. 2004). The ratio of Ce^{4+}/Ce^{3+} is found to be 77/23, which corresponds to a higher O/Ce ratio, of 2.7. Aluminum quantification results in a O/Al ratio of 1 instead of the expected 1.5. This could be a result of inefficient oxidation of the aluminum precursor in the preparation process (Haeberle et al. 2013).

Experimental design of the incubation

The strategy for analysing the standard dustiness levels and the potential role of storage conditions was to test the powder dustiness at three different relative humidities (30, 50 and 70 % RH), each tested with and without a physical compaction of the powder. The case of 50 % RH without compaction constitutes as the standard test within the EN15051. A value of 70 and 30 % RH was selected as the upper and lower normal boundary conditions in workplaces handling. The uniaxial pressure load was selected to be 160 kg/m^2, which corresponds approximately to the load pressure experienced by the bottom layer bags on a single Euro-pallet with 15 bags (five layers).

The samples tested at "standard 50 % RH conditions" were stored in darkness at laboratory room

conditions with 50 % RH and equilibrated in the test system for 3 min before testing was commenced in the rotating drum. This procedure is prescribed in EN15051.

The experiments with fully controlled humidities with/without uniaxial pressure were completed by incubating the samples for 7 days in an incubator using a 2 lpm inlet flow with a controlled RH of 30, 50 or 70 %, respectively. The variation in RH was measured to be ±2 %. The incubations were made by distributing the powder evenly in a flat-bottomed glass petri dish. Samples subjected to pressure load were weighed out in the same manner, and kept in the incubator for 24 h before the load was applied in order to ensure that the whole powder sample had equilibrated with the selected humidity conditions. The 2.7 kg load was applied on the inverted lid from the petri dish (14 cm OD) placed on top of the powder. The setup is illustrated in Fig. 1.

Dustiness testing

Data on dustiness for different materials and storage conditions were obtained using the down-scaled EN15051 dustiness drum as described in (Schneider and Jensen 2008). The humidifier and the sampling train were modified from the original design (Schneider and Jensen 2008) to allow simultaneous real-time measurement and sampling using up to five different samplers and to allow respirable dust fraction measurements by optionally inserting a GK2.69 cyclone (BGI, UK). For the humidity and pressure load experiments, an incubation chamber was connected in between the humidifier and the test chamber to ensure the same test conditions (Fig. 2).

In this study, real-time measurements were done for particle concentration and size distribution using the following systems:

- Fast Mobility Particle Sizer (FMPS 3091, TSI Inc., Shoreview, MN, USA) for particles in the range 5.6–560 nm. The measurement with the FMPS is done through combining size classification by electrical mobility and counting by particle charge after positive charge equilibration at a unipolar diffusion charger at the column inlet. To ensure no particle concentrations above the instrument limit, a recirculating HEPA-filtered 1:10 dilution system was placed in front of it.
- Aerodynamic Particle Sizer (APS 3321, TSI Inc., Shoreview, MN, USA), range 542 nm–20 µm. The particle size measured with the APS is an aerodynamic equivalent sizes where the reference is a sphere with a density of 1. To ensure no particle concentrations above the instrument limit, it was coupled with a 1:20 dilution system (3302A, TSI Inc., Shoreview, MN, USA).
- Sampling on grids for transmission electron microscopy (TEM) was done in parallel for all materials and conditions using a mixed cellulose ester (MCE) 0.8-µm filter-cassette for asbestos sampling with a holey-carbon-film-coated Cu-grid mounted on the MCE filter. Sampling was done from one of the outlet sampling lines using conductive tubing and performed at 1.5 lpm for 60 s. Due to insufficient loading of particles on TEM grids and later recognized uncertainties regarding their size-resolved sampling efficiencies, data from this work will only be presented in supplemental material.
- Respirable dust (PM_4) was sampled at 4.2 lpm on Teflon filters mounted in 0.8-µm Millipore dust sampling cassettes after the GK2.69 cyclone.

Fig. 1 Illustration of powder placement in the incubation experiments where the *left*- and *right*-hand image shows the petri dish for pure humidity and combined humidity–pressure load incubations, respectively

The standard dustiness tests were conducted at 50 % RH according to EN 15051 with the adjustment that sampling was continued 120 s after termination of powder agitation. This has been normal practise in tests using the small rotating drum even though the original EN15051 standard procedure sampling is to be terminated immediately after the rotation has been stopped. The reason for the prolonged measurement time is that we have observed that the dust cloud decays long time after rotation are stopped. Hence, a full analysis of the generated dust requires prolonged sampling time to collect the whole dust cloud.

All experiments were conducted at 11 rpm and a horizontal flow rate of 11 lpm to obtain the same number of powder parcels falling per minute and average horizontal flow velocity in the cylinder as in

the EN 15051 test, respectively. HEPA-filtered and humidified air was supplied to the drum inlet and exhausted to be distributed into the different sampling units at the other end of the drum (Fig. 2).

Loading of powders was done by first removing the exit cone of the drum and orient the drum with a lifter vane placed at lowest position of the rotation circle. As is the standard procedure in small rotating drum tests, 6 g of powder was carefully loaded in a pile on the upward moving side at the centre of the lifter vane. Then the system was closed, the humidity conditioned air-flow was applied and all flows were checked. The experiment was then initiated by leading the test atmosphere through the chamber for 180 s, during which the particle monitors reach background particle concentration levels and the dustiness test was initiated. After 60 s of rotation, the drum was stopped and sampling was maintained 120 s of particle sampling without rotation. This completed the rotation part of the dustiness test. Immediately after the conclusion of the test, the filter from the cyclone was retrieved. The mass of collected respirable dust was determined after conditioning the exposed filters and filter controls in a weighing room (22 °C; 50 % RH) using a Sartorius microbalance (Type R162 P; Sartorius GmbH, Göttingen, Germany). The measured mass was corrected for handling and conditional variations through the use of blind filters. The limit of quantification, calculated as three times the standard deviation of the blind filters, was 0.20 mg. The weighed mass was then used to calculate and categorize the dustiness levels of the powders according to EN15051.

Data treatment of dustiness data

All real-time measurements were done using an assumed density of 1 g/cm^3. FMPS and APS number concentrations were exported as dN/dlog D_p values for each particle size, D_p. Measured data were corrected for background based on the 40 s average size spectra sampled before the test was initiated. All reported size distributions are the average accumulated size distributions over the whole duration of the experiment based on three repeats ($N = 3$). For determination of

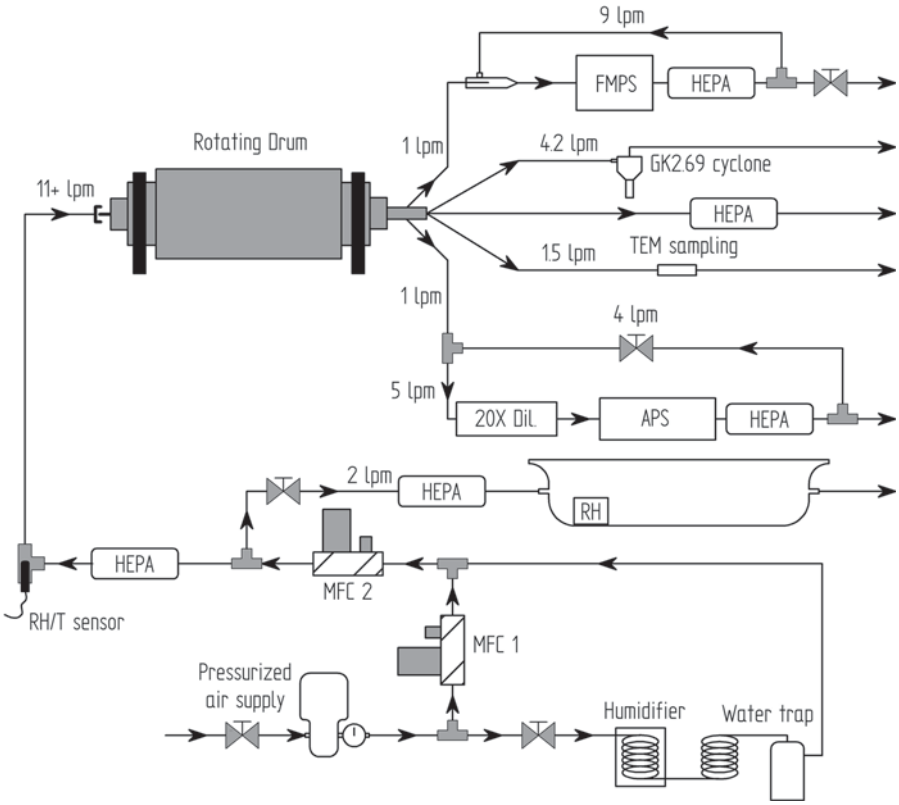

Fig. 2 The experimental setup of the dustiness drum, incubation chamber and real-time monitors

respirable dustiness, the differential mass measured on the filters was corrected for variations in the three blank control filters and divided by the actual mass of the tested sample. The final value is an average of three repeats. The respirable dustiness index (mg/kg) is then calculated as the amount of dust (mg) collected on the filter divided by the amount (kg) of the test material and multiplied by a factor of 4.2/11 to match total flow through the drum.

Measurement of adsorbed water and water uptake

As water uptake can occur by adsorption as well as due to chemical reaction with the samples, the extent of this was investigated using different methods. The amount of water adsorbed at 50 % RH standard conditions was determined as described in the EN15051 standards specification. Due to limited sample availability, the water uptake at the three incubation conditions was done only at 30, 50 and 70 % RH without pressure load. After 7 days incubation, triplicates of ca. 0.5 g powder were weighed into glass petri dishes and placed in an oven for 4 h at 110 °C, removed and weighed out immediately. The mass loss during heat treatment was assumed to correspond to the amount of adsorbed water alone. An attempt was also made to determine the hygroscopicity and point of condensation of water on the test materials by environmental scanning electron microscopy using a Peltier cooling stage in a FEI ESEM Quanta 200 FEG (FEI, Eindhoven, the Netherlands). However, the results did not show any immediate condensation until very high (>93.5 % RH) relative humidity (see supplemental material).

Consequences for risk assessment

To assess the potential consequences of the observed influences of storage conditions for risk assessment and associated risk management, a series of analyses were made for different principle exposure scenarios using the NanoSafer control banding and risk management tool. In this model, the exposure assessment is based on first-order exposure assessment modeling using dustiness data or default high values as one of the critical source strength input parameters. The tests were conducted using the dustiness values measured at 30, 50 and 70 % RH without loading to determine the NanoSafer exposure control band for each case. The tool has 5 exposure control bands ranking from 1 to 5 and is calculated for both process near-field and work room far-field concentrations for both Acute (15 min) and Chronic (8 h) exposure durations.

The studied scenarios were as follows:

- Small-scale activity; pouring of 5 × 2 kg into a mixer in a 3.5 × 5 × 2.9 m^3 workroom
- Intermediate scale activity; pouring of 5 × 20 kg into a mixer in a 4 × 5 × 3.5 m^3 workroom
- Large-scale industrial use activity; pouring one 800 kg big-bag into a dissolver in a 5 × 10 × 5 m^3 workroom.

More details of the scenario are collected in Table 2.

Table 2 Input parameters for three occupational exposure scenarios used in NanoSafer

	Scenario 1	Scenario 2	Scenario 3
Activity description-source domain	Scooping/filling bags in small-scale production	Pouring powder into twin-screw extruder	Wet mixing in dissolver
Activity energy factors level	0.1	0.5	0.75
Total amount used in the process	10 kg (5 × 2 kg)	100 kg (5 × 20 kg)	800 kg (1 × 800 kg)
Duration of the all process	75 min	30 min	5 min
Period between each cycle	6 min	1 min	0
Frequency of the process	1 time per day	1 time per day	1 time per day
Amount per each cycle	2 kg	20 kg	800 kg
Duration of each cycle	10 min	5 min	5 min
Room size	3.5 × 5 × 2.9	4 × 5 × 3.5	5 × 10 × 5
Ventilation rate	1 h^{-1}	5 h^{-1}	20 h^{-1}

It should be noted that control banding tools by definition do not give a quantitative values, but a qualitative precautionary risk assessments based on variable levels of quantitative and qualitative input and modelling depending on the tool. The aim of the test performed here is to illustrate through use of a real exposure assessment tool how important the observed differences caused by different storage conditions could be for exposure assessments.

Results and discussion

Gravimetrical respirable dustiness index

Dustiness testing showed a large variation in the respirable dustiness levels of the powders tested under standard EN15051 conditions (3 min, 50 % RH, no load) and is shown in Fig. 3, denoted as '50 %'. The lowest levels of respirable dustiness were observed for

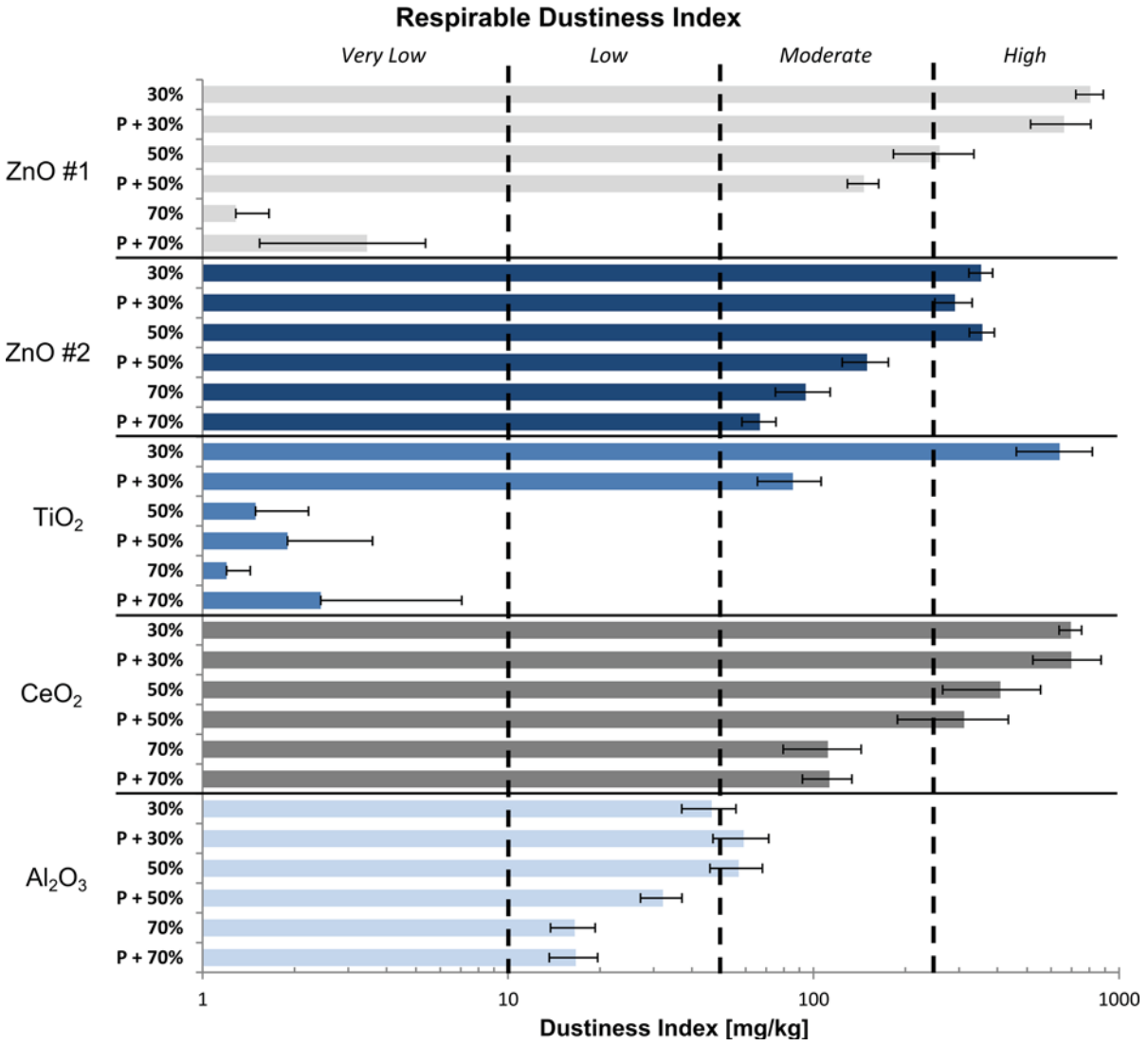

Fig. 3 Respirable dustiness index obtained at the different % RH and pressure load conditions. The percentage indicates relative humidity and 'P' the presence of 160 kg/m^2 pressure during incubation. The dustiness ranks are based on the thresholds in the EN15051 standard

TiO_2 (<limit of quantification) and Al_2O_3 (56.9 mg/kg). The highest levels were observed for CeO_2 (409 mg/kg), ZnO #1 (259 mg/kg) and ZnO #2 (357 mg/kg). The EN15051 convention for classifications of powder dustiness denotes indices as *Very Low* for <10 mg/kg, *Low* for between 10 and 50 mg/kg, *Moderate* between 50 and 250 mg/kg and *High* >250 mg/kg as indicated in Fig. 3. Hence, the standard dustiness tests reveal that two powders are categorized as *Very Low* (TiO_2) and *Moderate* (Al_2O_3) and three (CeO_2, ZnO #1 and ZnO #2) are in the category of powders with *High* dustiness.

Testing the influence of storage conditions showed different effects on the respirable dustiness indices, depending on the sample material (Fig. 3). Dustiness of Al_2O_3 was reduced or unaltered reducing the humidity, whereas the index was lowered to less than 60 % by compaction at 50 % humidity. Increasing RH to 70 % caused a more severe drop in dustiness. ZnO #2 followed almost the same pattern, however, with greater reduction in dustiness due to compaction at both 30 (19 % reduction), 50 % RH (58 % reduction) and 70 % RH (29 % reduction). ZnO #1 showed a similar behaviour at 30 % RH and 50 % RH, but at 70 % RH, there is an extreme drop in dustiness index (<10 mg/kg) for both the compressed and uncompressed versions. CeO_2 was seemingly unaffected by physical loading at all levels of RH and moderately lowered in dustiness with increasing RH. The most dramatic effect was observed with TiO_2 which went from below limit of quantification at 50 and 70 % RH to 85.7 and 693.3 mg/kg for compacted and uncompacted at 30 % RH, respectively. TiO_2 is the HNO_3 stabilized material, and based on our observations, incubation at these flow-through atmospheres caused release of corrosive vapours, which is ascribed to loss of the acidic HNO_3 stabilization.

All five materials had a statistically significant higher dustiness index at 30 % RH than at 70 % RH, both for compacted and un-compacted versions. A trend of higher values for 30 than 50 % RH can also be observed; however, it is not significant in all cases. No general pattern could be observed for changes in dustiness due to compaction, but in most cases compaction of the material decreased the dustiness. However, at higher humidities, the compaction appears to increase the dustiness. This might be due to compaction of the material limiting the uptake of water.

Water uptake

The measured water contents in the incubated powders are shown in Fig. 4 together with the corresponding dustiness indices. For ZnO #1 and TiO_2, there is a clear relation between increased water content and decreased dustiness index. Only small differences in water content for the different incubation humidities can be seen for the remaining three materials. For TiO_2, the high water uptake at all conditions, as compared to the other materials in the study, may be linked to the small primary particle size and high specific surface area.

Size distributions

All materials gave a typical bi-modal size-distribution at standard conditions with a smaller mode at

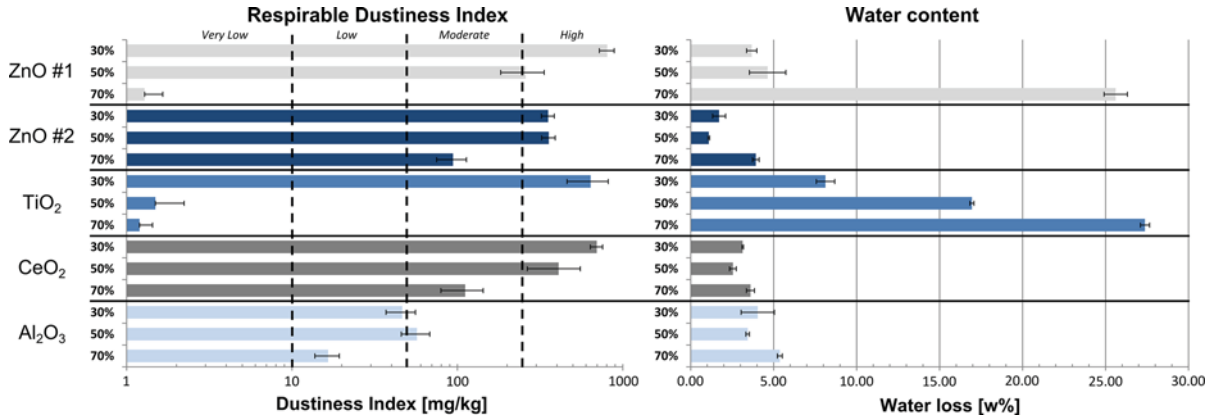

Fig. 4 Dustiness indices and water content of the five materials incubated at 30, 50 and 70 % RH

150–200 nm and a coarser at 2–3 μm, similar to size distributions reported in previous studies (Schneider and Jensen 2008; Jensen et al. 2009; Burdett et al. 2013; Levin et al. 2014). Figure 5 presents the accumulated size distributions as measured with FMPS and APS of TiO_2 and Al_2O_3 at 30, 50 and 70 % RH without loading to exemplify typical behaviour. Size distributions of all materials and storage conditions are available in supplemental material. The behaviour of the particle concentrations is well matched with that of the dustiness index, and the increase/decrease in particle numbers appears to be similar for all sizes. Presented data on particles <40 nm are due to electrometer noise accumulated over the course of the measurements.

Consequences for risk assessment

Table 3 presents the NanoSafer exposure risk-level bands obtained for the potential acute and chronic, near-field and far-field exposure levels for each powder and incubation conditions, respectively. It should be noted that NanoSafer consists of 5 bands for the allocation of the exposure potential ranking from 1 the lowest to 5 the highest. All materials give different control bands in one or more of the three scenarios due to incubation humidity. In two of the cases (ZnO#1 and TiO_2), a 20 % change in RH changes the exposure rank from the lowest to the highest level. For ZnO #1, this occurs when changing the % RH from 50 to 70 in scenario 2 and 3. For TiO_2, the drastic change in exposure rank is observed when going from 30 to 50 % RH in all three scenarios. The drastic effects can be observed in both near- and far-field concentrations and acute and chronic exposure times. The results from testing the powders in the NanoSafer control banding and risk management tool clearly show that the relative humidity and storage load play an important role on the emission potential of nanomaterial powders. In the worst case, an exposure- or risk-level estimated based on dustiness data produced under conditions different from reality may be extremely over- or underestimated depending on the material. This highlights the fact that the use of a single standard dustiness source term for control banding or quantitative exposure assessment may be critical if the test conditions vary considerably from the storage and use conditions. Unless such considerations are considered as safety margins or adopted into the tools or the dustiness data are actually generated

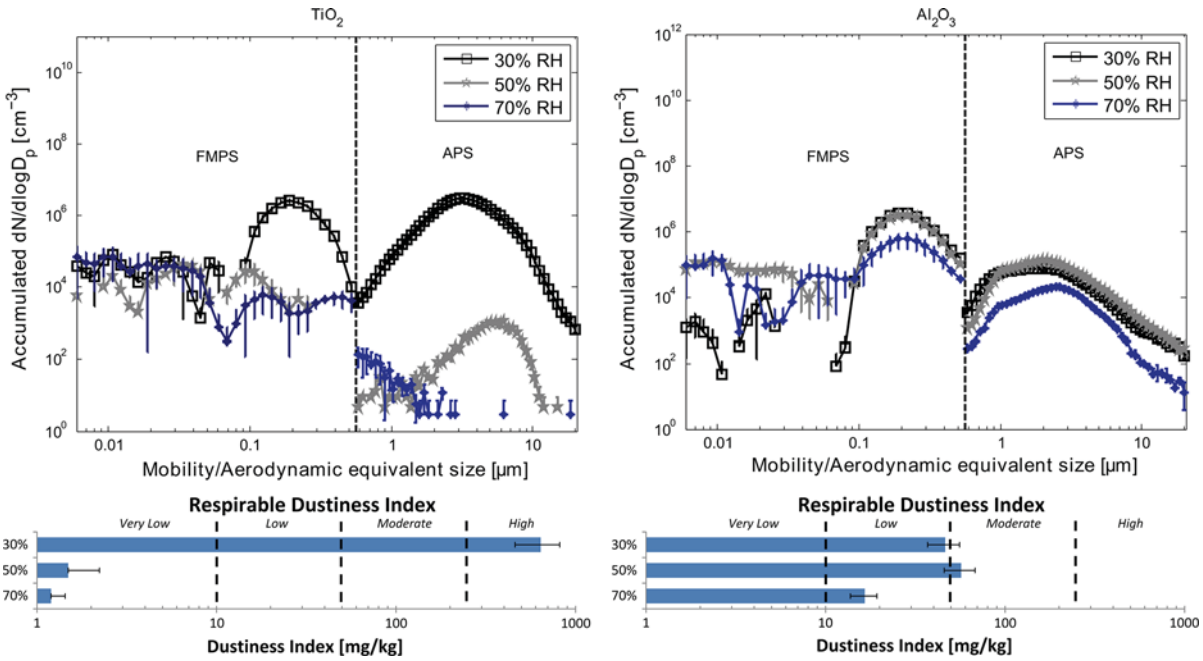

Fig. 5 Size distributions and corresponding gravimetrical dustiness levels of TiO_2 and Al_2O_3 at 30, 50 and 70 % RH

Table 3 NanoSafer exposure risk-level bands for acute exposure (15 min) and chronic exposure (8 h) calculated for each test material and incubation conditions

		Scenario 1				Scenario 2				Scenario 3			
		Near Field		Far Field		Near Field		Far Field		Near Field		Far Field	
	%RH	Acute	Chr.	Acute	Chr.	Acute	Chr.	Acute	Chr.	Acute	Chr.	Acute	Chr.
ZnO_1	30	4	3	3	3	5	5	5	5	5	5	5	5
	50	2	2	2	1	5	5	5	5	5	5	5	5
	70	1	1	1	1	1	1	1	1	3	1	1	1
ZnO_2	30	3	3	3	2	5	5	5	5	5	5	5	5
	50	3	3	3	2	5	5	5	5	5	5	5	5
	70	1	1	1	1	5	5	5	4	5	5	5	5
Al_2O_3	30	1	1	1	1	4	2	4	2	5	4	5	2
	50	1	1	1	1	5	2	4	2	5	5	5	3
	70	1	1	1	1	3	1	2	1	5	3	5	1
TiO_2	30	5	5	5	4	5	5	5	5	5	5	5	5
	50	1	1	1	1	2	1	1	1	5	2	3	1
	70	1	1	1	1	2	1	1	1	5	2	3	1
CeO_2	30	4	4	4	4	5	5	5	5	5	5	5	5
	50	4	3	4	3	5	5	5	5	5	5	5	5
	70	2	2	2	1	5	5	5	5	5	5	5	5

under comparable conditions, these effects add a major uncertainty to the results of exposure assessment.

Conclusions and recommendations

In this study, the effects of storage conditions such as relative humidity and physical loading on the dustiness of five inorganic nanomaterials were investigated. Gravimetrical dustiness index and particle size distributions were measured using rotating drum tests. Long-term water uptake of the powders was found to be an explanatory factor of the changes. Consequences of these varying storage conditions in exposure modelling were tested using the control banding and risk management tool NanoSafer.

The study shows that there is a material-dependent change in the dustiness index due to both humidity conditions and physical load during 7 days simulated storage. A general trend of reduced dustiness index with increased relative humidity was observed, although the magnitude varies with the materials. The effect of physical loading is more complicated, but the magnitude of the change is also generally smaller than that of the humidity condition.

The most severe effect was seen on the TiO_2 material which had a dustiness index below detection limit at standard dustiness conditions but ranked in as *Very high* (693.3 mg/kg) at 30 % RH incubation. This suggests that the effect of storage humidity on dustiness can be severe for certain powders and that the ±10 % RH gap allowed for in the EN15051 might be too broad. In this case, the major effect is ascribed to the HNO_3 stabilization used for this product.

Testing the consequences of the observed variation in dustiness using the NanoSafer control banding/risk management tool using three work scenarios also showed great variability in the exposure assessment. Of greatest concern, assessments based on high humidity conditions would seriously underestimate the need for increased ventilation and personal protection equipment compared to the same scenario at low humidity conditions.

To reduce the uncertainties associated with the effects of humidity during storage and work, we suggest that dustiness testing for exposure assessment should be expanded to include tests that also target the extreme ranges of the relative humidity at workplaces. Moreover, the allowed variation around the specified humidity levels should be reduced considerably from 10 % as given today in EN15051 and data on storage conditions may be essential. If data are to be used for more accurate predictive modelling, dustiness data on additional test conditions may be needed. Further studies to determine the effect of % RH in more detail are required to define more precisely the critical boundaries for the test conditions.

Acknowledgments This work was conducted as part of the Strategic Research effort at the National Research Centre for the Working Environment and the Danish Centre for Nanosafety (20110092173/3) from the Danish Working Environment Research Foundation and the EU Framework seven Programme HINAMOX (228825).

References

Aitken RA, Bassan A, Friedrichs S et al (2011) Specific advice on exposure assessment and hazard/risk characterisation for nanomaterials under REACH (RIP-oN 3)

Barr TL, Seal S (1995) Nature of the use of adventitious carbon as a binding energy standard. J Vac Sci Technol A 13:1239–1246. doi:10.1116/1.579868

Borm PJ, Robbins D, Haubold S et al (2006) The potential risks of nanomaterials: a review carried out for ECETOC. Part Fibre Toxicol 3:11. doi:10.1186/1743-8977-3-11

Brockel U, Wahl M, Kirsch R, Feise HJ (2006) Formation and growth of crystal bridges in bulk solids. Chem Eng Technol 29:691–695

Brouwer D (2010) Exposure to manufactured nanoparticles in different workplaces. Toxicology 269(2):120–127

Brouwer DH (2012) Control banding approaches for nanomaterials. Ann Occup Hyg 56:506–514. doi:10.1093/annhyg/mes039

BS EN:15051 (2006) EN15051 Workplace atmospheres: measurement of the dustiness of bulk materials—requirements and reference test methods

Burdett G, Bard D, Kelly A, Thorpe A (2013) The effect of surface coatings on the dustiness of a calcium carbonate nanopowder. J Nanoparticle Res 15:1311. doi:10.1007/s11051-012-1311-9

Cherrie JW, Gillies AT, Sleeuwenhoek A et al (2009) Modelling exposure to pharmaceutical agents. J Phys Conf Ser 151(1):012063

Engelhard M, Azad S, Peden CHF, Thevuthasan S (2004) X-ray photoelectron spectroscopy studies of oxidized and reduced CeO2(111) surfaces. Surf Sci Spectra 11:73–81. doi:10.1116/11.20050201

Freitag F, Kleinebudde P (2003) How do roll compaction/dry granulation affect the tableting behaviour of inorganic materials? Comparison of four magnesium carbonates. Eur J Pharm Sci 19:281–289

Gbureck U, Dembski S, Thull R, Barralet JE (2005) Factors influencing calcium phosphate cement shelf-life. Biomaterials 26:3691–3697

Haeberle J, Henkel K, Gargouri H et al (2013) Ellipsometry and XPS comparative studies of thermal and plasma enhanced atomic layer deposited Al2O3-films. Beilstein J Nanotechnol 4:732–742. doi:10.3762/bjnano.4.83

Hamelmann F, Schmidt E (2005) Methods for dustiness of industrial powders. China Particuol 03:90–93

Hämeri K, Lähde T, Hussein T et al (2009) Facing the key workplace challenge: assessing and preventing exposure to nanoparticles at source. Inhal Toxicol 21(Suppl 1):17–24. doi:10.3109/08958370903202804

Jensen KA, Koponen IK, Clausen PA, Schneider T (2009) Dustiness behaviour of loose and compacted Bentonite and organoclay powders: what is the difference in exposure risk? J Nanoparticle Res 11:133–146

Kristensen HV, Jensen KA, Koponen IK et al (2010) Nanopartikler i arbejdsmiljøet - Viden og inspiration om håndtering af nanomaterialer. Industriens Branchearbejdsmiljøråd, Branchearbejdsmiljørådet for Undervisning og Forskning samt Universitets og Bygningsstyrelsen, Copenhagen

Kuhlbusch TAJ, Asbach C, Fissan H et al (2011) Nanoparticle exposure at nanotechnology workplaces: a review. Part Fibre Toxicol 8:22. doi:10.1186/1743-8977-8-22

Levin M, Koponen IK, Jensen KA (2014) Exposure assessment of four pharmaceutical powders based on dustiness and evaluation of damaged HEPA filters. J Occup Environ Hyg 11:165–177. doi:10.1080/15459624.2013.848038

Li X, Lenhart JJ, Walker HW (2012) Aggregation kinetics and dissolution of coated silver nanoparticles. Langmuir 28:1095–1104. doi:10.1021/la202328n

Liden G (2006) Dustiness testing of materials handled at workplaces. Ann Occup Hyg 50:437–439

Liguori B, Hansen SF, Baun A, Jensen KA (Submitted) Comparative analysis of occupational exposure estimation tools for nanomaterials and their applicability for reach

Nishii K, Horio M (2007) Chapter 6 Dry granulation. In: Salman AD (ed) Handbook of Powder Technology. Elsevier Science B.V., pp 289–322

Paik SY, Zalk DM, Swuste P (2008) Application of a pilot control banding tool for risk level assessment and control of nanoparticle exposures. Ann Occup Hyg 52:419–428

Pérez-Campaña C, Gómez-Vallejo V, Martin A et al (2012) Tracing nanoparticles in vivo: a new general synthesis of positron emitting metal oxide nanoparticles by proton beam activation. Analyst 137:4902–4906. doi:10.1039/C2AN35863H

Pérez-Campaña C, Gómez-Vallejo V, Puigivila M et al (2013) Biodistribution of different sized nanoparticles assessed by positron emission tomography: a general strategy for direct activation of metal oxide particles. ACS Nano 7:3498–3505. doi:10.1021/nn400450p

Pujara CP (1997) Determination of factors that affect the generation of airborne particles from bulk pharmaceutical powders. Theses Diss Available ProQuest pp 1–155

Rasmussen K, Mech A, Mast J et al (2013) Synthetic amorphous silicon dioxide (NM-200, NM-201, NM-202, NM-203, NM-204): characterisation and physico-chemical properties JRC Repository: NM-series of representative manufactured nanomaterials

Rasmussen K, Mast J, de Temmerman P-J et al (2014) Titanium dioxide, NM-100, NM-101, NM-102, NM-103, NM-104, NM-105: characterisation and physico-chemical properties

Reed RB, Ladner DA, Higgins CP et al (2012) Solubility of nano-zinc oxide in environmentally and biologically important matrices. Environ Toxicol Chem 31:93–99. doi:10.1002/etc.708

Schmidt J, Vogelsberger W (2006) Dissolution kinetics of titanium dioxide nanoparticles: the observation of an unusual kinetic size effect. J Phys Chem B 110:3955–3963. doi:10.1021/jp0553611

Schneider T, Jensen KA (2008) Combined single-drop and rotating drum dustiness test of fine to nanosize powders using a small drum. Ann Occup Hyg 52(1):23–34

Schneider T, Brouwer DH, Koponen IK et al (2011) Conceptual model for assessment of inhalation exposure to manufactured nanoparticles. J Expo Sci Environ Epidemiol 21:450–463

Singh C, Friedrichs S, Levin M et al (2011) NM-series of representative manufactured nanomaterials—zinc oxide NM-110, NM-111, NM-112, NM-113: characterisation and test item preparation

Szepvolgyi J, Mohai I, Gubicza J (2001) Atmospheric ageing of nanosized silicon nitride powders. J Mater Chem 11: 859–863

Tardos GI (2005) Wet-granulation research with application to scale-up. China Particuol 3:191–195

Tielemans E, Schneider T, Goede H et al (2008) Conceptual model for assessment of inhalation exposure: defining modifying factors. Ann Occup Hyg 52:577–586

Van Duuren-Stuurman B, Vink SR, Verbist KJM et al (2012) Stoffenmanager nano version 1.0: a web-based tool for risk prioritization of airborne manufactured nano objects. Ann Occup Hyg 56(5):525–541

Witschger O, Jensen KA, Brouwer DH et al (2014) DUSTI-NANO: a CEN pre-normative research project to harmonize methods for manufactured nanomaterial powders. Aerosol Technology 2014, Karlsruhe. Abstract T230A09. Session APPVI Dustiness and Resuspension: http://www.gaef.de/AT2014/

Xia T, Kovochich M, Liong M et al (2008) Comparison of the mechanism of toxicity of zinc oxide and cerium oxide nanoparticles based on dissolution and oxidative stress properties. ACS Nano 2:2121–2134. doi:10.1021/nn800511k

Paper III

Aerosol Science and Technology, 49:556–565, 2015

ISSN: 0278-6826 print / 1521-7388 online
DOI: 10.1080/02786826.2015.1052039

Limitations in the Use of Unipolar Charging for Electrical Mobility Sizing Instruments: A Study of the Fast Mobility Particle Sizer

M. Levin,[1,2] A. Gudmundsson,[3] J. H. Pagels,[3] M. Fierz,[4] K. Mølhave,[1] J. Löndahl,[3] K. A. Jensen,[2] and I. K. Koponen[2]

[1]*Department of Micro and Nanotechnology, Technical University of Denmark, Kgs. Lyngby, Denmark*
[2]*Danish NanoSafety Centre, National Research Centre for the Working Environment, Copenhagen, Denmark*
[3]*Ergonomics and Aerosol Technology (EAT), Lund University, Lund, Sweden*
[4]*Institute of Aerosol and Sensor Technology, University of Applied Sciences Northwestern Switzerland, Windisch, Switzerland*

A comparison between three different types of particle sizing instruments (fast mobility particle sizer, FMPS; electrical low pressure impactor, ELPI; and scanning mobility particle sizer, SMPS) and one condensation particle counter (CPC) was made to compare instrument response in terms of size distributions and number concentration. Spherical oil droplets in 39 different sizes, with geometric mean diameter (GMD) ranging from 50 nm to 820 nm, were used as test particles. Furthermore, a characterization of the FMPS unipolar charger behavior was made to analyze the measured size distributions and number concentrations. The results show that all three sizing-instruments agree well for particle sizes below 200 nm, both in terms of size and number concentration, but the FMPS deviates clearly when particle sizes exceed 200 nm. Above this, the FMPS underestimates the particle size throughout the remainder of the size range, with an apparent upper limit for GMD of 300 nm. It also estimates a higher particle number concentration as compared to the other instruments. Analysis of the 22 FMPS electrometer currents and calculation of average number of charges per particle show a diameter dependence of response of $d_p^{1.21}$ for the FMPS unipolar charger. The resulting calculated electrical mobility showed a minimum in mobility for spherical particles at 577 nm, which indicates an interfering range of particles above the measurement range, but below the cut-off of the inlet pre-separator (1 μm). The study concludes that particle distributions with a true GMD above 200 nm cannot be measured reliably with the FMPS.

Received 28 February 2015; accepted 7 May 2015.
Address correspondence to M. Levin, Danish NanoSafety Centre, National Research Center for Working Environment, Lersø Park Alle 105, DK-2100 Copenhagen, Denmark. E-mail: mle@nrcwe.dk
Color versions of one or more of the figures in the article can be found online at www.tandfonline.com/uast.

1. INTRODUCTION

Measurement of airborne particle size and number concentration in the sub-micron size range is important for understanding the properties and mechanics of airborne particles within the atmosphere and its radiative forcing (Seinfeld and Pandis 2006). In addition, reliable measurements of exposures to particles from a few nanometers to several micrometers in size are increasingly becoming important in order to assess, measure, and manage the inhalation risk of airborne fine, ultrafine particles and manufactured nanomaterials that are increasingly documented to be of serious concern regarding our respiratory human health (Dockery et al. 1993; Oberdorster and Utell 2002; Donaldson et al. 2004; Oberdorster et al. 2005).

For studies performed at workplaces aiming at measuring manufactured nanostructured particles, the Scanning Mobility Particle Sizer (SMPS, Wang and Flagan 1990) is the most common instrument to be used for measurements of particle size distributions in the sub-micron range (Brouwer et al. 2009; Kuhlbusch et al. 2011). The potential downside of this technique is the relatively low time-resolution where a full scanning time takes from 16 s up to several minutes, depending on desired size resolution and instrument response time, which can cause erroneous measurements during transient concentrations (Yao et al. 2006; Asbach et al. 2014; Zimmerman et al. 2014). Other common instruments used for particle sizing in this range include the Fast Mobility Particle Sizer (FMPS, TSI Inc. Shoreview, MN, USA) and the Electrical Low Pressure Impactor (ELPI, Dekati Ltd., Finland), which both have the advantage of 1-s time resolution. However, it is imperative that the gain in time resolution should not come at a too high decrease in precision and accuracy in the determination of particle size and concentration.

Several studies have been carried out that compare these three instruments in different regards and during measurement of a large number of different aerosols. Asbach et al. (2009) compared three different commercial SMPS systems and one FMPS by measuring NaCl particles (geometric mean diameter, GMD, ~30 nm) and soot agglomerates (70–90 nm). They found that the FMPS consistently measured slightly lower GMD than the SMPS systems. In terms of concentration, the FMPS measurement was comparable to the SMPS systems for NaCl, but significantly higher for soot particles, likely due to the complex morphology of soot. Jeong and Evans (2009) compared the FMPS with a SMPS for measurements of urban ambient and indoor particles, rural ambient particles, and laboratory particles. They found a strong correlation between the two instruments in terms of total concentrations but poor agreement in the shape of the measured size distributions. All tested aerosols had a GMD below 100 nm. Leskinen et al. (2012) compared SMPS, FMPS, and ELPI along with additional instruments to aerosols relevant for occupational health measurements. They found that the SMPS, FMPS, and ELPI produced similar results for 30 nm ammonium sulfate particles in terms of concentration and GMD, but for larger size TiO_2 agglomerates and powder dusts with more complex morphology, the FMPS reported higher concentrations and smaller GMDs than the SMPS. Kaminski et al. (2013) compared eight commercial SMPS systems with three FMPSs using NaCl, Di-Ethyl-Hexyl-Sebacat (DEHS), and soot particles of various sizes. They found very good agreement for small nanosized (~40 nm) NaCl particles while FMPSs underestimated the 250 nm DEHS particles by 20–26% as compared to the SMPS systems. For the soot particles, the FMPS underestimated the particle sizes even more, up to 40%. The study concluded that the agreement between FMPS and SMPS is linked to the particle size and morphology. Hornsby and Pryor (2014) compared four SMPS systems and one FMPS for particles with GMDs between 10 nm and 100 nm. They found low deviation for the FMPSs from the GMD (±7.5%) as measured by the SMPS systems. Awasthi et al. (2013) compared the Engine Exhaust Particle Size (EEPS 3090; TSI Inc., Shoreview, MN, USA), which uses the same measurement design as the FMPS, with an SMPS for silver agglomerates, and showed that the EEPS consistently measured smaller number median mobility diameters and overestimated the total number concentration up to 67%. They also concluded that for small monodisperse particles (<80 nm), the EEPS measured diameters close to that of the SMPS but with a polydispersive distribution. No studies containing FMPS size distributions with a GMD higher than 200–250 nm could be found within the available literature by the authors.

This study was initiated by the observation that measuring the particle size distributions from powder agitation using rotating drum methods has been shown to produce inconsistent results when comparing size distributions measured with FMPS and ELPI, where the FMPS consistently showed a mode with the GMD of 200 nm, which is not observable in the ELPI data (Levin et al. In prep.). These data showing a mode with a GMD of 200 nm are consistent with data from several other dustiness studies, where the FMPS has been used to measure dust particles (Schneider and Jensen 2008; Jensen et al. 2009; Burdett et al. 2013; Levin et al. 2014).

Previously, efforts to establish correction algorithms for the FMPS have been presented by Jeong and Evans (2009) and Zimmerman et al. (2015). The first study proposed an adjustment of measured FMPS number concentration in channels below 93.1 nm through an empirical correction established by comparing FMPS size distributions with that of an SMPS. The second study extended this correction by proposing an adjustment of size bins starting at 80.6 nm and above which broadens the upper limit of the instrument to 857 nm to compensate for the underestimation of particle sizes. Furthermore, they normalized each size bin with the ratio in total concentration between the FMPS and a water-based condensation particle counter (CPC). There is, however, a need to further test if such a correction holds true for particles larger than 300 nm, which was the upper size range in Zimmerman et al. (2015). Since no information on the influence of particles with a GMD above the measurement range of the FMPS but below the pre-separator has been found by the authors, this possible error source needed to be addressed.

This study aims to investigate the apparent size-dependent deviations of FMPS when compared to other particle sizing instruments such as SMPS and ELPI. While a large amount of studies have compared the instruments for <200 nm particles, scarce data exist for particle size distributions with GMDs in the remainder of the claimed FMPS size range reaching up to 560 nm. Because the FMPS samples particles up to 1 μm in size by pre-selection through a $PM_{1.0}$ cyclone, we have also studied the effect of particle size distributions with GMDs above the FMPS size classification limit (560 nm) on the FMPS response. Finally, attempts were made to characterize the FMPS unipolar charger and calculate the charging profile with regard to particle size to further understand the instrument response to various particle sizes and possible interfering size ranges.

2. METHODS

2.1. Instrumentation

Three types of instruments designed for size measurements of particles in the sub-micron size range were included in the study. Additionally, a CPC was added as a reference instrument for comparisons of total number concentration.

2.1.1. Fast Mobility Particle Sizer (FMPS 3091, TSI)

The FMPS (TSI 2006) is a recently developed instrument based on the Electrical Aerosol Spectrometer (EAS; Tammet

et al. 2002). While the EAS consists of two parallel compartments for measuring particle mobility, one with diffusion charging and one with field charging, the FMPS only used the diffusion charger part, which positively charges the particles. In the EAS setup, information from the field charging part was used in the classification of particles larger than 300 nm due to the conversion from mobility to particle size in this region becoming ambiguous in the diffusion charging part (Tammet et al. 2002). After charging, the particles are separated in an electric field according to their electrical mobility and detected by 22 electrometers positioned in a vertical column. The measured currents are then corrected for multiple charges and image charges and then inverted from the 22 measured currents into 32 size channels ranging from 5.6 nm to 560 nm in electric mobility equivalent diameter. The measured size and concentration are therefore both dependent on the charging efficiency. Since the output contains more size channels than actual measurements, some assumptions must be made in the data inversion algorithm—these are, however, not disclosed by the manufacturer. The FMPS measures particle size distributions with a 1-s time resolution. Intake sampling for the FMPS is done at 10 l/min through a $PM_{1.0}$ cyclone. Two identical FMPS systems were used within this study, hereafter denoted as FMPS 1 and 2.

2.1.2. *Electrical Low Pressure Impactor (ELPI+, Dekati)*

The ELPI (Keskinen et al. 1992; Järvinen et al. 2014) uses a unipolar diffusion charger to charge the aerosol as it enters the instrument. The particles are size-separated according to their aerodynamic equivalent diameter in a cascade impactor where the particles are detected through charge measurements as they impact onto the 13 impactor plates. The final stage consists of a back-up filter stage. The measured currents in the ELPI+ are then corrected for multiple charges, image charges, and then converted into 14 concentrations specific for each size fraction ranging from 6 nm to 10 μm in aerodynamic equivalent diameter. Since the 14 measured currents directly correspond to the 14 size channels, and only concentration data is extracted from this, the data inversion is simpler and carries less assumptions than in the case of the FMPS. Intake sampling for the ELPI is done at 10 l/min and it measured particle size distributions with 1-s time resolution.

2.1.3. *Scanning Mobility Particle Sizer (SMPS)*

The SMPS (Wang and Flagan 1990) used in this study consisted of a ^{63}Ni aerosol neutralizer, a Differential Mobility Analyzer (DMA, Vienna type, 28 cm; Winklmayr et al. 1991), and a CPC (CPC 3010, TSI; Mertes et al. 1995). It was built and intercompared according to current technical standards for mobility size spectrometers as described by Wiedensohler et al. (2012). The sheath air was dried using silica gel. The SMPS measures the mobility equivalent size of the particles in the range of 10 nm to 1000 nm, which is within the operating range of the CPC. To increase size resolution, the measurement range only covered a limited range, e.g., 50–500 nm, were the actual size range was adjusted to match the particle size distributions being measured.

The SMPS was operated with two adjacent 90-s scans, one with increasing voltage and one with decreasing voltage. Data inversion was performed with a Labview (National Instruments, Austin, TX, USA) program (Löndahl et al. 2006), which also controlled the DMA and CPC. Particle charge correction was performed according to the bipolar charge distribution from Wiedensohler (1988) and, in the interval –2 to 2 elementary charges, from Fuchs (1963). The inversion of the SMPS data included correction for CPC smearing (Collins et al. 2002), CPC counting efficiency (Zhou 2001), and deviations from the ideal DMA transfer functions (Collins et al. 2004). The DMA was run with an aerosol flow of 1 l/min and a sheath air flow of 10 l/min.

2.1.4. *Condensation Particle Counter (CPC 3007, TSI)*

The CPC 3007 (TSI 2002) measures the total number concentration of particles larger than 10 nm in the concentration range up to 10^5 cm^{-3} (Hämeri et al. 2002) with a 1-s time resolution. The CPC 3007 samples inlet air with a flow of 0.7 l/min and has a manufacture stated concentration accuracy of $\pm$20%.

Sizing instruments were validated prior to the experiments using Polystyrene Latex Spheres (PSL, 80 nm and 150 nm) to ensure correct sizing and concentration. However, as reported previously, the FMPS is unable to properly measure the monodisperse distributions that the PSL should give rise to due to its data inversion where the measured particles always will be spread out over a minimum of five channels (TSI 2011; Leskinen et al. 2012; Awasthi et al. 2013). The CPC 3010 and CPC 3007 were also compared in terms of concentration to be within the manufacture-stated precision. More information regarding control of calibration can be found in the online supplementary information.

2.2. Particle Generation and Test Setup

Test particles for the comparative studies were created by first aerosolizing a solution of NH_4NO_3 and water with a constant output atomizer using pressurized air of 1.5–3 bar depending on desired conditions. This aerosol was then dried using a diffusion dryer with silica gel to form salt particles with diameters of 40–50 nm. The dried salt particles were then introduced to the Condensation Aerosol Generator (SLG 250; Topas, Dresden, Germany) where DEHS was condensed upon them to create spherical droplets. The oil droplet size could be varied from 50 nm up to 3 μm by varying the number of seed particles, oil temperature, and flow rate through the saturator.

The formed DEHS droplets were directly emitted into a 1.3 m^3 stainless steel chamber (Figure 1). The chamber was ventilated with HEPA-filtered air at 1 h^{-1} and used as a buffer volume to ensure stable concentrations. A joint aluminum sampling tube ($\phi = 140$ mm) with a constant airflow of 40 l/min was used to distribute the stainless steel sampling tubes, 10 mm diameter to the instruments. Theoretical concentration differences along the sampling tube due to diffusional and gravitational losses were estimated to be less than 1% for the size range of interest in this study, which were experimentally confirmed.

A total of 39 measurement runs was made with the desired particle GMD varying from 50 nm to 800 nm. The desired Geometric Standard Deviation (GSD) of the distribution was around 1.3 to minimize errors in FMPS inversion due to monodisperse aerosol. A measurement run constituted of 30 min of continuous measurement of a stable (±10% in concentration) aerosol. Before a measurement started, all instrument flows were controlled, zero-tests were conducted using HEPA-filters, and electrometers zeroed where it was necessary. After each measurement run was concluded, the chamber was flushed with HEPA-filtered air to lower the background concentration (<50 cm^{-3}) in preparation of the next run.

2.3. Unipolar Charging

In unipolar diffusion charging, the aerosol is introduced to a volume with a high concentration of gaseous ions of a specific charge, which are captured by the particles through the high-diffusion coefficient of the ions. Fuchs' limited sphere theory (Fuchs 1963) together with corrections by Hoppel and Frick (1986) describes the theory of this particle charging. After passing through the charger volume, an average charge per particle, $\overline{q}$, has been imposed onto the particles. The average charge depends on the particle diameter, d_p, the ion density within the charger volume, N_i, and the particle residence time within the charger volume, t. The latter two relate to charging conditions and are properties of the charger design; they are often described as the so-called $N_i t$-product. For a specific $N_i t$-product and within a specific particle size range, the average charge per particle can be related to the particle diameter through a power-law such as:

$$\overline{q} \propto d_p^x \qquad [1]$$

Besides the three parameters described above, unipolar charging may be influenced by several other factors such as particle morphology, particle dielectric constant, gas pressure temperature, as well as ion properties such as mass and mobility (Kulkarni et al. 2011).

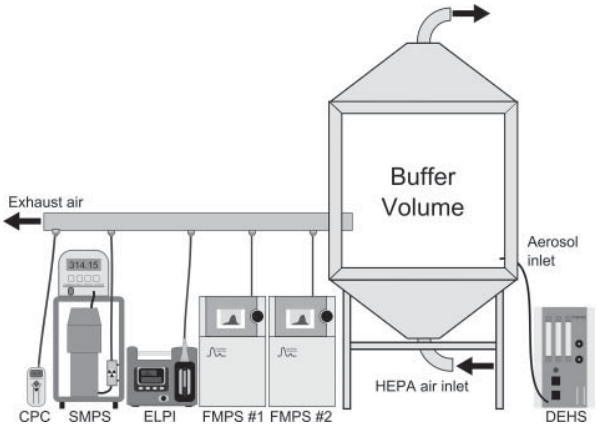

FIG. 1. Schematic overview of measurement setup. Tube lengths are not to scale.

2.4. Data Analysis

The raw data from the SMPS was inverted with regard to multiple-charge correction and diffusion losses. ELPI data was density-corrected with the DEHS density of 912 kg/m^3 adjusted for contribution of seed particle to density. To increase the comparability between instruments, the mobility diameter measured by FMPS and SMPS was converted into aerodynamic diameter using the assumption of spherical shape and the known density of DEHS using:

$$d_{aero}^2 \cdot C_{c,aero} = d_{mob}^2 \cdot C_{c,mob} \frac{\rho_p}{\rho_0} \qquad [2]$$

where d denotes particle diameter and C_c the Cunningham slip correction factor with subscripts *mob* and *aero* for mobility and aerodynamic equivalent diameters, respectively, ρ_0 is the standard density (1000 kg/m^3), and ρ_p is the particle density (Hinds 1999). All measurement data were corrected for diffusional and gravitational sampling losses in tubing and tubing bends (<5%).

For each measurement run, 30 min of stable conditions were selected and the data of the FMPS and ELPI were averaged down to the same resolution as the SMPS (180 s). Fitting of log-normal functions to these size distributions was done to parameterize them into GMD, GSD, and modal number concentrations using an automated algorithm (Hussein et al. 2005). In all cases of fitting, single-modal fitting was selected as the preferable choice. Means and standard deviations of the modal diameter and modal concentrations were then calculated. Data from the CPC was calculated into a mean value with standard deviations for the entire 30 min measurement run.

For further analysis of the FMPS, the raw current response from the 22 electrometers was studied. To remove the effect of concentration differences between different measurement runs, all electrometer currents, I, were normalized with the total concentration as measured with CPC 3007, N_{CPC}. Thus the average number of charges per particle, $\overline{n}$, which is equal

to the average charge per particle, $\overline{q}$, divided by elementary charge, e, was calculated as:

$$\overline{n} = \sum_{i=1:22} \left(\frac{I_i}{N_{CPC} \cdot Q_{FMPS} \cdot e} \right) \quad [3]$$

where Q_{FMPS} is the flow of the FMPS. By calculating this average number of charges of distributions with various GMD, an exponential fit was made to determine the exponent x as shown in Equation (1) and the number of charges can be extrapolated for a large range of particle sizes. Finally, the electrical mobility, Z, dependency on particle size for the FMPS unipolar charger can be calculated through:

$$Z = \frac{\overline{n} \cdot e \cdot C_C}{3 \cdot \pi \cdot \eta \cdot d_p} \quad [4]$$

where η is the viscosity of air.

3. RESULTS AND DISCUSSION

Figure 2 shows typical size distribution measurements within the sub-micron range as measured by FMPS, SMPS, and ELPI during four separate measurement runs. Visually, it appears that there is good agreement between all instruments for the distributions at 90 nm and 150 nm (Figures 2a and b, respectively). As the particle sizes increase to 350 nm (Figure 2c), the FMPS distribution appears to be situated at a lower size (200 nm) than that of the other instruments. This becomes even clearer as the particle sizes grow further to 500 nm (Figure 2d); here it obvious that the FMPS modal number concentration (at 200 nm) is higher than the other instruments. The apparent measured particles in the lowest stage of the ELPI with 10 nm mid-point value in Figures 2a, b, and d are due to the higher noise ratio of the filter stage of the ELPI.

Figure 3 presents the fitted GMDs with standard deviations from all 39 measurement runs for the four instruments. The comparison between SMPS and ELPI fitted GMDs falls close to the (1 to 1)-line against those of the SMPS ($R^2 = 0.98$), and no size-dependent shift in the comparison can be observed.

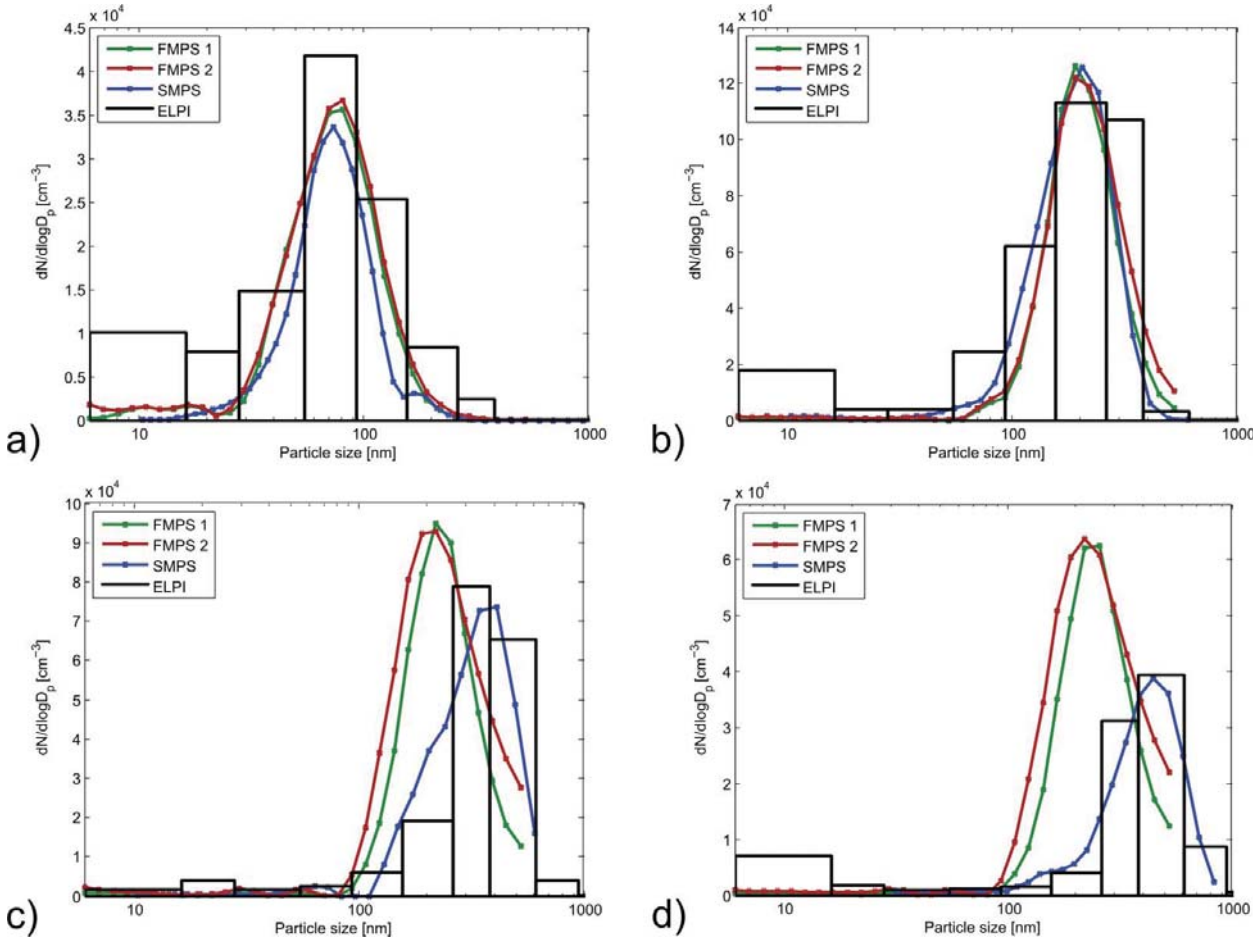

FIG. 2. (a–d) Size distributions as measured by FMPS, SMPS, and ELPI in the sub-micron size range (90, 150, 350, and 500 nm as measured by SMPS and ELPI).

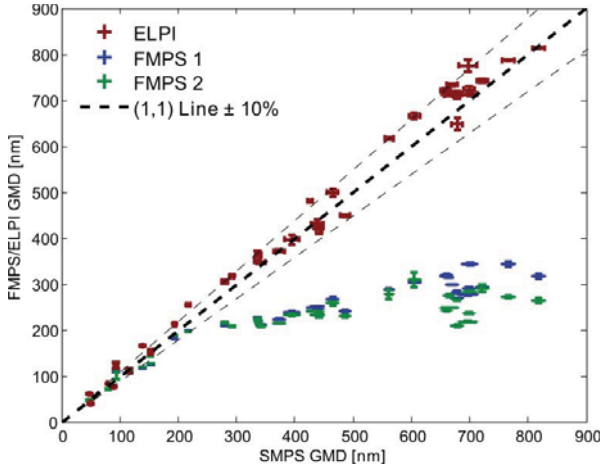

FIG. 3. Fitted GMDs from FMPSs and ELPI plotted against GMDs from SMPS.

The FMPS data appear to behave in two ways depending on the size range: Up to GMDs of ~200 nm, the data correlates well ($R^2 = 0.94$); however, above 200 nm, it is clear that both FMPSs underestimate the modal sizes as compared to both SMPS and ELPI. Thereafter, they continue to produce distributions with GMDs between 200 nm and 300 nm, well up into ranges above the 560 nm size-classification limit of the instrument. In no occurrence, as the particle sizes grew, did the FMPSs show only the tail end of a distribution, but rather showed a full particle mode.

The ratio in number concentrations contained in the particle modes for FMPS and ELPI against SMPS as well as the concentration ratio between CPC 3007 and the SMPS is shown in Figure 4. In general, the number concentrations were between $3{\cdot}10^4$ cm^{-3} and $6{\cdot}10^4$ cm^{-3}. There is a good correlation between SMPS and CPC (Ratio = 1.03 ± 0.04) and SMPS–ELPI (Ratio = 0.98 ± 0.14). For the SMPS–FMPS comparison, there is a similar scenario to that of the GMD comparison, where there is a good correlation up until 200 nm (Ratio = 0.99 ± 0.12). For GMDs larger than this, the FMPS number concentration starts to exceed that of the SMPS. The number concentration ratio peaks around 500 nm where the number concentration measured by the FMPS is twice than that of the SMPS. After the particle GMD reaches the FMPS upper size limit, the ratio decreases again; however, it remains above 1 until the GMD reaches 650 nm. At this point, the majority of the particle distribution should lie outside the FMPS range.

The correction algorithm suggested by Zimmerman et al. (2015) is based on particle measurements up to 300 nm. However, the fact that the GMD response in the FMPS is not continuously increasing with the GMD of the measured aerosol above this range, Figure 3 points toward an upper limit for such a correction of bin sizes. In addition, such an algorithm for correction would still misclassify results given by erroneous measurements of particles larger than the measured size range but smaller than the pre-separator cut-off. Furthermore, the size dependent concentration overestimation in Figure 4 suggests that a correction of FMPS concentration by that of a CPC would give an incorrect result in cases where a polydisperse aerosol is measured.

The concentration-normalized electrometer response for 22 different particle sizes, as measured with SMPS, between 50 nm and 800 nm is shown in Figure 5. From the response curves, it is clear that the particle size separation is more size sensitive for smaller particles than larger particles with the same size increment. In fact, particle GMDs between 550 nm and 800 nm give almost identical response and GMDs around 400–450 nm give a very similar response. It is also noticeable that even though the three last distributions have a true GMD outside the FMPS range, the response from the last electrometer is decreasing for all of them. This all shows that as the

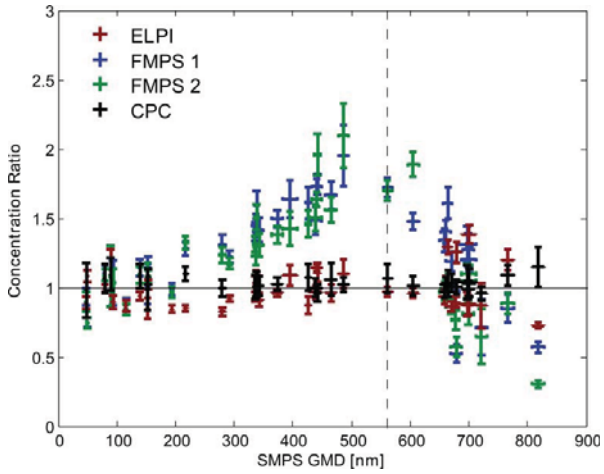

FIG. 4. Concentrations of FMPS, ELPI, and CPC normalized with that of SMPS. Dashed line indicates the upper measurement limit of the FMPS.

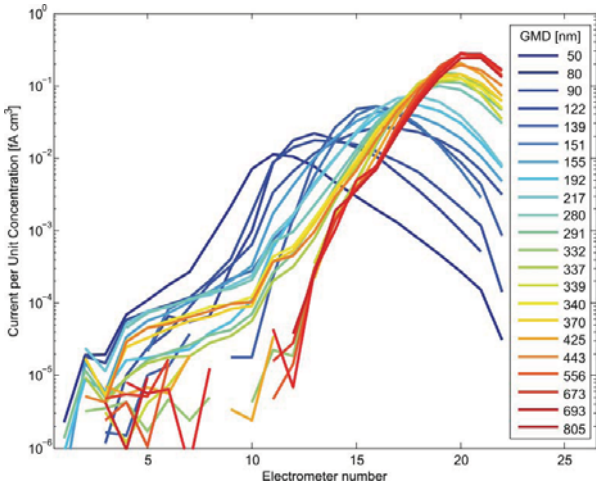

FIG. 5. Electrometer response distribution normalized by total concentration. GMD values as measured by SMPS.

particle size increases, it becomes more challenging to differentiate their particle size through this method.

The exponential fit of average number of charges per particle gave an exponent for the relationship between size and charge of 1.21 ± 0.02. It should be noted that there is an uncertainty in this value due to the polydisperse nature of the aerosols. In the ideal case, the charger would be characterized with monodisperse particles but due to the FMPS inversion being unable to cope with this (TSI 2011), distribution GSD varied from 1.25 to 1.35, as measured by SMPS, during the measurements. No previous value on the FMPS charger has been reported in literature, and these calculated values lie within the range of other reported values for unipolar chargers that lie between 1.32 and 1.91 for direct corona charges (Ntziachristos et al. 2004; Park et al. 2007), for indirect corona chargers between 1.11 and 1.36 (Liu and Pui 1975; Jung and Kittelson 2005; Fierz et al. 2007), and for turbulent jet chargers between 1.13 and 1.17 (Jung and Kittelson 2005; Fissan et al. 2007; Park et al. 2007).

This 1.21 exponent in the power law can now be used for further analysis of the FMPS response to investigate whether the incorrect measurements stem from misclassification of particle sizes. Figure 6 shows a corrected concentration ratio for the FMPS defined as:

$$Ratio = \frac{N_{FMPS}}{N_{SMPS}} \cdot \left(\frac{GMD_{FMPS}}{GMD_{SMPS}}\right)^{1.21}$$

This charging corrected ratio is now constant (0.94 ± 0.11) within the measurement range of the FMPS above which it starts to decline. This constant behavior clearly suggests that the particles are detected in the FMPS but misclassified, e.g., a 500 nm particle interpreted as a 200 nm particle will give an overestimation in concentration by a factor of approximately 3 due to it carrying the charge equivalent of a 500 nm particle.

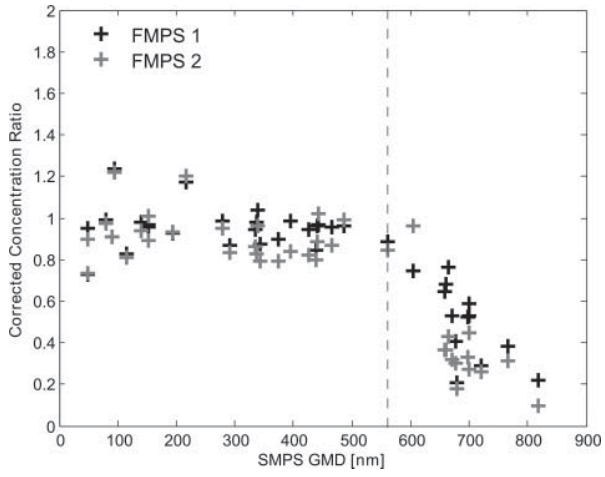

FIG. 6. Concentration ratio between FMPS and SMPS corrected with respective GMD and charging parameter.

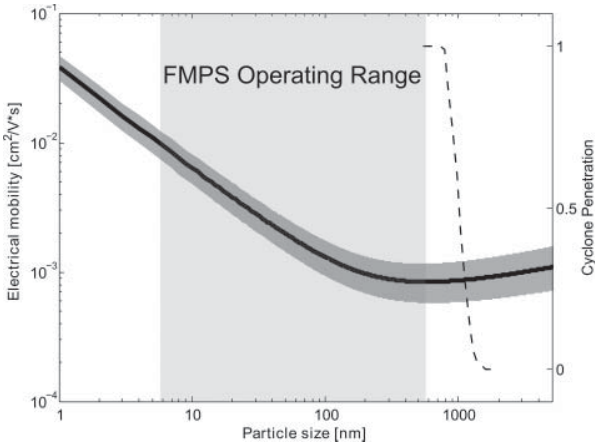

FIG. 7. Calculated electrical mobility as a function of particle size. Dark shaded area denotes 95% confidence bounds based on fitting, light shaded area the size range of the FMPS. Dashed line indicates penetration through FMPS inlet cyclone pre-separator.

Furthermore, the fact that such high concentrations are measured even at GMDs higher than the upper limit of the FMPS might be linked to the fact that the inlet cyclone of the FMPS has an aerodynamic cut-off diameter of 1μm. This means that particles in the size-range of 560 nm 1000 nm will still enter the instrument, become charged, and pass along the electrometer column. The calculated, Equation (4), particle electrical mobility of spherical particles after being charged by the FMPS charger as a function of size is presented in Figure 7. It is clear that the size dependency flattens out due to the Cunningham slip factor becoming a weaker function as the particle size grows and the electrical mobility reaches a minimum at 577 ± 54 nm. Above this point there is actually an increase in electrical mobility up to the inlet pre-separator D_{50} of 1000 nm, and above. This would effectively mean that differentiation of particles in this region based on electrical mobility analysis after unipolar charging is becoming impossible and that large particles may even be unintendedly detected by an electrometer stage aimed for particles of smaller size but similar electrical mobility. According to this extrapolation, a spherical 1 μm particle, which has a penetration of 0.5, would have the same electrical mobility and be similarly interpreted as a 360 nm particle. Its concentration response would, however, be higher due to it carrying a higher charge. Also, it should be noted that as the function for average charge per particle exceeds the measured size range, the calculated power-law may not be precise due to shifting conditions.

For non-spherical particles, Shin et al. (2010) showed that agglomerates are able to carry more charge after unipolar charging than a spherical particle of the same mobility size and that the size dependency is steeper than that for spherical particles. This would infer that the magnitude of incorrect particle sizing in the FMPS would increase since the electrical mobility, compared to that shown in Figure 7, would increase and that

the curve minima would move to smaller sizes. This would result in an incorrect response, both in terms of interpreted size and concentration, since a wider span of particle sizes within the measurement range will have the same electrical mobility. Furthermore, the influence of particles larger than the intended measurement range (>560 nm) but below the aerodynamic cut-off of the cyclone (1 μm) would have a higher risk of being detected in the instrument electrometers and interfere on the measurements. In the case of agglomerates, the particle effective density can often be below unit density that results in a shifted cyclone cut-off point to a larger equivalent mobility diameter, which extends the interfering range of large particles in the measurements. Therefore, post-measurement corrections of FMPS results are challenging and would need to take the particle shape into account and can therefore not be independent of the particle source. In the presence of particles with a diameter above the mobility minimum, such a correction would be impossible due to the measurement ambiguity.

A separate possible explanation for the occurrences of underestimated GMDs and overestimated concentrations is the data treatment in the FMPS where the signal from 22 electrometers is inverted to 32 size channels. Such data inversion includes some type of data-fitting, e.g., log-normal or polynomial. Such a fitting would be useful in many applications such as atmospheric measurements where the particles fall into well-known modes within the range of the instrument (Birmili 1998; Mäkelä et al. 2000). Similarly combustion processes mainly produce particle modes within this range. In many other applications such as dustiness testing, occupational powder handling, and other industrial processes the freshly emitted aerosol might not assume these otherwise common particle modes. Using log-normal fitting for these types of particle size distributions may result in forcing the particle GMD into the measurement range, while increasing the particle numbers as the actual current is registered from large particles.

Other instruments using unipolar diffusion charging, such as DISCmini (Fierz et al. 2011) and nanoTracer (Marra et al. 2009), are known to be using fitting of the data and therefore report upper and lower limits on the GMD that can be measured within the total measurement range. For the FMPS, however, there are no such GMD limits reported in literature. If such a fitting takes place in the instrument, an extremely important parameter to output would be the goodness of fit to ensure that the actual distribution is not an artifact of fitting.

4. CONCLUSIONS

In this study, we compared the measured particle size distributions of two FMPSs with that of one ELPI and an SMPS for 39 distributions of spherical DEHS particle distributions in a controlled test environment. The focus was put on the differences in the number size distribution log-normal fitted GMDs and the modal number concentrations as measured by the FMPSs compared to the other instruments.

The study showed that the ELPI and SMPS agreed well, both in terms of GMD ($R^2 = 0.98$) and number concentration (Ratio $= 0.98 \pm 0.14$), within the entire measured size range (50–850 nm). SMPS and ELPI also agreed well with the CPC in terms of total number concentration. The FMPSs agreed well with the other instruments for distributions with a GMD lower than 200 nm ($R^2 = 0.94$). However, for particle size distributions with a GMD higher than ~200 nm neither the particle size nor concentration can properly be measured using the FMPS. Furthermore, the size response of the FMPS was not continuously increasing with increasing true particle size, rendering a correction algorithm difficult.

Calculations on the measured electrometer currents showed an increasingly similar response as the particle size distribution GMD increased ending with sizes above 500 nm giving almost identical responses. Fitting of average number of charges per particle and power-law fit resulted in a diameter dependence of charge response as $d_p^{1.21}$ for the FMPS unipolar charger. The calculated electrical mobility showed a minimum in mobility for spherical particles at 577 nm, above which the electrical mobility increases with particle size. This indicates that there is an interfering range of particles above the measurement range, but below the cut-off (1 μm) of the inlet preseparator that will be erroneously detected.

Although further data might be needed for decisive conclusions, indications were given that measured distributions with a GMD above 200 nm cannot be deemed reliable as it may originate from a distribution of larger size being incorrectly measured, if not confirmed through other means of measurement, as it might be an artifact distribution. As many industrial processes, such as production, pouring, and packaging of nano-structured powder, are known to produce GMDs exceeding this or agglomerated particles where the effect will be even more pronounced, a secondary instrument should always be used to confirm particle observations. Based on this we recommend that reported size distribution with a GMD of 200 nm or above be further investigated as it might be caused by erroneous measurement.

FUNDING

This work was conducted as part of the Strategic Research effort at the National Research Centre for the Working Environment and the "Danish Centre for Nanosafety" (20110092173/3) from the Danish Working Environment Research Foundation, AFA Insurance (Grant no. 130122), and the EU Framework 7 Programme NANoREG (contract no. 310584). It was carried out within the Nanometer Structure Consortium (nmC@LU) at Lund University and the FORTE-centre METALUND.

SUPPLEMENTAL MATERIAL

Supplemental data for this article can be accessed on the publisher's website.

REFERENCES

Asbach, C., Aguerre, O., Bressot, C., Brouwer, D. H., Gommel, U., Gorbunov, B., Le Bihan, O., Jensen, K. A., Kaminski, H., Keller, M., Koponen, I. K., Kuhlbusch, T. A. J., Lecloux, A., Morgeneyer, M., Muir, R., Shandilya, N., Stahlmecke, B., and Todea, A. M. (2014). Examples and Case Studies, in *Handbook of Nanosafety*, U. Vogel, K. Savolainen, Q. Wu, M. van Tongeren, D. Brouwer, and M. Berges, eds., Academic Press, San Diego, CA, pp. 223–278.

Asbach, C., Kaminski, H., Fissan, H., Monz, C., Dahmann, D., Muelhopt, S., Paur, H., Kiesling, H., Herrmann, F., Voetz, M., and Kuhlbusch, T. (2009). Comparison of Four Mobility Particle Sizers with Different Time Resolution for Stationary Exposure Measurements. *J. Nanopart. Res.*, 11:1593–1609.

Awasthi, A., Wu, B.-S., Liu, C.-N., Chen, C.-W., Uang, S.-N., and Tsai, C.-J. (2013). The Effect of Nanoparticle Morphology on the Measurement Accuracy of Mobility Particle Sizers. *MAPAN-J. Metrol. Soc. India*, 28:205–215.

Birmili, W. (1998). *Production of New Ultrafine Aerosol Particles in Continental Air Masses (Dissertation)*. University of Leipzig, Leipzig.

Brouwer, D., van Duuren-Stuurman, B., Berges, M., Jankowska, E., Bard, D., and Mark, D. (2009). From Workplace Air Measurement Results Toward Estimates of Exposure? Development of a Strategy to Assess Exposure to Manufactured Nano-Objects. *J. Nanopart. Res.*, 11: 1867–1881.

Burdett, G., Bard, D., Kelly, A., and Thorpe, A. (2013). The Effect of Surface Coatings on the Dustiness of a Calcium Carbonate Nanopowder. *J. Nanopart. Res.*, 15:1311.

Collins, D. R., Cocker, D. R., Flagan, R. C., and Seinfeld, J. H. (2004). The Scanning DMA Transfer Function. *Aerosol Sci. Technol.*, 38:833–850.

Collins, D. R., Flagan, R. C., and Seinfeld, J. H. (2002). Improved Inversion of Scanning DMA Data. *Aerosol Sci. Technol.*, 36:1–9.

Dockery, D., Pope, C., Xu, X., Spengler, J., Ware, J., Fay, M., Ferris, B., and Speizer, F. (1993). An Association between Air-Pollution and Mortality in 6 United-States Cities. *N. Engl. J. Med.*, 329: 1753–1759.

Donaldson, K., Stone, V., Tran, C. L., Kreyling, W., and Borm, P. J. A. (2004). Nanotoxicology. *Occup. Environ. Med.*, 61:727–728.

Fierz, M., Burtscher, H., Steigmeier, P., and Kasper, M. (2007). *Field Measurement of Particle Size and Number Concentration with the Diffusion Size Classifier (Disc)*. SAE Technical Paper No. 2008-01-1179, SAE International, Warrendale, PA.

Fierz, M., Houle, C., Steigmeier, P., and Burtscher, H. (2011). Design, Calibration, and Field Performance of a Miniature Diffusion Size Classifier. *Aerosol Sci. Technol.*, 45:1–10.

Fissan, H., Neumann, S., Trampe, A., Pui, D. Y. H., and Shin, W. G. (2007). Rationale and Principle of an Instrument Measuring Lung Deposited Nanoparticle Surface Area. *J. Nanopart. Res.*, 9:53–59.

Fuchs, N. A. (1963). On the Stationary Charge Distribution on Aerosol Particles in a Bipolar Ionic Atmosphere. *Geofis. Pura E Appl.*, 56:185–193.

Hämeri, K., Koponen, I. K., Aalto, P. P., and Kulmala, M. (2002). The Particle Detection Efficiency of the TSI-3007 Condensation Particle Counter. *Aerosol Sci.*, 33:1463–1469.

Hinds, W. C. (1999). *Aerosol Technology: Properties, Behavior and Measurements of Airborne Particles*, 2nd ed. John Wiley, New York.

Hoppel, W. A., and Frick, G. M. (1986). Ion–Aerosol Attachment Coefficients and the Steady-State Charge Distribution on Aerosols in a Bipolar Ion Environment. *Aerosol Sci. Technol.*, 5:1–21.

Hornsby, K. E., and Pryor, S. C. (2014). A Laboratory Comparison of Real-Time Measurement Methods for 10-100-nm Particle Size Distributions. *Aerosol Sci. Technol.*, 48:571–582.

Hussein, T., Dal Maso, M., Petaja, T., Koponen, I. K., Paatero, P., Aalto, P. P., Hameri, K., and Kulmala, M. (2005). Evaluation of an Automatic Algorithm for Fitting the Particle Number Size Distributions. *Boreal Environ. Res.*, 10:337–355.

Järvinen, A., Aitomaa, M., Rostedt, A., Keskinen, J., and Yli-Ojanpera, J. (2014). Calibration of the New Electrical Low Pressure Impactor (ELPI Plus). *J. Aerosol Sci.*, 69:150–159.

Jensen, K. A., Koponen, I. K., Clausen, P. A., and Schneider, T. (2009). Dustiness Behaviour of Loose and Compacted Bentonite and Organoclay Powders: What is the Difference in Exposure Risk? *J. Nanopart. Res.*, 11:133–146.

Jeong, C.-H., and Evans, G. J. (2009). Inter-Comparison of a Fast Mobility Particle Sizer and a Scanning Mobility Particle Sizer Incorporating an Ultrafine Water-Based Condensation Particle Counter. *Aerosol Sci. Technol.*, 43:364–373.

Jung, H. J., and Kittelson, D. B. (2005). Characterization of Aerosol Surface Instruments in Transition Regime. *Aerosol Sci. Technol.*, 39:902–911.

Kaminski, H., Kuhlbusch, T. A. J., Rath, S., Goetz, U., Sprenger, M., Wels, D., Polloczek, J., Bachmann, V., Dziurowitz, N., Kiesling, H.-J., Schwiegelshohn, A., Monz, C., Dahmann, D., and Asbach, C. (2013). Comparability of Mobility Particle Sizers and Diffusion Chargers. *J. Aerosol Sci.*, 57:156–178.

Keskinen, J., Pietarinen, K., and Lehtimaki, M. (1992). Electrical Low-Pressure Impactor. *J. Aerosol Sci.*, 23:353–360.

Kuhlbusch, T. A. J., Asbach, C., Fissan, H., Goehler, D., and Stintz, M. (2011). Nanoparticle Exposure at Nanotechnology Workplaces: A Review. *Part. Fibre Toxicol.*, 8:22.

Kulkarni, P., Baron, P. A., and Willeke, K. (2011). *Aerosol Measurement: Principles, Techniques, and Applications*. 3rd ed. John Wiley, Hoboken, NJ.

Leskinen, J., Joutsensaari, J., Lyyranen, J., Koivisto, J., Ruusunen, J., Jarvela, M., Tuomi, T., Hameri, K., Auvinen, A., and Jokiniemi, J. (2012). Comparison of Nanoparticle Measurement Instruments for Occupational Health Applications. *J. Nanopart. Res.*, 14:718.

Levin, M., Koponen, I. K., and Jensen, K. A. (2014). Exposure Assessment of Four Pharmaceutical Powders Based on Dustiness and Evaluation of Damaged HEPA Filters. *J. Occup. Environ. Hyg.*, 11:165–177.

Levin, M., Witschger, O., Bau, S., Birkedal, R., Clausen, P. A., Jankowska, E., Koponen, I. K., Mølhave, K., Asbach, C., and Jensen, K. A. (In prep.). Can We Trust Online Measurements of the (Lung-Deposited) Surface Area Concentrations in Dust from Powder Nanomaterials?

Liu, B. Y. H., and Pui, D. Y. H. (1975). On the Performance of the Electrical Aerosol Analyzer. *J. Aerosol Sci.*, 6:249–254.

Löndahl, J., Pagels, J., Swietlicki, E., Zhou, J., Ketzel, M., Massling, A., and Bohgard, M. (2006). A Set-Up for Field Studies of Respiratory Tract Deposition of Fine and Ultrafine Particles in Humans. *J. Aerosol Sci.*, 37:1152–1163.

Mäkelä, J. M., Koponen, I. K., Aalto, P., and Kulmala, M. (2000). One-Year Data of Submicron Size Mods of Tropospheric Background Aerosol in Southern Finland. *J. Aerosol Sci.*, 31:595–611.

Marra, J., Voetz, M., and Kiesling, H.-J. (2009). Monitor for Detecting and Assessing Exposure to Airborne Nanoparticles. *J. Nanopart. Res.*, 12:21–37.

Mertes, S., Schroder, F., and Wiedensohler, A. (1995). The Particle-Detection Efficiency Curve of the Tsi-3010 Cpc as a Function of the Temperature Difference between Saturator and Condenser. *Aerosol Sci. Technol.*, 23, 257–261.

Ntziachristos, L., Giechaskiel, B., Ristimaki, J., and Keskinen, J. (2004). Use of a Corona Charger for the Characterisation of Automotive Exhaust Aerosol. *J. Aerosol Sci.*, 35:943–963.

Oberdorster, G., Maynard, A., Donaldson, K., Castranova, V., Fitzpatrick, J., Ausman, K., Carter, J., Karn, B., Kreyling, W., Lai, D., Olin, S., Monteiro-Riviere, N., Warheit, D., and Yang, H. (2005). Principles for Characterizing the Potential Human Health Effects from Exposure to Nanomaterials: Elements of a Screening Strategy. *Part. Fibre Toxicol.*, 2:8.

Oberdorster, G., and Utell, M. J. (2002). Ultrafine Particles in the Urban Air: To the Respiratory Tract - And Beyond? *Environ. Health Perspect.*, 110: A440–A441.

Park, D., Kim, S., An, M., and Hwang, J. (2007). Real-Time Measurement of Submicron Aerosol Particles Having a Log-Normal Size Distribution by Simultaneously Using Unipolar Diffusion Charger and Unipolar Field Charger. *J. Aerosol Sci.*, 38:1240–1245.

Schneider, T., and Jensen, K. A. (2008). Combined Single-Drop and Rotating Drum Dustiness Test of Fine to Nanosize Powders Using a Small Drum. *Ann. Occup. Hyg.,* 52:23–34.

Seinfeld, J. H., and Pandis, S. N. (2006). *Atmospheric Chemistry and Physics: From Air Pollution to Climate Change*. 2nd ed. John Wiley, Hoboken, NJ.

Shin, W. G., Wang, J., Mertler, M., Sachweh, B., Fissan, H., and Pui, D. Y. H. (2010). The Effect of Particle Morphology on Unipolar Diffusion Charging of Nanoparticle Agglomerates in the Transition Regime. *J. Aerosol Sci.*, 41:975–986.

Tammet, H., Mirme, A., and Tamm, E. (2002). Electrical Aerosol Spectrometer of Tartu University. *Atmos. Res.*, 62:315–324.

TSI. (2002). *Model 3007 Condensation Particle Counter: Operation and Service Manual*. TSI Inc., Shoreview, MN.

TSI. (2006). *Fast Mobility Particle Sizer Spectrometer: Operation and Service Manual*. TSI Inc., Shoreview, MN.

TSI. (2011). *Fast Moblity Sizers— FMPS 3091, EEPS 3090: Standard Operating Procedure—Recommendations, Quality Assurance*. TSI Inc., Shoreview, MN. Available at: ftp://ftp.tsi.com/pub/Lo_Charles/SOP%20-%20good%20practice-TJ.pdf.

Wang, S., and Flagan, R. (1990). Scanning Electrical Mobility Spectrometer. *Aerosol Sci. Technol.*, 13:230–240.

Wiedensohler, A. (1988). An Approximation of the Bipolar Charge-Distribution for Particles in the Sub-Micron Size Range. *J. Aerosol Sci.*, 19:387–389.

Wiedensohler, A., Birmili, W., Nowak, A., Sonntag, A., Weinhold, K., Merkel, M., Wehner, B., Tuch, T., Pfeifer, S., Fiebig, M., Fjaraa, A. M., Asmi, E., Sellegri, K., Depuy, R., Venzac, H., Villani, P., Laj, P., Aalto, P., Ogren, J. A., Swietlicki, E., Williams, P., Roldin, P., Quincey, P., Hueglin, C., Fierz-Schmidhauser, R., Gysel, M., Weingartner, E., Riccobono, F., Santos, S., Gruening, C., Faloon, K., Beddows, D., Harrison, R. M., Monahan, C., Jennings, S. G., O'Dowd, C. D., Marinoni, A., Horn, H.-G., Keck, L., Jiang, J., Scheckman, J., McMurry, P. H., Deng, Z., Zhao, C. S., Moerman, M., Henzing, B., de Leeuw, G., Loeschau, G., and Bastian, S. (2012). Mobility Particle Size Spectrometers: Harmonization of Technical Standards and Data Structure to Facilitate High Quality Long-Term Observations of Atmospheric Particle Number Size Distributions. *Atmos. Meas. Tech.*, 5:657–685.

Winklmayr, W., Reischl, G., Lindner, A., and Berner, A. (1991). A New Electromobility Spectrometer for the Measurement of Aerosol Size Distributions in the Size Range from 1 to 1000 Nm. *J. Aerosol Sci.*, 22:289–296.

Yao, X. H., Lau, N. T., Fang, M., and Chan, C. K. (2006). On the Time-Averaging of Ultrafine Particle Number Size Spectra in Vehicular Plumes. *Atmos. Chem. Phys.*, 6:4801–4807.

Zhou, J. (2001). *Hygroscopic Properties of Atmospheric Aerosol Particles in Various Environments* (Ph.D. thesis). Department of Nuclear Physics, Lund University, Lund, Sweden.

Zimmerman, N., Jeong, C.-H., Wang, J. M., Ramos, M., Wallace, J. S., and Evans, G. J. (2015). A Source-Independent Empirical Correction Procedure for the Fast Mobility and Engine Exhaust Particle Sizers. *Atmos. Environ.*, 100:178–184.

Zimmerman, N., Pollitt, K. J. G., Jeong, C.-H., Wang, J. M., Jung, T., Cooper, J. M., Wallace, J. S., and Evans, G. J. (2014). Comparison of Three Nanoparticle Sizing Instruments: The Influence of Particle Morphology. *Atmos. Environ.*, 86:140–147.

Paper IV

Can we trust real time measurements of lung deposited surface area concentrations in dust from powder nanomaterials?

Marcus Levin[1,2*], Olivier Witschger[3], Sébastien Bau[3], Elzbieta Jankowska[4], Ismo K. Koponen[2], Antti J. Koivisto[2], Per A. Clausen[2], Alexander Jensen[2] Kristian Mølhave[1], Christof Asbach[5], Keld A. Jensen[2]

[1]*Department of Micro and Nanotechnology, Technical University of Denmark, Kgs. Lyngby, DK-2800, Denmark.*
[2]*National Research Centre for the Working Environment, Lersø Parkallé 105, DK-2100 Copenhagen, Denmark.*
[3]*Institut National de Recherche et de Sécurité, Rue du Morvan, FR-54500 Vandoeuvre les Nancy, France.*
[4]*Natl Res Inst, Cent Inst Labour Protect, Zaklad Zagrozen Chem Pylowych & Biol, Ul Czerniakowska 16, PL-00701 Warsaw, Poland.*
[5]*Institut für Energie- und Umwelttechnik (IUTA),47229 Duisburg, Germany*

Abstract

A comparison between various methods for real-time measurements of lung deposited surface area (LDSA) using spherical particles and powder dust with specific surface area ranging from 0.03 to 112 m^2/g was conducted. LDSA concentrations measured directly using Nanoparticle Surface Area Monitor (NSAM) and Aerotrak and were compared to LDSA concentrations recalculated from size distribution measurements using Electrical Low Pressure Impactor (ELPI) and Fast Mobility Particle Sizer (FMPS). FMPS and ELPI measurements were also compared to dust surface area concentrations estimated from gravimetrical filter measurements and specific surface areas.

Measurement of LDSA showed very good correlation in measurements of spherical particles (R^2 > 0.97, Ratio 1.0 to 1.04). High surface area nanomaterial powders showed a fairly reliable correlation between NSAM and Aerotrak (R^2 0.73-0.93) and a material-dependent offset in the ratios (1.04-2.8). However, the correlation and ratio were inconsistent for lower LDSA concentrations. Similar levels of correlation were observed for the NSAM and the FMPS for high surface area materials, but with the FMPS overestimating the LDSA concentration. The ELPI showed good correlation with NSAM data for high LDSA materials (R^2 0.87-0.93), but not for lower LDSA concentrations (R^2 0.50-0.72). Comparisons of respirable dust surface area from ELPI data correlated well (R^2 > 0.98) with that calculated from filter samples, but materials-specific exceptions were present.

We conclude that there is currently insufficient reliability and comparability between methods in the measurement of LDSA concentrations. Further development is required to enable use of LDSA for reliable dose metric and regulatory enforcement of exposure.

Keywords: lung deposited surface area; exposure assessment; aerosol measurement; dustiness

* Corresponding author. Tel: +4539165274; Fax: +4539165201

E-*mail address*: mle@nrcwe.dk

Introduction

There is increasing evidence that the pulmonary toxicological response of ambient air-pollution and manufactured nanomaterials may, at least partially, be driven by the specific surface area dose of the test materials (Oberdorster 2000; Maynard and Kuempel 2005; Duffin et al. 2007; Jacobsen et al. 2009; Giechaskiel et al. 2009; Donaldson et al. 2013; Saber et al. 2014). Therefore, it is of high interest to include airborne particle surface area measurements to offer a potentially more biologically relevant metric in exposure and risk assessment. To meet these new developments, it is also of interest to include surface area measurements in dustiness testing; the latter tests are performed to rank the ability of powders to generate dust and used in e.g., new modeling approaches and regulatory exposure assessment (BS EN:15051 2006; Aitken et al. 2011; Jensen et al. 2015).

The surface area of airborne dust particles may be determined by either direct or indirect methods. There are currently no commercially available real-time methods to determine the geometric surface area concentration of airborne particles. In principle the most correct method would be direct determination of the specific surface area on filters using the BET inert gas-adsorption technique. Even-though this method has been demonstrated (Lebouf et al. 2011a; LeBouf et al. 2011b), the method is in reality not yet straight-forward and changes could potentially occur in the aerosol during filter-sampling and storage that might change the surface area. Therefore, this method may not be generally applicable.

Another approach is to estimate the surface area concentrations based on airborne particle number size distributions assuming particle shape. Particle number-size-distributions can be measured using a range of different optical, aerodynamic, electrical mobility and charging techniques. Therefore, the comparability in these measurements and the reliability in conversions from number and volume

concentrations metrics is still not well documented for non-spherical particles such as aggregates and agglomerates commonly observed in dustiness tests, covering a wide range of sizes from nano- to µm-size (Ibaseta and Biscans 2007; Schneider and Jensen 2008; Jensen et al. 2009; Tsai et al. 2009; Levin et al. 2014; Koivisto et al. 2015; Koponen et al. 2015). Even in case of direct release from an airborne synthesis processes, primary particles can already start to agglomerate or aggregate in the reactor and may further coagulate at or very near the point of release with similar result (Makela et al. 2009; Hameri et al. 2009; Schneider et al. 2011; Koivisto et al. 2012; Koivisto et al. 2015). Measurements are therefore challenging when the aerosol structure is not known, because this in principle prevents the possibility to convert number-size-distribution measurements into reliable surface area values (Fissan et al. 2013).

To overcome the uncertainties in size-distribution conversion, the lung deposited surface area (LDSA), i.e. the fraction of the total airborne particle geometric surface area concentration that would deposit in the human lung, of aerosols can be measured in real-time. Based on particle unipolar diffusion charging and subsequent current measurement with electrometers (Fissan et al. 2007; Shin et al. 2007), this principle is used by several instruments such as the Aerotrak (Aerotrak 9000, TSI inc, MN, USA) and the Nanoparticle Surface Area Monitor (NSAM 3550, TSI Inc, MN, USA). It should be noted that this surface area is not the same as the surface area determined by nitrogen or krypton gas-adsorption using the BET technique for powders (Bau et al. 2010).

Recently, a few studies reported measurements comparing the results of different number size-distribution and surface area monitors challenged to equidimensional or spherical and aggregated particles. For aerosol monitors, Asbach et al. (2012) investigated the correlation between Aerotrak (Aerotrak 9000, TSI inc, MN, USA) and Fast Mobility Particle Sizer (FMPS 3091, TSI inc, MN, USA) with polydisperse aerosols of different sizes and morphologies (35 nm cubic NaCl, 190 nm spherical Di-Ethyl-Hexyl-Sebacat (DEHS) oil particles and 50 nm agglomerated soot particles; all

modal diameters), and found good agreement (mostly within ±15 % difference) and correlation for NaCl ($R^2 \geq 0.985$) and soot ($R^2 \geq 0.997$) but poorer agreement for DEHS with deviations up to 50% ($R^2 \geq 0.989$). The comparability in the tests with DEHS decreased when the spherical particle sizes exceeded 400 nm, which has been reported to be the upper limit for accurate measurement with this type of instruments. Levin et al. (2015) compared the particle sizing and counting of the FMPS, Electrical Low Pressure Impactor (ELPI, Dekati, Finland) and a Scanning Mobility Particle Sizer (SMPS) for spherical particles in the size range of 50-900 nm. While ELPI and SMPS data agreed well within the tested size-range, the FMPS was unable to size particle larger than 200 nm correctly. This led to it severely underestimating the particle size and overestimating the concentration.

Leavey et al. (2013) compared the Aerotrak with LDSA concentrations calculated from size distributions measured with a SMPS for a range of different particle types and morphologies with mean particle diameters ranging from 30 to 140 nm. They found a strong correlation (R^2 0.78 – 0.99) between the two methods but a moderate dependency on particle type. In most cases, the SMPS data overestimated the LDSA as compared to the Aerotrak. Leskinen et al. (2012) compared LDSA concentrations measured with NSAM and SMPS and found that for TiO_2 agglomerates and dust agglomerates and found that values from NSAM were higher than those of the SMPS.

Todea et al. (Subm.) compared the measured LDSA from Aerotrak and NSAM for monodisperse spheres and agglomerates with the calculated value based on number concentration from a Condensational Particle Counter (CPC) and knowledge of particle size. They found that for spherical particles the NSAM and Aerotrak data both generally agreed within ±30% with the calculated value from the CPC in the size range of 20 to 346 nm. For spheres larger than 400 nm, LDSA concentration was underestimated by both instruments. For agglomerated particles, the

instruments based on unipolar diffusion charging generally overestimated the LDSA concentration compared to the CPC value, but mostly still within ±30%.

These previous results indicate that both method- and size-specific differences exist in the results given by different measurement devices used for sub-µm sized particles. Additional differences may arise when such devices are used to measure agglomerates with even wider size-distributions and different highly complex agglomerate structures, which may be found in dust generated from nanopowders. Since most applicable instrument(s), and potentially also the reliability of measurement results, will depend on the characteristics of the airborne particles and their size-distribution and all aerosol instruments in principle are calibrated and report their data assuming spherical equivalent diameters, it is difficult to measure and report true particle exposure values. This is because the assumptions required for generating the correct values are usually not known or are very complex in true exposure situations, and it is still poorly understood how instrument responses vary with the many different material characteristics and properties.

The aim of this study was to investigate the comparability of the results in a performance test of four commonly used real-time monitoring particle measuring instruments when challenged to pigment and nanomaterial powder dusts which resemble dust from occupational powder handling. For comparison with a morphologically simple aerosol, we also demonstrate the performance of the measurement devices challenged to a spray product forming nm-size condensate particles (Norgaard et al. 2009). Because all currently commercially available surface area monitors report the biologically relevant alveolar lung deposited surface area, this work also involves an analysis of potential procedures of conversion between measured number size distribution data and LDSA and their comparability. Finally, the real-time measurement data are compared with interpretations from gravimetric measurements of collected respirable dust samples.

The test powder materials were specifically selected to challenge the monitoring instruments based on their variations in primary particle size and specific surface areas as determined by the BET technique. Dust aerosols released from such powders may pose some measurement problems due to their level of agglomeration, size-distribution and multimodality, which may not be revealed in tests using standard testing particles such as PSL, NaCl or DEHS. However, documentation of these problems and their levels is important to understand the ability to use such instruments for monitoring and regulatory exposure assessment.

Materials and Methods

Instrumentation

Four different real-time monitoring instruments were used in this study as listed below. Two of them are particle sizing instruments while the other two are LDSA concentration monitors. All instruments were calibrated by the manufactures prior to the study.

- **Fast Mobility Particle Sizer (FMPS; TSI model 3091, TSI Inc., Shoreview, MN, USA).** In the FMPS, particles are charged through a dual unipolar diffusion charger prior to size classification according to particles electrical mobility based on their trajectory in an electrical field. The electrical charge carried by the size classified particles is measured with 22 electrometers which currents are corrected for multiple charges and image charges and further inverted to size distribution having 32 bins between 5.6 and 560 nm. The FMPS was used to measure particle number size distributions. The alveolar deposited surface area concentration and respirable surface area concentration were further calculated assuming spherical particles with unit density. Sampling for the FMPs is done using a PM_1-cyclone to remove micron-sized particles.

- **Electrical Low Pressure Impactor (ELPI, Dekati, Finland).** In the ELPI (Keskinen et al. 1992; Marjamaki et al. 2005), particles are charged using a unipolar diffusion charger after which the particles are collected in a low pressure cascade impactor which fractionates the particle sizes based on their aerodynamic properties into 12 channels spanning from 30 nm to 10 µm. The electrometer detected current in each stage is corrected for multiple charges, image charges and inverted to a size distribution. In this study the ELPI was used to measure particle number size distributions and further calculate alveolar deposited surface area concentration and respirable surface area concentration.
- **Nanoparticle Surface Area Monitor (NSAM; TSI model 3550, TSI Inc., Shoreview, MN, USA).** The NSAM uses unipolar diffusion charging and a Faraday cup electrometer to measure a current which was found to be proportional to the lung deposited surface area concentration. By changing the voltage of the instrument ion trap, different proportionalities can be applied to mimic that of alveolar or tracheobronchial deposition as described by ICRP (1994). The inlet of the NSAM is mounted with a PM_1-cyclone. In this study, only the alveolar deposited surface area measured by the NSAM was investigated.
- **Aerotrak (Aerotrak 9000, TSI Inc., Shoreview, MN, USA).** The Aerotrak is a field-portable version of the NSAM. In all other functions it is identical to the NSAM. The inlet of the Aerotrak is mounted with a PM_1-cyclone. The Aerotrak has previously been compared with the NSAM and good agreement has been confirmed (Bau et al. 2012).

Case of spherical particles challenging the instruments

The first experiment was carried out in a 20 m^3 stainless steel chamber which was ventilated using a HEPA-filtered outdoor air which was well mixed within the chamber using two fans. A well-studied surface cleaning and maintenance product Multicover (Nanocover, Denmark) was applied for 10 seconds from a distance of 20 cm onto a metal sheet (Norgaard et al. 2009; Norgaard et al.

2010). Approximately 5 minutes after spraying a nucleation event took place, which formed nm-size droplet particles anticipated to be due to nucleation through limonene oxidation that slowly grew in size through condensation.

Airborne particles were sampled from the room at the same point using separate conductive tubes for each instrument. The tube lengths were adjusted so that residence times were equal for each instrument to avoid differences in particle losses. As spray condensation particles are considered to be highly spherical, this experiment on one hand served as a calibration check of the instruments as well as a challenge to a simple aerosol within the optimum application ranges of all instruments.

Case of dust particles challenging the instruments

Seven different powders (**Table 1**) were selected so that primary particle sizes varied from 16 nm to over 100 nm, specific surface areas from 0.03 to 113 m^2/g, (Volume-Specific Surface Area (VSSA) from 0.3 to 437 m^2/cm^3 calculated using the nominal material densities from 2.7 to 10.4 g/cm^3). The variation in specific surface areas was used to indicate the potential level of aggregation in the powder particles. The extraordinary low specific surface area was observed for the PVP-stabilized AgNP powder, which appears as large aggregates with a water-soluble PVP matrix. The highest specific surface area material was UF TiO_2, which also had the smallest primary particle size (16 nm).

The powders were aerosolized using the miniaturized EN15051 dustiness drum (Schneider and Jensen 2008). The system has been made to correspond to the EN15051 standard drum so relative dimensions have been maintained and the 33 drops per minute is ensured by three lifter vanes in the drum and an 11 rpm rotation. The inlet air to the drum was controlled at 50 % RH and HEPA-filtered to ensure a particle-free background. The measurements were split into two separate sampling trains in order to maintain 11 lpm flow through the drum (**Fig. 1**). Before starting the test,

2 g of powder was loaded into the drum, which was then rotated for 60 seconds to ensure that all surfaces were saturated with particles. After the drum had been emptied, 6 g of test material were loaded into it and 60 seconds of background measurements were done without the drum rotating to ensure a particle free test atmosphere. The experiment was then initiated by rotating the drum for 60 seconds during which particles were emitted and led through the airflow to the sampling train. After the drum was stopped, measurement of remaining airborne particles was conducted for another 120 seconds. This completed the rotational test. The measurement was then repeated an additional two times and the results here are presented as averages over the three experiments.

In the first experimental set-up (**Fig. 1a**), respirable dust (as defined by EN 481 (1993), D_{50} = 4 µm) was collected with a GK2.69 cyclone at 4.2 lpm (BGI Inc., Waltham, MA, USA), and particle concentrations were measured with the FMPS, NSAM and Aerotrak. In addition, an Electrostatic Precipitator (ESP, Asbach, 2015) was used to deposit particles onto 25 mm silica wafers for analysis by Scanning Electron Microscopy (SEM) using a FEI ESEM Quanta 200 FEG (FEI, Eindhoven, the Netherlands) and Energy-Dispersive X-ray Spectroscopy (EDX) to determine elemental composition of the particles. The respirable dust mass was determined using a Sartorius microbalance (Type R162 P; Sartorius GmbH, Göttingen, Germany), after conditioning the filters and control filters in a weighing room (22°C; 50 %RH) before and after sampling. The measured mass was used to calculate the gravimetrical powder dustiness index and categorize the powder dustiness level according to EN15051.

In the second experimental set-up (**Fig. 1b**), particle size distributions were measured by using the ELPI and FMPS. The FMPS was used to validate that the measurements were comparable with the measurements performed in the first experimental set-up.

Particle concentrations analysis

1) Comparison of LDSA concentrations

For both FMPS and ELPI, alveolar particle number concentration fractions were calculated by multiplying measured particle number size distributions with the alveolar deposition fraction, DF_{alv} (ICRP 1994). The alveolar deposition fraction is based on aerodynamic diameter; therefore we assumed spherical particle shape and unit density while calculating the FMPS alveolar particle number concentrations. Particle number size distributions measured by the ELPI were also multiplied with the NSAM PM_1-cyclone penetration efficiency to simulate the cyclone placed upstream of the NSAM, Aerotrak and FMPS. For direct comparison of the measured LDSA concentrations between the 4 instruments, time series data were converted into running 5 second averages. Due to NSAM and Aerotrak measuring alveolar deposited surface area, $LDSA_{alv}$, the ELPI and FMPS (without PM_1 fractions) had to be recalculated according to:

$$LDSA_{alv} = \pi \sum_{Dp} n(D_p) \cdot D_p^2 \cdot DF_{alv}(D_p) \cdot PM_1(D_p) \text{ [m}^2\text{]} \quad (1)$$

with $n(D_p)$ being the number of particles with diameter D_p, DF_{alv} and PM_1 being the alveolar deposition fraction and cyclone penetration fraction for the specific particle size, respectively.

2) Comparison of respirable surface area concentrations

A second analysis was completed to investigate the comparability between the theoretical geometric surface area of the respirable dust collected on the filter for dustiness categorization and the theoretical accumulated respirable surface area concentrations of the airborne dusts measured with the FMPS and ELPI.

On the one hand, respirable LDSA values were compared with the respirable particle surface area calculated from the respirable gravimetric measurements [g] multiplied by their respective specific surface areas [m^2/g] (**Table 1**).

On the other hand, FMPS and ELPI particle number size distributions were converted to geometric surface area size distributions, assuming spherical particles (SA_{sph}). The latter is then integrated during the sampling period (180 s), and, transformed to the corresponding respirable fractions, *RF*. It should be noted that the FMPS was included in comparison, despite not covering the entire range of the respirable fraction. It is therefore expected that the FMPS data will underestimate the surface area in cases where a considerable number of particles are larger than 560 nm.

$$SA_{sph} = \pi \cdot \frac{Q_{drum}^2}{Q_{instr}} \cdot \int_0^{\tau} \sum_{D_p} \left[n\left(D_p, t\right) \cdot D_p^2 \cdot RF\left(D_p\right) \right] dt \quad (2)$$

where $Cn\left(D_p, t\right)$ is the number size distribution (FMPS, ELPI) at time t, Q_{drum} the total air flowrate of the drum, Q_{instr} the instrument flow and τ the sampling time.

Another approach is based on particle volume size distribution, combined with the respirable fraction, material density, ρ, and specific surface area, *SSA*:

$$SA_{ssa} = \frac{\pi}{6} \cdot \rho \cdot SSA \cdot \frac{Q_{drum}^2}{Q_{instr}} \cdot \int_0^{\tau} \sum_{D_p} \left[n\left(D_p, t\right) \cdot D_p^3 \cdot RF\left(D_p\right) \right] dt \quad (3)$$

Unlike the first approach this uses the assumption of spherical shape to calculate a total volume which then is recalculated into a surface area using known properties of the material.

Results and discussion

Dustiness

Fig. 2 shows an overview of the measured gravimetrical respirable dustiness indices for the 7 materials used in the study along with the regions of classification of powder dustiness according to EN15051. The materials covers a wide range of dustiness from Very *Low* (TiO_2 Pigment, TiO_2 AFDC, $CaCO_3$ #2) to *Low* (AgNP) and *High* (ZnO, $CaCO_3$ #1, UF TiO_2).

Real-time measurements

Particle size distribution measurements by the FMPS and ELPI showed a good agreement on the droplets formed in the chamber measurements (**Fig. 3a**). The small rotating drum shows in general good repeatability even though differences may occur in the modal diameter as well as the shape of the (number size) distribution. However, large discrepancies/deviations between FMPS and ELPI number size distributions were observed for all non-spherical powder particles generated using the small rotating drum (**Fig. 3b-h**). More precisely, the FMPS shows consistently higher particle number concentrations within its measurement size range (<560 nm) as compared to the ELPI. In the FMPS, particle concentrations often abruptly decreased in particle sizes below 100 nm (**Fig. 3a,b,d,g, and h**) while particles concentrations were specifically predominant in the size region of 150-200 nm. On contrary, the ELPI did not show any increased particle concentrations in this size range (**Fig. 3b-h**). For powders, the ELPI peak particle number concentrations were generally located in the size range of 0.5 to 2 µm. It should be remembered that the FMPS classifies particles according to their *electrical mobility equivalent* diameter while the ELPI measures *aerodynamic*

equivalent diameter, which are equal if particles are spherical and have unit density (1 g/cm^3). In the chamber experiment, particles are presumably spherical with a density close to 1 g/cm^3. Thus, the FMPS and ELPI particle number size distributions were found to be similar (**Fig. 3a**). However, in the rotating drum experiments, airborne particles are highly agglomerated, with particle effective densities that are likely to be significantly different from unity. For powder particles, an order of magnitude difference in measured modal diameter was observed. This difference cannot be explained alone by particles shape and density; it would require two orders of magnitude difference in effective density as estimated by using the relation between the mobility diameter and aerodynamic diameter as described by Kelly and McMurray (1992). The deviating FMPS measurement is explained by Levin et al. (2015) where it is shown that FMPS is unable to measure distributions of spherical particles with a Geometric Mean Diameter (GMD) higher than 200 nm. This is partly because the electrical mobility size dependency flattens out within the FMPS size range and particles become harder to size-separate based on this technique. Furthermore, secondary effects in the FMPS current inversion seem to affect the final size distribution. For distributions having a GMD above 200 nm, it still shows them as having a GMD of 200-300 nm, and overestimates the number concentration. Furthermore, Shin et al. (2010) showed that agglomerated particles have higher unipolar charging efficiency than spherical particles having the same mechanical mobility. Thus, after unipolar charging, the electrical mobility of an agglomerate is higher than the electrical mobility of a spherical particle having equivalent mechanical mobility as the agglomerate. Increased agglomeration level is seen in the FMPS measurements as a decrease in electrical mobility size and an increase in concentration. It also moves the minima in electrical mobility into the FMPS size range, making size-classification based on this ambiguous (Levin et al. 2015). In the ELPI measurements, agglomeration increases the measured concentration due to increased charging capabilities.

Electron Microscopy

Typical dust particles from each material used in the dustiness drum and collected using the ESP is shown in **Fig. 4**. The AgNP appears in irregular aggregates with no clear primary particles visible by SEM (**Fig. 4g**) while other powder particles appear as aggregates of fused primary particles. The special appearance of the AgNP is explained by the abundant matrix encapsulating the AgNP (see Nymark et al. (2013) for TEM images of the primary AgNP particles). It was impossible to generate statistical data on particle size-distributions and morphologies due to insufficient number of particle counts on the images obtained. However, qualitatively, the fractal dimensions of the particles studied are all rather close to 3, which correspond to compact particles (Virtanen et al. 2004). This would mean that the unipolar charging done in the instruments should not be affected too much by the particle morphology.

Surface area comparison

The first step in the comparison was a benchmark comparison between the NSAM and Aerotrak, which are specifically designed for LDSA concentration measurements. Since both instruments are based on the same design, they were expected to give very similar results. **Fig. 5a** shows the LDSA concentration measured by the NSAM plotted against that of Aerotrak for all test particles. The LDSA concentration measured from spherical test particles was well within the manufacturer's given accuracy (both instruments are specified to have a ±20% measurement accuracy in the region of 20 to 200 nm) and had an average ratio of 1.06 (**Table 2**). In general the surface area monitors showed good comparability with a few exceptions. For low surface area materials, $CaCO_3$ #2 and TiO_2 Pigment, the Aerotrak gave notably higher concentrations of surface area and the correlation between the instruments was poor. TiO_2 AFDC, while having a poor correlation, gave values within ±20% of the NSAM. For the powders with higher specific surface area, the Aerotrak appears to give slightly higher values than NSAM, but with better correlation factors.

The calculated LDSA concentration measured using FMPS data are shown in **Fig. 5b**, with correlation factors and ratios in **Table 2**. It shows that the LDSA concentration measured using the FMPS appears to correlate well with that of the NSAM for certain powder materials such as $CaCO_3$ #1, ZnO, AgNP and UF-TiO_2 throughout their whole spectra of LDSA concentration levels. For most powders the FMPS appears to consequently give higher values than the NSAM, with the exceptions of UF-TiO_2 where the ratio is 0.77. The disagreement between the methods increases slightly at lower surface areas, i.e. for TiO_2 Pigment. No powder material has an average ratio within the ±20% boundaries. The underestimation of the NSAM as compared to the FMPS could be explained by the fact that NSAM underestimates LDSA concentrations for particles larger than 400 nm (Asbach et al. 2009). The assumption of spherical particle shape and unit density could also affect the results.

The LDSA concentration of particles below the 1 µm cut-off measured with the ELPI is shown in **Fig. 5c**. The correlation of LDSA concentrations between the ELPI calculated values and the NSAM was fair (R^2 0.87-0.93) for the high surface area powders but poorer (R^2 0.5-0.72) for the low surface area ones (**Table 2**). The ELPI calculated LDSA concentrations were underestimated as compared to the ones measured by the NSAM. Only UF-TiO_2 has an average ratio within the ±20% boundary. It should be noted that the ELPI was not measuring on the same aerosol as the surface area monitors but on separate repetitions of the same experiment, due to limitations in the total available volume-flow through the drum. However, measurements done with FMPS during both setups showed a good comparability between the two setups ($R^2 > 0.95$).

Fig. 6 shows that the accumulated respirable dust surface area calculated from gravimetric samples and calculated using **Eq. 2** and **3** from the ELPI and FMPS measurements were only similar for a few powders. With the exception of AgNP, the respirable dust surface areas calculated directly by assumption of spherical particles (**Eq. 2**) is greatly underestimated as compared to the respirable

dust surface area assigned from gravimetric measurements. This exception is likely due to its very low SSA as a bulk material. When the specific density and SSA is considered (**Eq. 3**) the values for airborne dust as measured by the ELPI generally correlates well with the values for filter-based calculations (R^2 0.98, Ratio 1.17). The corresponding values for the FMPS do not have a general trend towards approaching the gravimetrical value (Ratio 0.23). From this it is evident that using the relative density in the assessment of airborne dust surface area measured with the ELPI improves the comparability with the surface area derived from the respirable dust mass. However, large differences between the two estimates of released dust surface area may still arise for certain materials.

Conclusions

This study analyzes the comparability of lung deposited surface area (LDSA) concentrations as measured by or derived from four commonly used devices and approaches (FMPS, ELPI, NSAM, and Aerotrak) for both spherical particles and seven different powders aerosolized using the small rotary drum to simulate realistic workplace-like nanostructured dust particles. Test aerosol LDSA concentrations ranged from 0.1 to 10^4 μm^2 cm^{-3} as measured by NSAM, where spherical particles were mainly below 100 nm, while powder-borne particles covered the range from 0.1 to 10 µm, based on ELPI measurements. Powders dustiness indices varied from *Very Low* up to *High* according to the EN:15051 classification.

Test of spherical droplets after application of a surface coating product showed a good correlation ($R^2 > 0.97$, Ratio between 1.0 and 1.04) between NSAM, FMPS and Aerotrak for alveolar LDSA.

Dustiness testing of the seven highly different powders showed only fairly reliable correlation (R^2 between 0.73 and 0.93) and concentration ratio (1.04 to 2.8) between the two surface area monitors

tested for the high surface area range of materials. However, the comparison was inconsistent for the lower surface area concentrations and varied considerably. Similar levels of correlation were observed comparing the data from the NSAM and the FMPS for high surface area materials, but with the FMPS overestimating the concentration. Finally, the re-calculated ELPI LDSA concentrations showed good correlation at high concentrations (R^2 between 0.87 and 0.93), with somewhat lower correlation at the lower end (R^2 between 0.50 and 0.72). The LDSA concentration ratios were between 1.12 to 5.19 and 1.35 to 4.43, respectively.

Using a different approach, we evaluated the comparability between accumulated surface areas derived from on-line particle size-distribution measurements using FMPS and ELPI and a theoretical respirable dust surface area calculated based on the mass of respirable dust collected on filters. The results show that dust surface area converted from ELPI data may generally correlate well (R^2 > 0.98, Ratio 1.17) with the theoretical mass-based surface area of the generated dust particles. However, some large deviations were observed for the same calculations using FMPS data which may be due to particle morphology (agglomeration/aggregates), effective densities, and other previously mentioned issues regarding online measurement of particle size-distributions and surface areas. Further studies are required to validate the results using this approach for assessment of airborne dust particle LDSA with ELPI as it shows promise.

As an over-arching conclusion, the observed lack of data agreement between the different state-of-the-art measurement equipment is important and the apparent discrepancies encourage the need for further metrological research. If LDSA is to become a metric of choice in toxicology and occupational exposure assessments as well as regulatory enforcement, then a method of choice has to be decided or developed as current techniques give material dependent results and do not have the appropriate comparability. Results from different techniques can therefore not be trusted to

represent comparable levels of LDSA concentrations. The results should have implications for development of new measurement devices developed.

Acknowledgements

This work was conducted as part of the Strategic Research effort at the National Research Centre for the Working Environment and the 'Danish Centre for Nanosafety' (20110092173/3) from the Danish Working Environment Research Foundation, and the EU Framework 7 Programme NANODEVICE (NMP4-LA-2009-211464). We thank Signe H. Nielsen for technical assistance during dustiness testing and being responsible for gravimetric measurements of filters from dustiness testing and FIOH for donation of the samples in connection with the NANODEVICE project.

References

Aitken RA, Bassan A, Friedrichs S, et al (2011) Specific advice on exposure assessment and hazard/risk characterisation for nanomaterials under REACH (RIP-oN 3).

Asbach C (2015) Exposure Measurements at Workplaces, In: NanoEngineering – Global Approaches to Health and Safety Issues, ed. by Patricia Dolez. Elsevier Publishing (in press)

Asbach C, Fissan H, Stahlmecke B, et al (2009) Conceptual limitations and extensions of lung-deposited Nanoparticle Surface Area Monitor (NSAM). J Nanoparticle Res 11:101–109.

Asbach C, Kaminski H, Von Barany D, et al (2012) Comparability of Portable Nanoparticle Exposure Monitors. Ann Occup Hyg 56:606–621. doi: 10.1093/annhyg/mes033

Bau S, Witschger O, Gensdarmes F, et al (2010) A TEM-based method as an alternative to the BET method for measuring off-line the specific surface area of nanoaerosols. Powder Technol 200:190–201. doi: 10.1016/j.powtec.2010.02.023

Bau S, Witschger O, Gensdarmes F, Thomas D (2012) Evaluating three direct-reading instruments based on diffusion charging to measure surface area concentrations in polydisperse

nanoaerosols in molecular and transition regimes. J Nanoparticle Res 14:1217. doi: 10.1007/s11051-012-1217-6

BS EN:481 (1993) Workplace atmospheres. Size fraction definitions for measurement of airborne particles.

BS EN:15051 (2006) EN15051 Workplace Atmospheres: Measurement of the Dustiness of Bulk Materials - Requirements and Reference Test Methods.

Donaldson K, Schinwald A, Murphy F, et al (2013) The Biologically Effective Dose in Inhalation Nanotoxicology. Acc Chem Res 46:723–732. doi: 10.1021/ar300092y

Duffin R, Tran L, Brown D, et al (2007) Proinflammogenic effects of low-toxicity and metal nanoparticles in vivo and in vitro: Highlighting the role of particle surface area and surface reactivity. Inhal Toxicol 19:849–856. doi: 10.1080/08958370701479323

Fissan H, Kaminski H, Asbach C, et al (2013) Rationale for Data Evaluation of the Size Distribution Measurements of Agglomerates and Aggregates in Gases with Extended SMPS-Technology. Aerosol Air Qual Res 13:1393–1403. doi: 10.4209/aaqr.2013.02.0050

Fissan H, Neumann S, Trampe A, et al (2007) Rationale and principle of an instrument measuring lung deposited nanoparticle surface area. J Nanoparticle Res 9:53–59. doi: 10.1007/s11051-006-9156-8

Giechaskiel B, Alfoeldy B, Drossinos Y (2009) A metric for health effects studies of diesel exhaust particles. J Aerosol Sci 40:639–651. doi: 10.1016/j.jaerosci.2009.04.008

Hameri K, Lahde T, Hussein T, et al (2009) Facing the key workplace challenge: assessing and preventing exposure to nanoparticles at source. Inhal Toxicol 21 Suppl 1:17–24. doi: 10.3109/08958370903202804

Ibaseta N, Biscans B (2007) Ultrafine Aerosol Emission from the Free Fall of TiO2 and SiO2 Nanopowders. Kona-Powder Part 25:190–204.

ICRP (1994) Human respiratory tract model for radiological protection.

Jacobsen NR, Moller P, Jensen KA, et al (2009) Lung inflammation and genotoxicity following pulmonary exposure to nanoparticles in ApoE(-/-) mice. Part Fibre Toxicol 6:2. doi: 10.1186/1743-8977-6-2

Jensen KA, Koponen IK, Clausen PA, Schneider T (2009) Dustiness behaviour of loose and compacted Bentonite and organoclay powders: What is the difference in exposure risk? J Nanoparticle Res 11:133–146.

Jensen KA, Levin M, Witschger O (2015) Methods for testing dustiness. In Ratna Tantra (Ed.) Nanomaterial Characterization: An introduction. John Wiley & Sons Inc (Accepted).

Kelly W, Mcmurry P (1992) Measurement of Particle Density by Inertial Classification of Differential Mobility Analyzer Generated Monodisperse Aerosols. Aerosol Sci Technol 17:199–212. doi: 10.1080/02786829208959571

Keskinen J, Pietarinen K, Lehtimaki M (1992) Electrical Low-Pressure Impactor. J Aerosol Sci 23:353–360. doi: 10.1016/0021-8502(92)90004-F

Koivisto AJ, Jensen ACØ, Levin M, et al (2015) Testing the near field/far field model performance for prediction of particulate matter emissions in a paint factory. Environ Sci Process Impacts 17:62–73. doi: 10.1039/c4em00532e

Koivisto AJ, Lyyranen J, Auvinen A, et al (2012) Industrial worker exposure to airborne particles during the packing of pigment and nanoscale titanium dioxide. Inhal Toxicol 24:839–849. doi: 10.3109/08958378.2012.724474

Koponen IK, Koivisto AJ, Jensen KA (2015) Worker Exposure and High Time-Resolution Analyses of Process-Related Submicrometre Particle Concentrations at Mixing Stations in Two Paint Factories. Ann Occup Hyg. doi: 10.1093/annhyg/mev014

Leavey A, Fang J, Sahu M, Biswas P (2013) Comparison of Measured Particle Lung-Deposited Surface Area Concentrations by an Aerotrak 9000 Using Size Distribution Measurements for a Range of Combustion Aerosols. Aerosol Sci Technol 47:966–978. doi: 10.1080/02786826.2013.803018

LeBouf RF, Ku BK, Chen BT, et al (2011) Measuring surface area of airborne titanium dioxide powder agglomerates: relationships between gas adsorption, diffusion and mobility-based methods. J Nanoparticle Res 13:7029–7039. doi: 10.1007/s11051-011-0616-4

Lebouf RF, Stefaniak AB, Chen BT, et al (2011) Measurement of airborne nanoparticle surface area using a filter-based gas adsorption method for inhalation toxicology experiments. Nanotoxicology 5:687–699. doi: 10.3109/17435390.2010.546951

Leskinen J, Joutsensaari J, Lyyranen J, et al (2012) Comparison of nanoparticle measurement instruments for occupational health applications. J Nanoparticle Res 14:718. doi: 10.1007/s11051-012-0718-7

Levin M, Gudmundsson A, Pagels JH, et al (2015) Limitations in the use of Unipolar Charging for Electrical Mobility Sizing Instruments: A Study of the Fast Mobility Particle Sizer. Aerosol Sci Technol 0:00–00. doi: 10.1080/02786826.2015.1052039

Levin M, Koponen IK, Jensen KA (2014) Exposure Assessment of Four Pharmaceutical Powders Based on Dustiness and Evaluation of Damaged HEPA Filters. J Occup Environ Hyg 11:165–177. doi: 10.1080/15459624.2013.848038

Makela JM, Aromaa M, Rostedt A, et al (2009) Liquid flame spray for generating metal and metal oxide nanoparticle test aerosol. Hum Exp Toxicol 28:421–431. doi: 10.1177/0960327109105154

Marjamaki M, Lemmetty M, Keskinen J (2005) ELPI response and data reduction - I: Response functions. Aerosol Sci Technol 39:575–582. doi: 10.1080/027868291009189

Maynard AD, Kuempel ED (2005) Airborne nanostructured particles and occupational health. J Nanoparticle Res 7:587–614.

Norgaard AW, Jensen KA, Janfelt C, et al (2009) Release of VOCs and Particles During Use of Nanofilm Spray Products. Environ Sci Technol 43:7824–7830. doi: 10.1021/es9010468

Norgaard AW, Larsen ST, Hammer M, et al (2010) Lung Damage in Mice after Inhalation of Nanofilm Spray Products: The Role of Perfluorination and Free Hydroxyl Groups. Toxicol Sci 116:216–224. doi: 10.1093/toxsci/kfq094

Nymark P, Catalan J, Suhonen S, et al (2013) Genotoxicity of polyvinylpyrrolidone-coated silver nanoparticles in BEAS. Toxicology 313:38–48. doi: 10.1016/j.tox.2012.09.014

Oberdorster G (2000) Toxicology of ultrafine particles: in vivo studies. Philos Trans R Soc Lond Ser -Math Phys Eng Sci 358:2719–2739. doi: 10.1098/rsta.2000.0680

Saber AT, Jacobsen NR, Jackson P, et al (2014) Particle-induced pulmonary acute phase response may be the causal link between particle inhalation and cardiovascular disease. Wiley Interdiscip Rev-Nanomedicine Nanobiotechnology 6:517–531. doi: 10.1002/wnan.1279

Schneider T, Brouwer DH, Koponen IK, et al (2011) Conceptual model for assessment of inhalation exposure to manufactured nanoparticles. J Expo Sci Environ Epidemiol 21:450–463.

Schneider T, Jensen KA (2008) Combined Single-Drop and Rotating Drum Dustiness Test of Fine to Nanosize Powders Using a Small Drum. Ann Occup Hyg mem059–.

Shin WG, Pui DYH, Fissan H, et al (2007) Calibration and numerical simulation of nanoparticle surface area monitor (TSI model 3550 NSAM). J Nanoparticle Res 9:61–69. doi: 10.1007/s11051-006-9153-y

Shin WG, Wang J, Mertler M, et al (2010) The effect of particle morphology on unipolar diffusion charging of nanoparticle agglomerates in the transition regime. J Aerosol Sci 41:975–986. doi: 10.1016/j.jaerosci.2010.07.004

Todea AM, Beckmann S, Kaminski H, Asbach C (Subm.) Accuracy of electrical aerosol sensors measuring lung deposited surface area concentrations.

Tsai CJ, Wu CH, Leu ML, et al (2009) Dustiness test of nanopowders using a standard rotating drum with a modified sampling train. J Nanoparticle Res 11:121–131.

Virtanen A, Ristimaki J, Keskinen J (2004) Method for measuring effective density and fractal dimension of aerosol agglomerates. Aerosol Sci Technol 38:437–446. doi: 10.1080/02786820490445155

List of Table Titles

Table 1. Physico-chemical properties of powders.

Powder name	**Producer**	**Reference Code (Producers names)**	**XRD-Structure**	**XRD size [nm]**	**Nominal Density [g/cm^3]**	**SSA [m^2/g][a]**	**VSSA[b] [m^2/cm^3]**	**Mass-loss[d] [wt%]**	**Organic coating**
$CaCO_3$ #1	SkySpring Nanomaterials Inc, Houston, TX, USA	NRCWE-012 ($CaCO_3$ for water-based latex paint)	Calcite	73±3	2.7	31.9	86	4	Fatty acid methyl ester
$CaCO_3$ #2	SkySpring Nanomaterials Inc, Houston, TX, USA	NRCWE-011 ($CaCO_3$)	Calcite	> 100	2.7	11.6	31	-	N/D
UF TiO_2	Kemira Oyj, Helsinki, Finland	UF TiO_2[e] (UV Titan M111)	Anatase	16±1	3.9	112	437	4.5	Not detected (N/D)
TiO_2 AFDC	Kemira Oyj, Helsinki, Finland	TiO_2 AFDC[e] (TiO_2 AFDC)	Rutile	> 100	4.3	6.0	26	-	N/D
TiO_2 Pigment	NaBond Technologies Co., Ltd, Shenzhen, China	NRCWE-004 (Titanium oxide Nano-powder; Rutile-TiO_2)	Rutile	94±4	4.3	9.7	42	-	N/D
ZnO	Umicore N.V. Brussels, Belgium	UMICORE ZANO[e] (ZANO)	Zincite	40±1	5.6	22	123	-	N/D
AgNP	Nanogap sub-nm-powder, S.A., A Coruña, Spain	NRCWE-009 (NGAP NP)	Metallic	41±2[c]	10.4[c]	0.03[c]	0.3[c]	15[c]	PVP[c]

[a]As measured with Krypton-BET on bulk material. [b] Estimated VSSA using nominal densities and neglecting the potential presence of organic-chemical surface modifications and coatings. [c]Data from Nymark et al. (2013). [d]Thermogravimetric analysis, 10 °C/min up to 1000 °C. [e]Original sample name at the Finnish Institute of Occupational Health.

Table 2. Correlation coefficients and ratios between LDSA determined by Aerotrak, FMPS and ELPI against NSAM.

Instrument:	**Aerotrak**		**FMPS**		**ELPI**	
Material:	R^2	Ratio	R^2	Ratio	R^2	Ratio
Droplets	0.99	1.06±0.01	0.99	1.01±0.01	0.98	1.03±0.04
$CaCO_3$ #1	0.96	1.68±0.2	0.97	1.51±0.27	0.93	2.14±0.11
$CaCO_3$ #2	0.34	6.97±0.03	0.26	10.05±0.01	0.53	6.17±0.03
UF TiO_2	0.73	2.81±0.7	0.89	0.77±0.08	0.92	1.12±0.48
TiO_2 AFDC	0.45	1.18±0.4	0.37	1.77±1.08	0.72	2.84±2.46
TiO_2 Pigment	0.05	7.12±1.2	0.01	11.23±0.76	0.50	4.43±0.63
ZnO	0.94	2.40±0.4	0.93	3.29±1.71	0.93	5.19±0.44
AgNP	0.74	1.04±0.04	0.96	4.38±1.88	0.87	1.35±0.294

List of Figure Captions

Figure 1. Schematic overview of measurement setups connected to dustiness drum.

Figure 2. Measured dustiness indices and classification regions according to EN15051. Whiskers denote one standard deviation.

Figure 3. Size distributions of sprayed droplets (**a**) and seven materials form the dustiness drum (**b-h**) as measured by FMPS and ELPI.

Figure 4. SEM images of a) $CaCO_3$ #1 b) $CaCO_3$ #2 c) UF TiO_2 d) TiO_2 AFDC e) TiO_2 Pigment f) ZnO g) AgNP

Figure 5. Comparison alveolar deposited surface area measured by NSAM and (a) Aerotrak, (b) FMPS, and (c) ELPI. Grey area denotes ±20 % uncertainty.

Figure 6. Calculated respirable fraction surface area from FMPS, ELPI as described in **Eq. 2 and 3**, and calculated value from filter sampling.

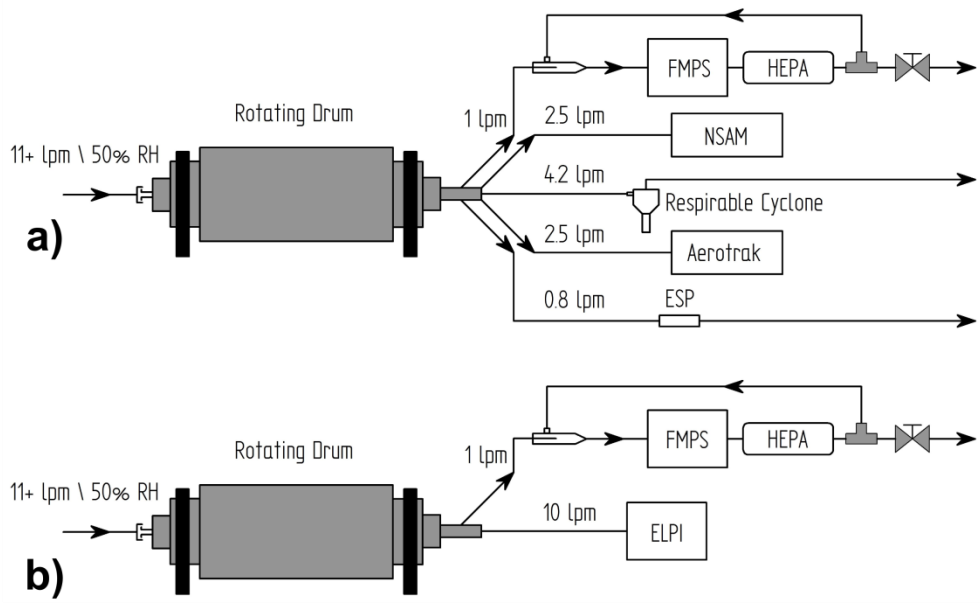

Figure 1. Schematic overview of measurement setups connected to dustiness drum.

Figure 1

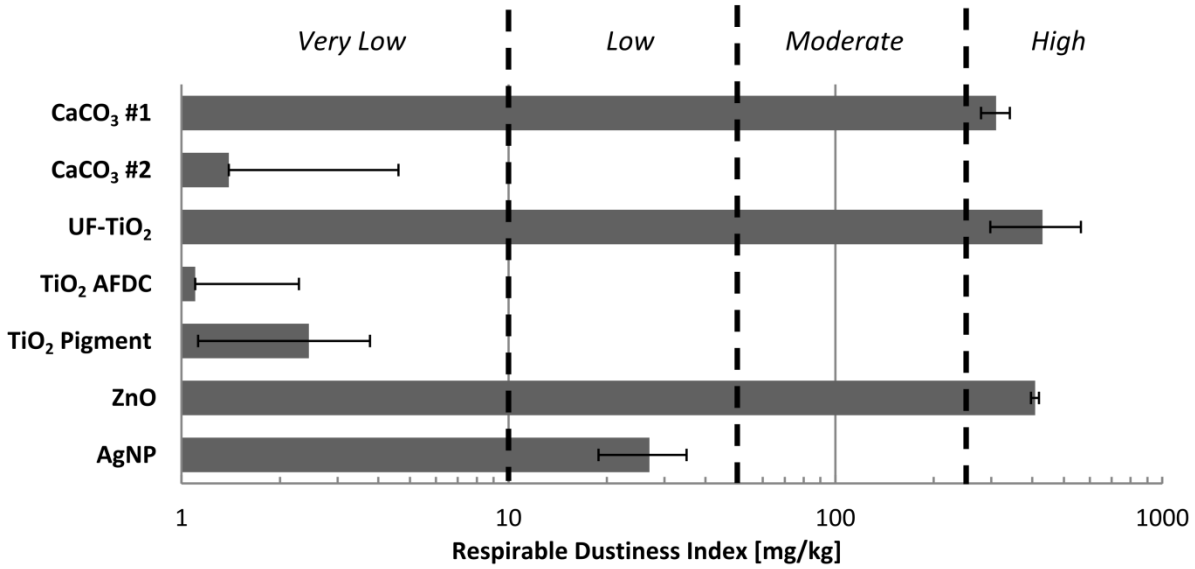

Figure 2. Measured dustiness indices and classification regions according to EN15051. Whiskers denote one standard deviation.

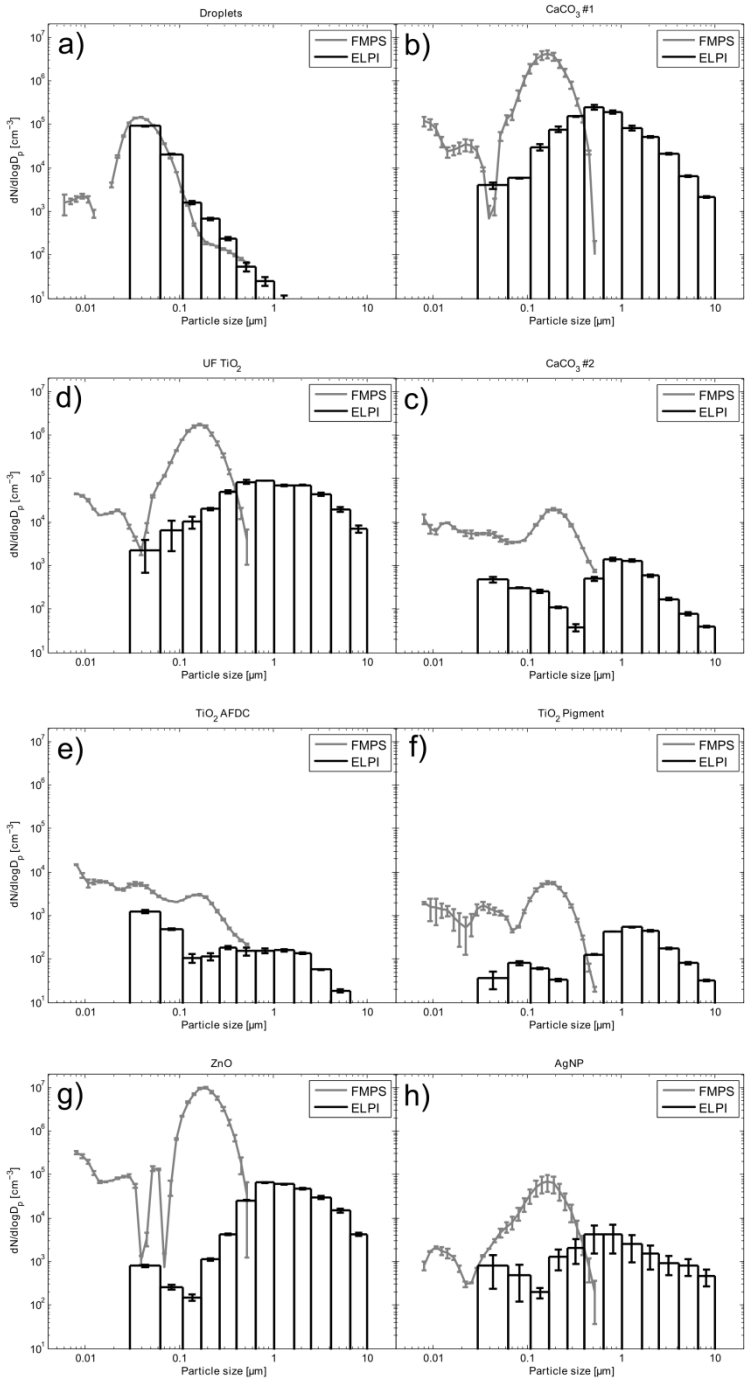

Figure 3. Size distributions of sprayed droplets (**a**) and seven materials form the dustiness drum (**b-h**) as measured by FMPS and ELPI.

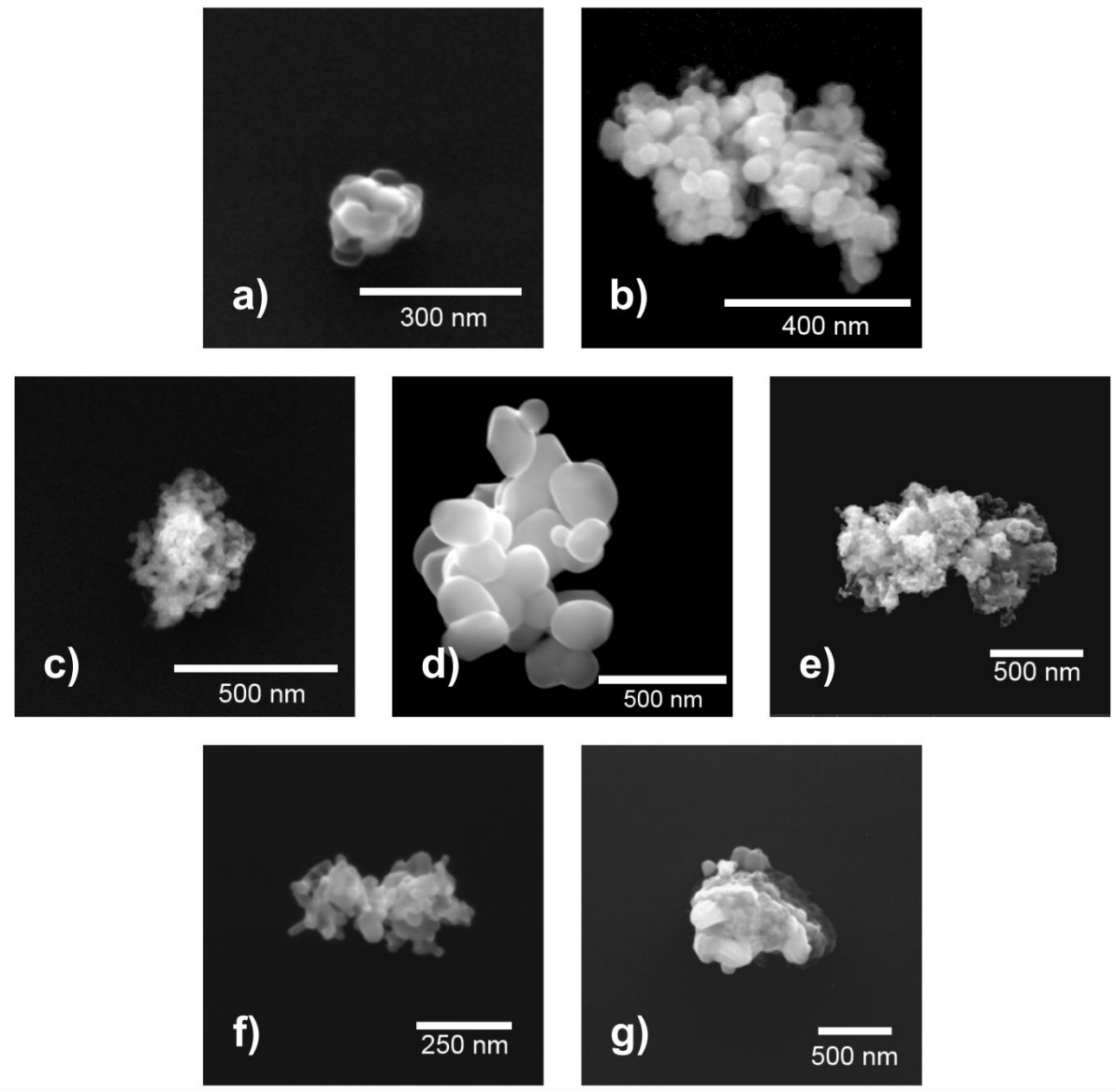

Figure 4. SEM images of a) $CaCO_3$ #1 b) $CaCO_3$ #2 c) UF TiO_2 d) TiO_2 AFDC e) TiO_2 Pigment f) ZnO g) AgNP

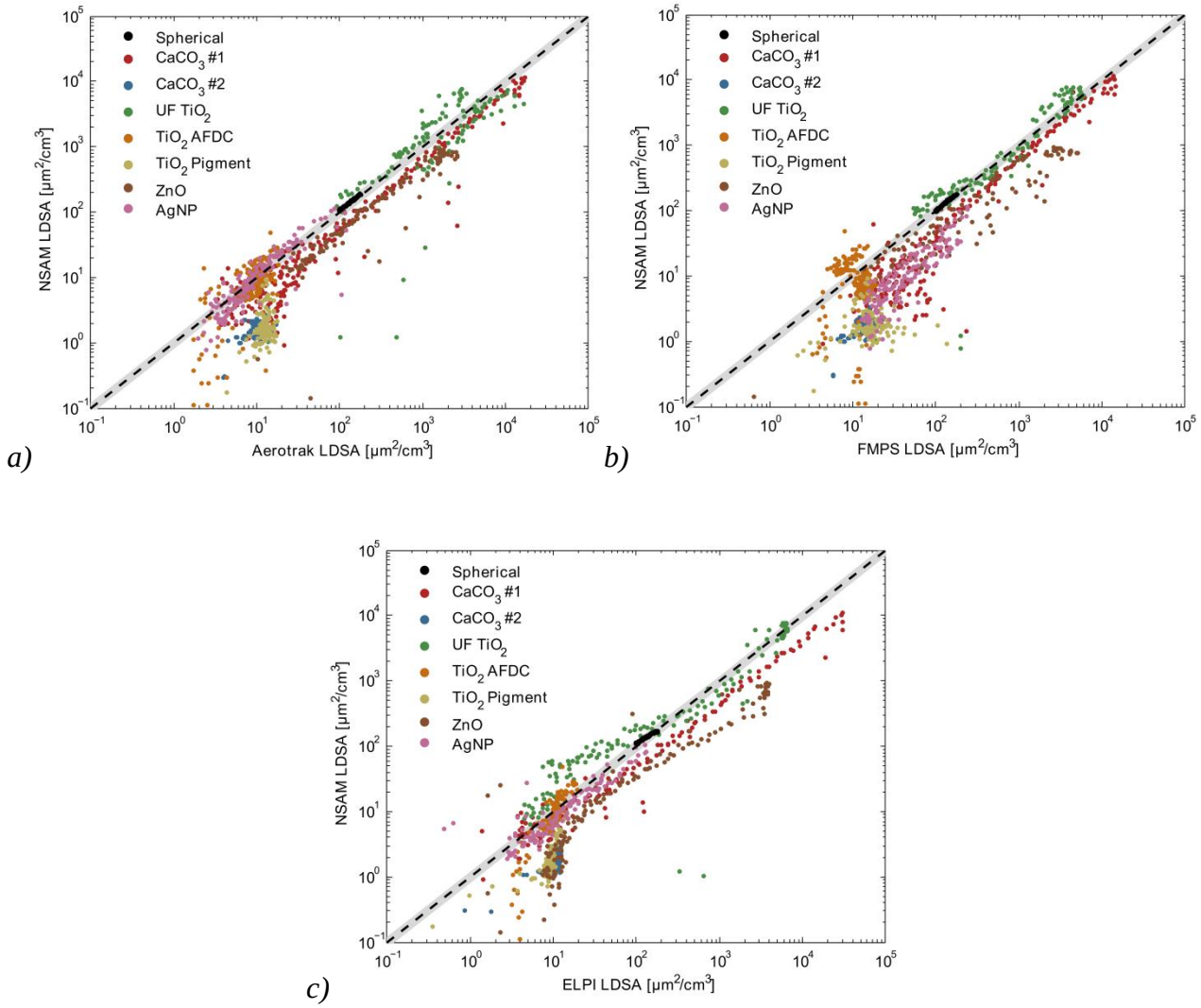

Figure 5. Comparison alveolar deposited surface area measured by NSAM and (a) Aerotrak, (b) FMPS, and (c) ELPI. Grey area denotes ±20 % uncertainty.

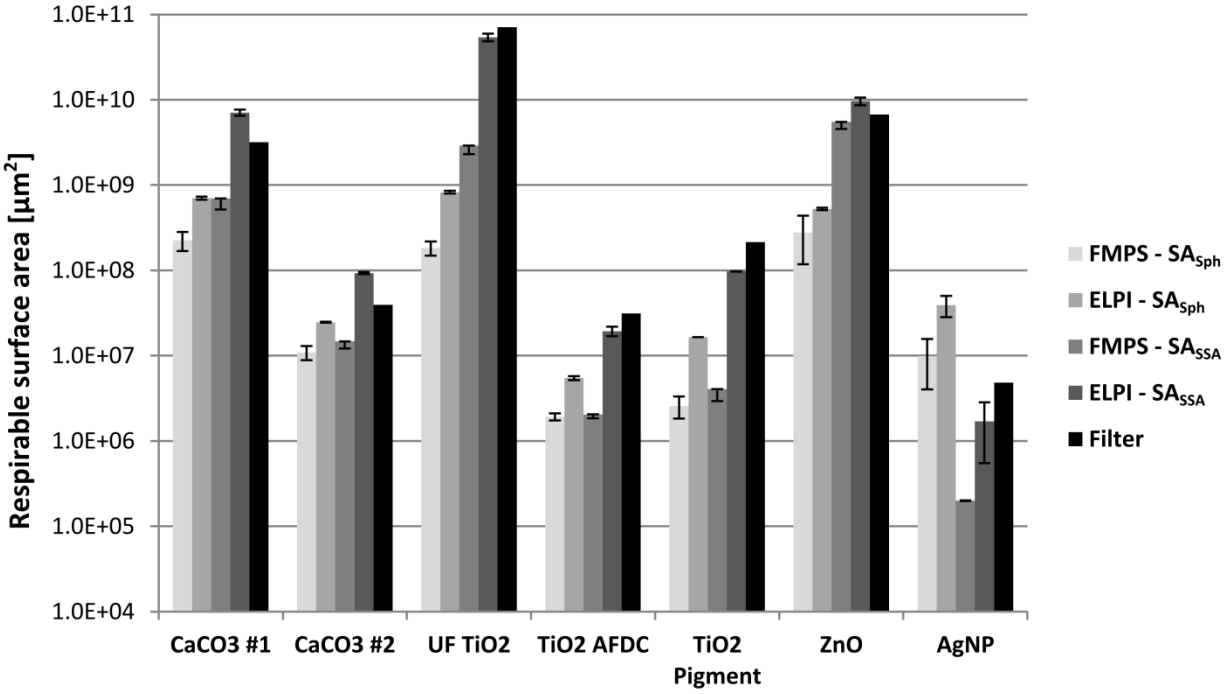

Figure 6. Calculated respirable fraction surface area from FMPS, ELPI as described in **Eq. 2 and 3**, and calculated value from filter sampling.

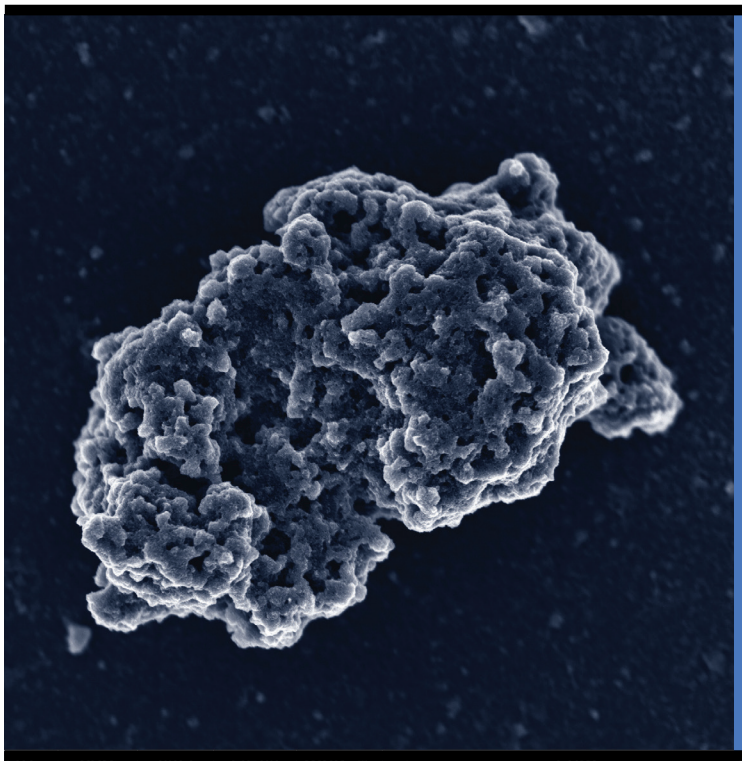

Published by:
DTU Nanotech
Department of Micro- and Nanotechnology
Technical University of Denmark
Ørsteds Plads, building 345B
DK-2800 Kgs. Lyngby